The Role of the *Axon Guidance* Molecule Slit2 in Pancreatic Cancer

Dissertation

zur Erlangung des akademischen Grades

doctor rerum naturalium

(Dr. *rer. nat.)*

im Fach Biologie

eingereicht an der

Mathematisch-Naturwissenschaftlichen Fakultät I

der Humboldt-Universität zu Berlin

von

M.Sc. Andreas Johannes Göhrig

Präsident der Humboldt-Universität zu Berlin

Prof. Dr. Jan-Hendrik Olbertz

Dekan der Mathematisch-Naturwissenschaftlichen Fakultät I

Prof. Stefan Hecht, PhD

Gutachter/in: 1. Prof. Dr. Ulrike Stein

2. Prof. Dr. Ann Ehrenhofer-Murray

3. PD Dr. med. Thorsten Cramer

Tag der mündlichen Prüfung: 30. September 2014

The study was conducted at the Experimental and Clinical Research Center, a joint cooperation between the Charité Medical Faculty and the Max-Delbrück Center for Molecular Medicine, Berlin-Buch, Germany, under supervision of Dr. med. Christian Fischer.

Index of Contents

Abbreviations

°C	Celsius
µg	Microgram
µl	Microliter
µM	Micro molar
5-FU	5-fluoruracil
aa	Amino acid
ALPS	Agrin, Laminin, Perlecan, Slit
Ang	Angiopoietin
ARF	ADP-ribosylation factor
Arp	Actin-Related Protein
bFGF	Basic fibroblast growth factor
bp	Base pair
BRCA2	Breast cancer type 2 susceptibility protein
BSA	Bovine serum albumin
CA-CX	Uterine cervical carcinoma
CAFs	Cancer associated fibroblasts
CAM assay	Chorio-allantoic membrane assay
CCR2	C-C chemokine receptor type 2
CD31	Cluster of differentiation 31
CDC42	Cell division control protein 42 homolog
cDNA	complementary DNA
cm	Centimeter
ctr	Control
CXCR4	C-X-C chemokine receptor type 4
DAPI	4',6-diamidino-2-phenylindole
DCC	Deleted in colorectal carcinoma
Dll4	Delta-like protein 4
DNA	Deoxyribonucleic acid
DOC	Deoxycholic acid
Dock	Dreadlock
Dox	Doxycycline
DPC4	Deletion target in pancreatic carcinoma 4
DRG	Dorsal root ganglion
DTT	Dithiothreitol
e.g.	for example (*exempli gratia*)
ECM	Extracellular matrix
EDTA	Ethylene-di-amine-tetra-acetic acid
EGF	Epidermal growth factor

EMT	Epithelial-to-mesenchymal transition
Eph	Ephrin receptor
Erk	Extracellular signal-regulated kinases
EtBr	Ethidium bromide
EZH2	Enhancer of zeste homolog 2
FAK	Focal adhesion kinase
FBS	Fetal bovine serum
Fc	Fragment crystallizable region
FITC	Fluorescein isothiocyanate
Fn3	Fibronectin type III repeats
FOLFIRINOX	Folinic acid, fluoruracil, irinotecan, oxaliplatin
fw	Forward
G	Gauge
g	Gram
GAPDH	Glyceraldehyde 3-phosphate dehydrogenase
GAPs	GTPase-Activating Proteins
GDNF	Glial cell line-derived neurotrophic factor
GEF	Guanine nucleotide exchange factor
GFRα	GDNF family receptor alpha
Glu	Glutamine
GTPase	Guanosine triphosphatases
h	Hour
HCC	Hepatocellular carcinoma
HDMEC	Human Dermal Microvascular Endothelial Cells
HE stain	Hematoxylin and eosin stain
HEK293	Human Embryonic Kidney 293 cells
Hh	Hedgehog
His-tag	Polyhistidine tag
HPDE	Human pancreatic duct epithelial cells
HRP	horseradish peroxidase
hu	Human
HUVEC	Human Umbilical Vein Endothelial Cells
i.e.	that is (*id est*)
Ig superfamily	Immunoglobulin superfamily of adhesion molecules
IHC	Immunohistochemistry
IL8	Interleukin 8
IPMNs	Intraductal papillary mucinous neoplasms
kDa	Kilodalton
Kras	Kirsten rat sarcoma viral oncogene homolog

LB	Lysogeny broth
LOH	Loss of heterozygosity
LRR	Leucine-rich domains
MAPK	Mitogen-activated protein kinase
MCNs	Mucinous cystic neoplasms
Mek (also MAPK)	Mitogen-activated protein kinases
mg	Milligram
Min	Minute
ml	Milliliter
mM	Millimolar
n	Number
NaCl	Sodium chloride
NCAM	Neural Cell Adhesion Molecule
ng	Nanogram
NGF	Nerve growth factor
NI	Neural invasion
NK	Natural killer cell
NRP	Neuropilin
ns	not significant
NSCLC	Non-small cell lung cancer
P+S	Penicillin + Streptomycin
$p16^{ink4a}$ (CDKN2A)	Cyclin-dependent kinase inhibitor 2A,
p53	Protein 53 (tumor protein 53)
PAA	Polyacrylamide
PanIN	Pancreatic intraepithelial neoplasia
PaSCs	pancreatic stellate cells
PBS	Phosphate buffered saline
PcG	Polycomb group
PDAC	Pancreatic ductal adenocarcinoma
PDGF	Platelet Derived Growth Factor
PFA	Paraformaldehyde
PI3K	Phosphatidyl-inositide 3 kinases
PlGF	Placental growth factor
Plxn	Plexin
qRT-PCR	Quantitative polymerase chain reaction
Rac1	Ras-related C3 botulinum toxin substrate 1
Raf	Rapidly Accelerated Fibrosarcoma
Ret	Ret proto-oncogene
rev	Reverse

Rho	Ras homology
RIPA	Radio-immunoprecipitation assay buffer
RNA	Ribonucleic acid
Robo	Roundabout receptor
Rpm	Revolutions per minute
RT	Room temperature
RT-PCR	Reverse transcription polymerase chain reaction
s or sec	Second
SCID	Severe combined immunodeficiency
SCLC	Small cell lung cancer
scr	scrambled
SDF1	Stromal cell-derived factor 1
SDS	Sodium dodecyl sulfate
SDS-PAGE	Sodium Dodecyl Sulfate-Polyacrylamide Gel Electrophoresis
Sema	Semaphorin
SH	Src-homology
shRNA	Small hairpin RNA
Slit-C	C-terminal fragment of Slit
Slit-N	N-terminal fragment of Slit
Sos	Son of sevenless
srGAP	Slit-Robo GAP
SWC	Schwann cells
TAE	Tris base, acetic acid and EDTA
TCA	Trichloroacetic Acid
Tet	Tetracycline
$TetO_2$	Tetracycline operator 2
TetR	Tet repressor
TGF-alpha	Transforming growth factor-alpha
TGF-beta	Transforming growth factor-beta
TRIS	Trisamine (2-Amino-2-hydroxymethyl-propane-1,3-diol)
TRITC	Tetramethylrhodamine B isothiocyanate
TrkA	Tyrosine kinase receptor A
UV	Ultraviolet
VEGF	Vascular endothelial growth factor
w/v	Weight per volume
WASP	Wiskott–Aldrich Syndrome Protein
wt	Wildtype

Abstract

The *Axon Guidance* Molecule Slit2 impairs pancreatic cancer metastasis *in vivo* and neural invasion *in vitro*

Background and aim: Early dissemination of pancreatic ductal adenocarcinoma (PDAC) via vascular routes and neural invasion limits curative therapy in this devastating disease, suggesting a central role for the interaction of tumor cells with blood vessels and nerves in the tumor stroma. Slit2 and its receptors, Robo1 and Robo4, constitute a system of guidance cues that function in axon guidance, angiogenesis and epithelial morphogenesis, respectively. More recently, a tumor suppressor function of Slit2 was proposed. Here, we studied the expression of Slit2 in PDAC and its function for tumor growth and dissemination.

Methods and results: Quantitative RT-PCR revealed a reduced Slit2 mRNA expression in specimens of human PDAC as compared to non-transformed pancreas. Clinically, reduced Slit2 mRNA expression correlated with a higher incidence and a higher extent of lymphatic metastasis. In contrast, the Slit2 receptors Robo1 and Robo4 were uniformly present in clinical samples of PDAC and healthy pancreas and displayed differential localization on epithelial tumor cells (Robo1) and tumor vasculature (Robo4) in immunohistochemical analyses. Moreover, pancreatic nerves exhibited strong Robo1 immunoreactivity. Consistent with reduced Slit2 mRNA levels in PDAC specimens, Slit2 was found substantially reduced or lost in poorly-differentiated human PDAC cell lines, respectively. Stable or inducible re-expression of Slit2 in PDAC cell lines inhibited their migration and invasion in transwell assays, an effect that was prevented by co-treatment with a soluble Robo1 decoy receptor or a soluble Robo1-Fc fragment. Tumor cell derived Slit2, furthermore, suppressed VEGF-induced lamellipodia formation, as well as migration of primary endothelial cells. Finally, *in vivo* studies in orthotopic human xenograft and mouse syngeneic pancreatic cancer models revealed that re-expression of Slit2 in PDAC cells inhibited tumor growth, invasion, metastasis and angiogenesis. Consistently, functional inactivation of Slit2 in Slit-competent PDAC cells via lentiviral-mediated Robo1 receptor knockdown stimulated tumor cell migration *in vitro*, and enhanced invasion and metastasis *in vivo*. In order to evaluate the effects of Slit2 on neural invasion we used co-cultures of tumor cells with dorsal root ganglia (DRGs) to monitor PDAC cell movement along the conduit provided by outgrowing neurites. Induction of Slit2 in PDAC cells impaired the unidirectional migration along outgrowing neurites.

Conclusion: These data confirm the notion of Slit2 as a tumor suppressor in PDAC. Slit2 suppresses motility and invasion of PDAC cells as well as their angiogenic and metastatic capacity. Thus, disruption of Slit2 dependent signaling pathways likely supports the aggressive phenotype of PDAC cells. In particular, the loss of Slit2 mediated repulsive signals may create a permissive environment for PDAC cell migration along pancreatic nerves, thereby facilitating neural invasion.

Keywords

Angiogenesis

Axon guidance

Invasion

Metastasis

Neural invasion

Orthotopic tumor growth

Pancreatic ductal adenocarcinoma (PDAC)

Robo receptors

Slit2

Xenograft

Zusammenfassung

Das *Axon Guidance* Molekül Slit2 inhibiert neurale Invasion und Metastasierung des Pankreaskarzinoms

Einleitung und Ziele: Lokale Invasion und Ausbreitung von Tumorzellen entlang von Nerven und Gefäßen limitieren den Erfolg kurativer Therapien und die Prognose von Patienten mit Pankreaskarzinom (PDAC). Slit2 und seine Robo-Rezeptoren, Robo1 und Robo4 sind *axon guidance* Faktoren, welche die Navigation von Nerven und Gefäßen sowie die Motilität von Epithelzellen steuern. Sie stellen somit attraktive Regulatoren der klinisch bedeutsamen Ausbreitungswege des PDAC dar. Neuerdings konnte für Slit2 auch eine tumor-suppressive Wirkung belegt werden. Zielsetzung der vorgelegten Arbeit war die Charakterisierung der Expression von Slit2 im PDAC und seiner Funktion für Tumorwachstum und -ausbreitung.

Methodik und Resultate: Quantitative Expressionsanalysen belegten eine deutliche Reduktion der Slit2 mRNA-Expression in humanen PDAC Proben im Vergleich zu gesundem Gewebe. Bei Patienten mit verminderter Slit2 Expression waren Slit2 mRNA-Werte unterhalb des Medians mit einer höheren Inzidenz lymphatischer Metastasierung und einem gesteigerten Prozentsatz befallener Lymphknoten verbunden. Im Gegensatz dazu zeigten immunhistochemische Untersuchungen der Slit2-Rezeptoren Robo1 und Robo4 vergleichbare Immunreaktivität in den PDAC-Proben und im gesunden Gewebe, wobei eine differentielle Lokalisation in epithelialen Tumorzellen (Robo1) und Tumorgefäßen (Robo4) zu beobachten war. Darüber hinaus, wiesen intra-pankreatische Nerven eine starke Immunreaktivität für Robo1 auf. Ähnlich den humanen PDAC Proben wiesen auch schlecht-differenzierte humane PDAC Zelllinien eine stark verminderte mRNA-Expression oder einen Verlust von Slit2 auf. Die stabile oder induzierbare Re-Expression von Slit2 in solchen Slit2-defizienten Zelllinien führte zu einer Hemmung der gerichteten Migration und

Invasion, ein Effekt, welcher durch die gleichzeitige Gabe des löslichen Robo1-Rezeptors oder eines löslichen Robo1-Fc-Fragments aufgehoben werden konnte. Außerdem hemmte Slit2-konditioniertes Medium aus Tumorzellen die VEGF-induzierte Bildung von Lamellipodien und die Migration primärer Endothelzellen. Schließlich zeigten *in vivo* Studien an orthotopen humanen Xenograft-Modellen und an einem murinen, syngenen pankreatischen Tumormodell, dass die Re-Expression von Slit2 in PDAC Zellen Tumorwachstum, Invasion, Metastasierung und Angiogenese reduziert. Umgekehrt zeigten PDAC Zellen mit endogener Slit2 Expression nach Unterbrechung der Slit/Robo1 Interaktion durch lentiviral-vermitteltem Robo1-Rezeptor *knockdown* verstärkte Tumorzell-Migration *in vitro,* sowie vermehrte Invasion und Metastasierung *in vivo*. Effekte von Slit2 auf die neurale Invasion wurden in Ko-Kulturen von Tumorzellen mit Spinalganglien (Hinterwurzelganglien) geprüft, die es erlaubten die gerichtete Migration der Tumorzellen entlang aussprießender Neuriten zu verfolgen. Die Induktion von Slit2 in PDAC Zellen verminderte die gerichtete Migration von Tumorzellen entlang aussprießender Neuriten.

Schlussfolgerung: Diese Daten weisen Slit2 die Funktion eines Tumorsuppressors im duktalen Pankreaskarzinom zu. Auf funktionaler Ebene inhibiert Slit2 die Motilität und Invasion von PDAC Zellen, sowie deren angiogene und metastatische Kapazität. Es liegt daher nahe, dass eine Störung des Slit2-Robo Signalweges einen aggressiveren Phänotyp von PDAC Zellen begünstigt. Insbesondere der Verlust, Slit2-vermittelter, repulsiver Signale könnte daher Bedingungen schaffen, welche die Migration von PDAC Tumorzellen entlang pankreatischer Nerven ermöglicht und so neurale Invasion begünstigt.

1. Introduction

1.1 Pancreatic Ductal Adenocarcinoma (PDAC)

Pancreatic ductal adenocarcinoma (PDAC) is among the leading causes of cancer related deaths in the western world [1, 2]. The high mortality of pancreatic cancer [3] is reflected by a 5-year survival rate of less than 5 % [1, 4].

A late onset of clinical symptoms and, consequently, a late diagnosis combine unfavorably with an aggressive course of the disease and an extremely poor efficacy of systemic therapies [5]. Median overall survival times are therefore 4 to 6 months in patients with metastatic disease and 8 to 14 months in patients with unresectable locally advanced disease [1, 6]. Whenever feasible, surgery is the treatment of choice for PDAC, increasing median survival up to 23 months [4, 6]. However, due to the lack of symptoms and the concealed anatomical location of the pancreas, PDAC remains frequently undetected until metastatic disease is present [7-9]. Consequently, only 10 % of the patients are diagnosed with resectable tumors, and even in this favorable subgroup most patients will experience disease recurrence, either at the original tumor site or in the form of distant metastasis [10, 11].

Therapeutic interventions for recurrent systemic or primary metastatic disease have been based on the nucleoside analogue gemcitabine, palliative medicine and pain management [12, 13]. 5-fluoruracil (5-FU) is as effective as gemcitabine and recent data from meta-analyses suggest that a combination of gemcitabine and capecitabine may be beneficial [5, 13-16]. Also, the epidermal growth factor (EGF) receptor tyrosine kinase inhibitor erlotinib in combination with gemcitabine, has recently been added to the first line treatments [17], and FOLFIRINOX (folinic acid, fluoruracil, irinotecan, oxaliplatin) has recently been introduced for patients with a good clinical performance and risk profile [18-20]. Furthermore, combination regimes of gemcitabine with oxaliplatin or paclitaxel nanoparticles, are now considered as second line therapies [21-29]. Despite the increasing number of systemic treatment options however, survival benefits have remained small for most patients with PDAC. [Reviewed in 5, 30]

For those patients that are eligible for surgery, adjuvant treatments are gaining importance. Unfavorable prognostic factors in patients with intended curative surgery include tumor spread into lymph nodes and the presence of neural invasion [4, 5, 31, 32], suggesting that

therapeutic targeting of these processes may constitute a way to improve survival in PDAC.

1.1.1 PDAC – a multi-step genetic disease

There are few accepted risk factors for PDAC, such as chronic pancreatitis, advanced age or smoking, and a several familial predispositions are associated with an increased susceptibility [5, 33-37]. Molecular analyses of resected pancreatic tumor specimens have yielded important advances in our understanding of pancreatic pathogenesis over the past decade. By now, a widely accepted multistep model of PDAC has evolved, which provides a molecular and histological framework from premalignant precursor lesions to systemic metastatic disease [38-40].

Pancreatic transformation is reflected by morphologic changes of the affected cells and re-organization of the microenvironment. The first detectable histological abnormalities are non-invasive, pre-neoplastic lesions [35, 41]. So far, three precursor lesions have been identified: intraductal papillary mucinous neoplasms (IPMNs), mucinous cystic neoplasms (MCNs) and pancreatic intraepithelial neoplasia (PanIN) [41, 42]. Most frequent and relevant to PDAC are PanINs, which comprise different stages from PanIN-1 to PanIN-3 [2, 40]. They are characterized by increasing morphological changes and genetic alterations, with PanIN-3 reflecting many properties of invasive PDAC [41, 42]. [Reviewed in 43]

The most prevalent molecular alteration in PDAC is the presence of oncogenic $Kras^{G12D}$ in more than 90 % of cases, which can already be found in early stage premalignant PanIN lesions (PanIN-1) and occasionally in chronic pancreatitis, a risk factor for PDAC [35, 44, 45]. Oncogenic activation of Kras is followed by additional alterations that affect cellular senescence induction, in particular by inactivation of the tumor suppressor $p16^{ink4a}$ [46-48]. Further frequent somatic mutations occur in the tumor suppressor genes p53, DPC4 and BRCA2 [38, 39, 45, 48, 49]. Invasive PDAC also features frequent chromosomal losses, gene amplifications, and telomere shortening, which likely account for the considerable genomic instability observed in PDAC [Reviewed in 48]. Systematic sequencing of PDAC genomes has identified a large number of less frequent, additional genetic alterations, which however could be allocated to 12 core signaling pathways, including developmental pathways such as Wnt/ß-catenin and Hedgehog (Hh) [35, 50]. [Reviewed in 43]

Genetically engineered mouse models, which recapitulate several aspects of the human disease have been established and provided additional information regarding the molecular pathogenesis [Reviewed in 51-53]. Data from these models emphasize the importance of oncogenic activation of Kras and have localized precursor cells that are susceptible to transformation in the acinar epithelial compartment. Induction of mutant Kras in acinar cells supports the acinar to ductal cell metaplasia, which typically precedes the formation of low grade PanIN lesions. Additional genetic changes, such as loss of p16 or p53, may then promote progression to higher grade PanINs and eventually to carcinoma *in situ*, in models with prenatal expression of the initiating genetic lesions [53]. A different situation unfolds, when these genetic lesions are induced in the adult mouse pancreas, in which transformation does not occur unless an inflammatory insult (e.g. experimental pancreatitis) is provided [54]. Combined with experimental pancreatitis however, oncogenic Kras is sufficient to promote the formation of PanINs and their progression towards PDAC [55, 56].

1.1.2 PDAC – Tumor microenvironment

A most abundant desmoplastic stroma is one of the characteristic features of human PDAC specimens, and is increasingly perceived as a key aspect of PDAC pathogenesis [57-59]. The desmoplastic reaction likely reflects a substantial contribution of inflammatory mechanisms [58, 59], which is consistent with the long known clinical observation of chronic pancreatitis as a risk factor for the development of PDAC [33]. The desmoplastic stroma consists of extracellular matrix (ECM) proteins, pancreatic stellate cells (PaSCs) or cancer associated fibroblasts (CAFs) which produce fibrinogen and collagen-1 [35, 57]. The stroma also attracts immune cells, which secret cytokines, such as interleukin 8 (IL8) and transforming growth factor (TGF)-beta, creating an inflammatory environment, which in turn promotes tumor growth and metastasis [60, 61]. Notably, the dense stroma in PDAC is considered rather hypovascular, which has been proposed as an explanation for the chemoresistance of PDAC [62, 63]. At the same time, PDAC stroma is particularly rich in nerves, which are used by tumor cells as conduits for invasive spread, a process referred to as perineural invasion (please refer to 1.2.1). Indeed, a variety of neurotrophic factors, e.g. nerve growth factor (NGF) and Artemin are found expressed within the stroma compartment, supporting nerve hypertrophy and neoneurogenesis [64]. On the other hand, pancreatic cancer cells are attracted by neuronal structures within the pancreas and migrate along

them to the neuronal plexus, in a process associated with the clinical symptom of neuropathic pain and with poor prognosis [Reviewed in 65].

Identifying key genetic alterations for PDAC has led to a better understanding of the molecular events occurring during tumor initiation and progression. Unfortunately, these advances are not yet translated into improved therapies. Early blood-borne metastasis and neural invasion are still major causes of disease recurrence [4] and targeting these events could thus contribute to improved treatment of the disease. First trials with anti-angiogenic agents for the treatment of pancreatic cancer increased disease free survival, but failed to improve overall/mean survival [66-69] [Reviewed in 30, 70], indicating the need for alternative targets. Although clinical studies have identified neural invasion as a strong independent prognostic factor [4, 71], the knowledge about the driving molecular mechanisms of neural invasion is still limited [71]. Thus, new insights into the molecular mechanisms of neural invasion could possibly contribute to an improvement of PDAC treatment.

1.2 The neurovascular link – axon and vessel guidance molecules

The similar branching patterns displayed by vessels and nerves throughout the entire body has been recognized early in history [72]. The concept of a structural congruency between nerves and vessels has since been confirmed on the cellular and molecular level and has finally led to the current concept of the neurovascular link [Reviewed in 72, 73].

The navigation and maturation of developing neuronal and vascular circuits is coordinated and tightly controlled by many intra- and extracellular signals, that influence a variety of cell types like neurons, Schwann cells and glia cells, endothelial cells, mural cells (pericytes and smooth muscle cells), macrophages and fibroblasts [74-82]. For instance, during embryonic development of the mouse retina, nerve fibers are the first to innervate the retina [75]. Subsequently, endothelial cells navigate along these newly formed neuronal scaffolds in order to generate a vascular network [75] (Figure 1A). At the cellular level the growing vessel consists of various differentiated cell types. The tip cells at the leading front of the protruding vessel exhibit membrane protrusions that explore and scan the environment for guidance cues, thereby directing the growing vessel to its final destination [75] (Figure 1B). Stalk cells are less proliferative, build the lumen and connect the nascent vessel to the existing vascular network [75]. This process of angiogenic sprouting in turn resembles many

structural features of an axon growth cone with its protruding neurites that scan the environment for guidance cues [72, 75, 83] (Figure 1C).

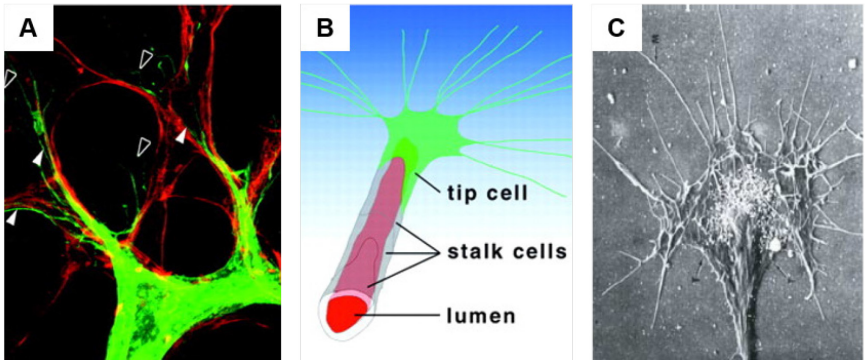

Figure 1: Interdependent and coordinated navigation and maturation of developing neuronal and vascular circuits during embryologic processes

(A) During embryonic development of the mouse retina, endothelial cells (green) navigate along previously formed neuronal scaffolds (red) creating a new vascular network with structural congruency to the neuronal compartment [75] (Reprinted under noncommercial purposes according to the permission and licensing terms of The Rockefeller University Press). **(B)** Schematic representation of a growing vessel (angiogenic sprout) with its various differentiated cell types [72, 75] (Reprinted under noncommercial purposes according to the permission and licensing terms of The Rockefeller University Press). **(C)** The angiogenic sprout resembles many structural features of an axon growth cone with its protruding neurites [72, 75, 83] (D; Reprinted with permission from [83]).

The structural congruency of the nervous and vascular systems suggests that the development of both networks is orchestrated by similar molecular mechanisms [84]. Most likely, some of the structural features and molecular mechanisms that had already been established by the evolutionary earlier evolved nervous system were taken over by the emerging vasculature [72]. Hence, tightly regulated interactions between various guidance cues have been shown to control the navigation of both growing axons and vessel sprouts [Reviewed in 72, 85]. Indeed, vascular endothelial growth factor (VEGF), which was initially characterized as the major angiogenic factor involved in physiological and pathological angiogenesis has since been recognized as a modulator of the nervous system displaying neurotrophic properties [72, 84, 86]. Similarly, members of the axon guidance family, such as Slit/Robo, Netrin/DCC/UNC, Semaphorin/NRP/Plexin and Eph/Ephrin, which control neuronal cell migration and axonal growth, have now emerged as important regulators of vessel guidance and maturation [72, 87].

Neural and vascular structures not only align with each other during developmental processes and share the same molecular cues but also exhibit a functional interdependence [88]. Thus, nerves and vessels not only provide each other with nutrients, oxygen and electric stimuli [89, 90] but they also mutually interact with each other via expression of certain membrane receptors and secretion of various guidance cues and survival factors to adapt to changes in navigation cues released from the microenvironment [Reviewed in 90, 91]. These navigation cues can be of repulsive or attractive nature (or both depending on the context) [72, 92]. Thus, endothelial cells migrate towards their target location by following gradients of attractive cues, while avoiding regions with increased local expression of repulsive cues, altogether providing the molecular infrastructure for the establishment of a new functional vessel network [85, 91].

A deregulation of both axon guidance and vessel guidance factors has been reported to contribute to excessive axon branching and vessel sprouting in various pathological conditions [Reviewed in 89, 90]. Aberrant expression of these factors also contributes to an aggressive phenotype of solid tumors characterized by excessive vessel sprouting, immature vessels and chemoresistance [93, 94]. For instance, the semaphorin and VEGF-165 receptor NRP1 was found to increase microvessel density *in vivo*, thereby promoting hepatocellular carcinoma (HCC) growth and progression [95]. Furthermore, overexpression of NRP1 in pancreatic cancer cells activated MAPK signaling and provided chemoresistance against gemcitabine and 5-FU *in vitro* [93], whereas a functional blocking peptide of VEGF-NRP1 interactions had a synergistic effect on 5-FU induced inhibition of lung and prostate cancer cell proliferation *in vitro* [96].

1.2.1 The neurovascular link: a concept that likely fits the pathobiology of PDAC

Early tumor cell dissemination via blood vessels and nerves is a hallmark of PDAC, and contributes to disease recurrence and poor prognosis [4, 97]. Various pre-clinical studies have confirmed the importance of tumor angiogenesis for the progression of pancreatic cancer and identified several angiogenic factors such as PlGF, Ang2, or PDGF that were overexpressed in PDAC [1, 98-100]. Among these were also members of the axon guidance family. In this context, recent studies revealed that re-expression of the axon guidance factor Netrin1 in the pancreatic cancer cell line MiaPaCa inhibits sprouting angiogenesis in xenograft tumor models, and that this inhibitory effect

depends on the expression of its receptor UNC5B on tumor vessels [94, 101].

Independent from lymphatic and hematogenous metastasis, neural invasion has emerged as a key pathologic feature of PDAC and represents a distinct route of tumor cell spread [65, 97, 102]. A dense neuronal network and the anatomical location of the pancreas, surrounded by extrapancreatic neural plexus in the retroperitoneal space, provide an optimal route for tumor cells to disseminate along the neuronal structures [7, 8]. The clinical relevance of neural invasion is meanwhile accepted, as its occurrence is associated with disease recurrence and poor clinical outcome [4]. However, despite the clinical importance of neural invasion in PDAC, the molecular mechanisms underlying the process of neural invasion are only now starting to unravel [65, 103] [Reviewed in 71].

Evidence is emerging that neural invasion depends on the mutual interaction of cancer cells with nerves, with both cell types secreting various factors, including neurotrophins, cytokines and chemokines to stimulate attraction, proliferation and invasion [97, 103, 104] [Reviewed in 71].

Cancer cells, nerves and endoneurial macrophages show increased expression levels of neurotrophic factors belonging either to the family of NGF or glial cell line-derived neurotrophic factor (GDNF) and their cognate receptors, respectively [97, 105]. Recently, their function for neural invasion in PDAC has been established. Indeed, neurotrophic factors have been found to enhance neural invasion in *ex vivo* co-cultures between pancreatic cancer cells and nerves. Moreover, the frequency of neural invasion in PDAC specimens correlated with the gene expression of neurotrophic factors [103, 104, 106]. Thus, increased expression of NGF, and its receptor TrkA were found to correlate with a higher incidence and a higher degree of neural invasion in pancreatic cancer [106], oral squamous cell carcinoma [107] and cutaneous cell carcinoma [108]. Moreover, upregulation of the GDNF receptors GFRα2 and neurturin were found to induce neuroplasticity in chronic pancreatitis a risk factor of malignant PDAC [109]. Axon guidance factors have also been implicated in PDAC. For instance, semaphorin3A (Sema3A) and neuropilin1 (NRP1) were found overexpressed in metaplastic ducts, malignant cells and nerves of PDAC specimens, and increased mRNA expression levels of Sema3A and NRP1 correlated with shorter patients' survival [110].

1.2.2 Function of axon guidance molecules in the (patho-) biology of epithelial organs

Apart from their role in neurogenesis and angiogenesis, axon guidance molecules have also been implicated in epithelial cell biology. With respect to cancer it is particularly interesting that axon guidance molecules are involved in the regulation of epithelial morphogenesis. Thus, they were found to control the development of various epithelial organs, such as the mammary gland [111, 112], the kidney [113], the foregut [114], the lung [115-119], the heart [120-122], the placenta [123], and the pancreas [124] [Reviewed in 125]. The function of axon guidance factors in developing and adult epithelial organs is not restricted to vascularization and innervation of these organs [123, 126-128], but also extends to the regulation of migration of epithelial (progenitor) cells and the coordination of ductal branching morphogenesis and organ homeostasis [111, 115, 124, 129-136].

Indeed, netrins are expressed in the fetal pancreas and were further shown to mediate pancreatic epithelial cell migration and differentiation, presumably via interaction with integrins [132, 137, 138] [Reviewed in 124]. Furthermore, the semaphorin family of axon guidance molecules and their cognate receptors were found in several organs to regulate branching morphogenesis. For instance, a study on kidney development demonstrated that Semaphorin4C (Sema4C) stimulates branching of ureteric epithelium via PlexinB2 (Plxnb2) in wildtype kidney explants, but not in $Plxnb2^{-/-}$ explants [136]. The authors further showed that PlexinB2 interacts with Ret, a co-receptor of GDNF-GFRα, in embryonic kidneys and that $Plxnb2^{-/-}$ ureteric buds fail to respond to GDNF, thus postulating that Sema4C-Plexin-B2 regulates ureteric branching via modulation of the GDNF-Ret signaling axis [136]. Moreover, developing mice with a deletion of Neuropilin2 (NRP2) in the mammary-gland, displayed aberrant branching morphogenesis and ductal outgrowth [135]. Interestingly, the effects of NRP2 on mammary branching were linked to VEGF and activation of focal adhesion kinase (FAK) and not to its semaphorin ligands, indicating that during these processes various signaling pathways are integrated [135]. In addition, Sema3A was shown to inhibit branching morphogenesis of fetal mouse lungs via NRP1 [133].

Complementary to studies that demonstrate expression and function of axon guidance molecules in epithelial organs during physiological processes, aberrant expression of these molecules was suggested to lead to pathological changes within the affected organ [139, 140]. Indeed, plasma netrin1 was found to be overexpressed in patients with adenomas of the breast, kidney and prostate [141].

In this context numerous studies ascribe to axon guidance molecules either tumor suppressive or promotive functions dependent on the cellular and molecular context [95, 142-145]. Evidently, treatment of breast cancer cells with Sema3A increased integrin levels, tumor cell adhesion to collagen-1 and inhibited tumor cell migration [146], whereas semaphorin3E-PlexinD1 induced tumor cell motility and mediated EMT in ovarian endometrioid cancer cells [147]. Moreover, in an invasive chorioallantoic membrane (CAM) assay, Netrin-1 was shown to protect pancreatic tumor cells and endothelial cells against apoptosis and to promote tumor cell invasion [148].

Taken together, axon guidance factors have been implicated in biological processes at the interface of epithelial cells, neurons and vessels that could be at most relevance to the pathobiology of pancreatic cancer. Consequently, a perturbation of this tightly controlled homeostasis might contribute to PDAC spread and progression.

1.3 The axon guidance factor Slit and its Robo receptors

Slits were initially characterized as secreted axon guidance factors in Drosophila [149, 150], binding to Roundabout (Robo) receptors [151] [Reviewed in 152, 153]. Three Slit (1-3) homologues have been identified in mammalians so far (60 % aa-sequence homology between Slits) [151, 152, 154]. The full-length-protein consists of 1469 amino acids (~200 kDa), which are arranged in several modular regions (Figure 2A). Four leucine-rich domains (D1-D4; LRR) are located at the N-terminus [155], followed by seven to nine epidermal growth factor (EGF)-like repeats [151, 156] and a C-terminal cysteine-knot [157]. The EGF domains are separated by an ALPS domain (Agrin, Laminin, Perlecan, Slit) [158-160]. [Reviewed in 152]

Slits are proteolytically cleaved within the sixth EGF domain (starting with aa 1110 (SPPMVLPRT) [152, 162] resulting in a 140 kDa N-terminal Slit (Slit-N) and a shorter C-terminal fragment (Slit-C) of 55-60 kDa [162]. Both, the N-terminal fragment and full-length Slit were reported to bind Robo receptors. Furthermore, they both elicited repulsion of olfactory bulb neurites [162]. In contrast, N-terminal Slit was found to induce growth cone collapse and branching, whereas full-length Slit itself had no effect on its own, but antagonized the N-terminal fragment [152, 162]. While the N-terminal fragment and full-length Slit were shown to be active, no specific function is yet associated with the short C-terminal Slit fragment, though it was shown

to associate with heparan sulfates at the cell surface [163] und thus might serve as a short range cue with orphan functions.

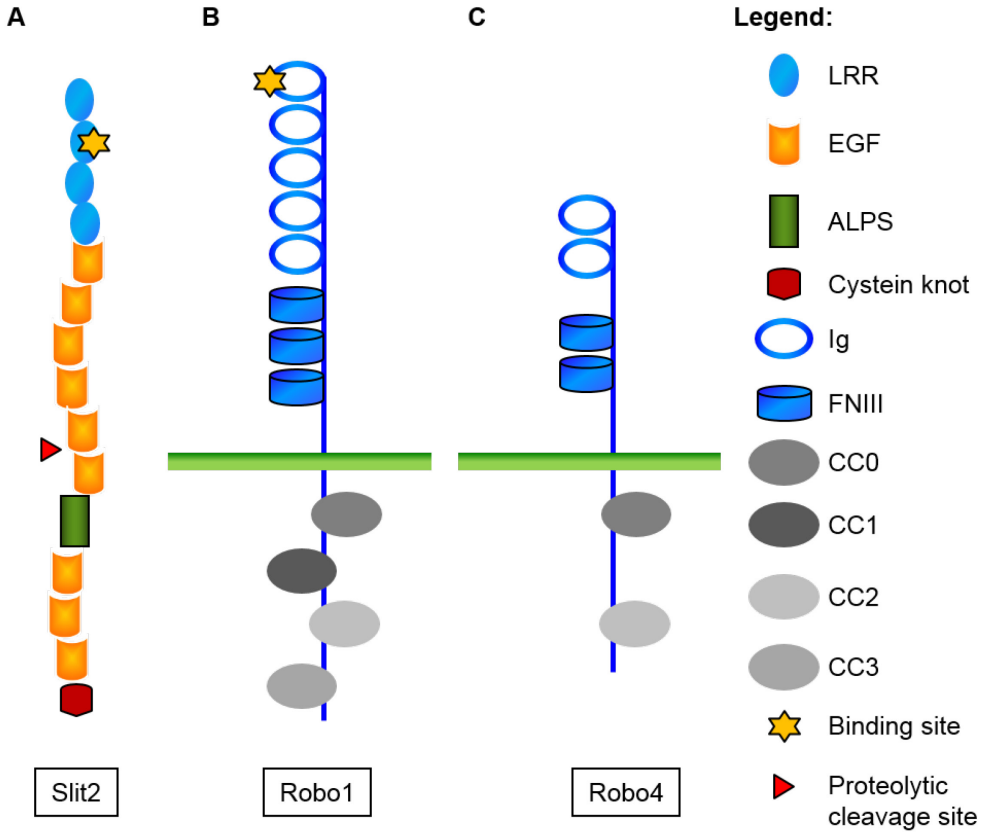

Figure 2: Schematic representation of the axon guidance molecule Slit2 and its receptors Robo1 and Robo4

(A) Structural domains of Slit2. Full-length Slit2 ligand consists of 1469aa (~200 kDa), comprising four leucine-rich domains (LRR), located at the N-terminus, followed by nine epidermal growth factor (EGF)-like repeats, which are separated by an ALPS domain (Agrin, Laminin, Perlecan, Slit) and a cysteine knot at the C-terminus. Full-length Slit2 is proteolytically cleaved at aa1110-1118 (SPPMVLPRT) creating an additional N-terminal (~140 kDa) and a C-terminal (~60 kDa) fragment. **(B, C)** Structural domains of Robo1 and Robo4. The single transmembrane receptors Robo1 and Robo4 belong to the immunoglobulin (Ig) superfamily of adhesion molecules. The extracellular domain consist of several Ig domains and fibronectin type III repeats (Fn3), with varying numbers between the receptor isoforms. The cytoplasmic domains do not possess intrinsic catalytic activities, but several adaptor proteins are recruited to conserved cytoplasmic motifs (CC0-CC3), which also vary between Robo receptors. (Adapted with permission from [161]).

Four Robos have been identified in mammals so far, which are single pass transmembrane receptors that belong to the immunoglobulin (Ig) superfamily of adhesion molecules [164, 165] (Figure 2B, C). Like their Slit ligands, Robo receptors are multi-domain proteins that consist of an extra-cellular domain with five Ig- and three fibronectin type III repeats (Fn3) [165, 166]. The cytoplasmic domains do not possess intrinsic catalytic activities, but upon Slit binding several adaptor proteins are recruited to conserved cytoplasmic motifs (CC0-CC3) [123, 167]. These adaptor proteins comprise proteins like Slit- Robo-GTP*ases* activating proteins (srGAPs) and CrossGAP/ Vilse [168-170] or the SH2-SH3 adaptor protein Dreadlock (Dock/Nck), which in turn recruits guanine nucleotide exchange factor (GEF) Son of sevenless (Sos) [171]. They further link Slit-Robo signaling to downstream effector pathways via Rho family of guanosine triphosphatases (GTPases), e.g. Rho, CDC42 and Rac1 that are involved in many cellular processes like axon repulsion, migration and adhesion [172]. Slit also induces cytoskeletal rearrangements via WASP and Arp2/3 in endothelial cells [173, 174]. As the availability of such adaptors and effectors varies between different cell types, the biological effects of Slit2 highly depend on the cellular context [175, 176]. [Reviewed in 161, 168]

1.3.1 Slit and its Robo receptors – repulsive guidance cues in the developing and adult nervous system

First analyses of the biological function of Slits and Robos revealed that these molecules serve as repulsive axon guidance cues regulating navigation and midline crossing of commissural axons [171, 177-180]. The processes during midline crossing are regulated by an orchestrated interplay of diffusible and membrane-bound cues that either attract or repulse axons [165, 179]. Netrin and its receptor DCC play an important role in the attraction of commissural axons to the midline [179] [Reviewed in 168]. After crossing the midline, these axons are prevented from re-crossing by the spatial and temporal expression of Slit proteins and their Robo receptors [179, 181-183].

Although Slit2 has originally been discovered as a repulsive guidance cue, which controls commissural axon pathfinding, Slit2 has since been also characterized as an attractive guidance factor [184-188]. For instance, the N-terminal fragment of Slit2 purified from brain tissue extracts stimulated elongation and branching of sensory axons in an *in vitro* collagen assay [184]. As mentioned above, Slit2 is cleaved into two major fragments, which were shown to differ in receptor binding

and/or biological effects from the full-length protein [184]. Therefore, differences in the outcome of Slit2 stimulation *in vivo* may reflect differences in the extent of proteolytic processing and depend on the availability of proteases.

Furthermore, the responsiveness to Slit gradients might also depend on the composition of Robo receptors expressed by each cell type [180-182, 186]. The expression of Slits and Robos in turn, is tightly regulated at the level of mRNA expression, secretion and their availability on the cell surface or extracellular matrix [178, 189-192]. Heterophilic interactions with other guidance molecules, such as Netrin-DCC and Semaphorin-Plexin, increase the complexity of Slit-Robo signaling, resulting in a context-dependent biological function for these axon guidance molecules [179, 193-196].

1.3.2 Slit and its Robo receptors – axon guidance factors and the neurovascular link

The discovery of Slit and Robo axon guidance factors on blood, and possibly also lymph vessels, implies that these axon guidance factors have retained a conserved function in the vascular system [197-199]. Indeed, a data mining approach identified an endothelial-specific gene with homology to Robo1, which was termed Robo4 [198, 200]. Robo4 shows the most structural divergence from the other Robo receptors [198] (Figure 2C). It lacks most of the extracellular domains with only three Igs and two Fn motifs and misses two of the cytoplasmic conserved domains [198]. Robo4 expression was found to be predominant in stalk cells of retinal blood vessels [201], and it was further postulated that Slit-Robo4 signaling might antagonize Notch-Dll4 induced tip cell formation, thereby supporting the maturation and maintenance of vascular structures [Reviewed in 202].

Evidence for a function of Robo4 in the regulation of angiogenesis *in vivo* came from gene knockdown and overexpression approaches in zebrafish [203]. These functional analyses revealed that Robo4 regulates a coordinated sprouting of intersomitic vessels (IVS) and prevents excessive IVS sprouting during zebrafish development [203]. Excessive vessel branching and sprouting is often associated with immature, malfunctioning vessels, as observed during pathologic VEGF-driven tumor vascularization [75, 204-207]. Interestingly, Slit2-dependent activation of Robo4 reduced VEGF-induced migration and vascular permeability *in vitro*, while deletion of Robo4 increased angiogenesis and vascular leak in mouse models of retinal vascular disease, providing further evidence for a functional role of Robo4 in

angiogenesis [201, 208]. These studies delineated an anti-angiogenic function for Slit2-Robo4 signaling, by restricting excessive vessel sprouting and stabilizing the vasculature in pathological conditions and in response to pro-angiogenic factors such as VEGF. Furthermore, Slit-Robo anti-angiogenic function also comprises the inhibition of endothelial cell migration *in vitro* as reported by various independent studies [197, 201, 209].

In apparent contradiction to the observed anti-angiogenic effects of Slit2-Robo, stimulation of endothelial and lymph-endothelial cell migration by Slit2, as well as tube formation *in vitro* were also reported [173, 175, 210, 211], suggesting a more complex, context- and disease-specific situation for Slit2-Robo signaling in angiogenesis. The context-dependent utilization of Slit2-Robo signaling and the different biological outcome in angiogenesis are reminiscent of the multiples role of Slit2-Robo during neurogenesis (please refer to 1.3.1).

1.3.3 Slit and its Robo receptors – regulators of ductal epithelial morphogenesis

Expression patterns of the Slit-Robo axon guidance members suggest that Slit-Robo activity is not restricted to the developing brain but also functions in developmental processes outside the nervous system [118, 212-217]. Indeed, Slit2 confines stereotypic and polarized branching morphogenesis of several epithelial organs during embryonic development [218], such as the mammary gland, the kidney and the lungs. For instance, during murine mammary gland development, Slit2 and Robo1 are expressed in duct epithelial cells and regulate branching duct morphogenesis [111, 218]. More specifically, Slit2 negatively regulates the proliferation of basal cells in the mammary duct, restricting epithelial branching [111] [Reviewed in 112]. Conversely, loss of Slit2-Robo1 function resulted in disrupted ductal structures and abnormal end bud formation [111].

Slit2 and Robo2 expression and function were also detected in the developing kidney, where they guide the correct formation of the developing ureteric bud, presumably by restricting GDNF signaling [113, 219] [Reviewed in 125]. Furthermore, mice with a targeted deletion of the Robo1 gene frequently die at birth because of respiratory complications [115]. Surviving mice exhibited bronchial epithelial abnormalities and hyperplasia [115].

These data not only provide evidence for a physiological expression and function of Slits and Robos in developing organs outside the nervous system but also demonstrate that a deregulated expression of these axon guidance molecules is associated with structural changes and aberrant branching morphogenesis within affected epithelial organs.

1.3.4 Slit and its Robo receptors – suppressors of tumor cell migration and metastasis

As outlined above, Slit2-Robo regulate a number of signaling pathways that control the correct localization and function of epithelial cells within their microenvironment and organ-context. In line with the deregulation of these pathways in cancer, altered Slit2-Robo function has been implicated in a number of human malignancies.

For instance, Slit2-Robo signaling has been linked to epithelial-to-mesenchymal transition (EMT) in mammary epithelial cells and migration and invasion of cancer cells in certain cancer entities [111, 220, 221]. It was thus shown that stimulation of lung and breast cancer cells with purified or ectopically expressed Slit2 inhibited tumor cell migration and consequently increased intercellular contacts via modulation of β-catenin and stabilization of E-cadherin [221]. Low Slit2 expression levels in lung cancer patients were prognostic for earlier disease recurrence [221]. Moreover, Slit2-Robo signaling integrates the response to various mitogenic attractants important for tumor cell migration and chemotaxis [222]. For instance, Slit2-Robo1 signaling attenuated hepatocyte growth factor (HGF)-induced epithelial branching in mammary organoid cultures [111], whereas silencing of Slit2, or functional inactivation of Slit2 signaling, promoted HGF-mediated migration and invasion of breast cancer cells via upregulation of CDC42 and decrease of RAC1 activity [222]. Similarly, loss of Slit-Robo signaling in the mammary epithelial gland induced upregulation of SDF1-CXCR4, concomitant with hyperplastic changes in the epithelium and desmoplastic transformation of the surrounding stroma [223]. Consequently, overexpression of Slit2 in breast cancer cell lines resulted in reduced expression of CXCR4 and inhibition of tumor growth [223]. Hence, restoration of Slit2-Robo within the mammary epithelium or tumor compartment perturbed autocrine SDF1-CXCR4 signaling [223], suggesting that loss of auto-/paracrine Slit2-Robo signaling might be beneficial for tumor progression. Moreover, expression and secretion of Slit2 by stromal fibroblasts, likewise, reduced tumor progression by interfering with PI3K/AKT/ß-catenin signaling [224]. In this case Slit2 secreted from stromal fibroblasts

binds to Robo1 and thereby prevents ß-catenin-induced transcription of the important cell-cycle proteins c-myc and cyclin D1 [224]. In breast cancer specimens, high Robo1 expression in breast cancer cells was correlated with increased survival and low Slit2 expression in stromal fibroblasts correlated with enhanced lymph node metastasis [224].

These observations are representative for numerous studies that provide evidence for an anti-metastatic and tumor-suppressive function of Slit2 (please refer to chapter 1.3.5). Nevertheless, other reports suggest that Slit2 acts as a promoter of tumor progression and metastasis. In this respect, overexpression of Slit2 in pancreatic islet tumors of a Rip1-Tag2 tumor model increased lymphatic metastasis [211].

1.3.5 Slit and its Robo receptors - potential prognostic factors, frequently lost or epigenetically inactivated in human cancer

Experimental data suggest that Slit-Robo signals can modify cancer growth. In line with this observation, mutations and altered expression of Slit2-Robo have been found in human cancer entities [Reviewed in 161]. Integrated analyses from small cell lung cancer (SCLC) exomes, genomes and transcriptomes revealed frequent mutations of Slit2 and listed Slit2 as a likely driver gene [225]. Similarly, mutations of Slit2 and Robo receptors have been identified in pancreatic cancer [45]. Moreover, loss of heterozygosity (LOH), at chromosome 4, the chromosomal location of the Slit2 gene, has been reported for mesothelioma, SCLC and NSCLC, as well as lung, breast and colorectal cancer [226-228]. Deletions in chromosome 4, together with the high incidence of promoter hypermethylation, suggest Slit2 as a tumor suppressor in uterine cervical carcinoma (CA-CX) and colorectal cancer [229, 230]. Other studies also report an epigenetic inactivation, either of Slit ligands and/or its Robo receptors [231]. Indeed, inactivation of the Slit2 gene was reported for human colorectal cancer and cancer cell lines mainly through promoter hypermethylation [228]. Similar results were obtained for Slit2 in gliomas [232] and breast cancer [227]. A comparison of the methylation status in human blood samples from various cancer entities, detected the highest methylation frequency in adult chronic lymphocytic leukemia (80 %) [233], and Slit2 was found to be (partly) methylated in the corresponding leukemia cell lines [233]. Slit was also shown to be down-regulated in 83 % of primary human hepatocellular carcinoma (HCC), which correlated with

CpG island hypermethylation [234]. Accordingly, 75 % of the HCC cell lines exhibited reduced Slit2 levels, which were related to the degree of promoter methylation. A genome-wide location analysis in prostate cancer cell lines identified Slit2 as a target of the polycomb group (PcG) protein EZH2. Polycomb proteins bind as complexes to the promoter region of target genes and thereby suppress the expression of these genes [231]. Promoter hypermethylation of $p16^{INK4A}$, $p14^{ARF}$, CyclinD2 and Slit2 was detected in the serum and tumor DNA of breast cancer patients with Slit2 bearing the highest frequency of methylation [235].

While many studies reported that Slit2 is lost or otherwise functionally inactivated in most cancers, there are also studies that report an up-regulation of Slit2 and Robo receptors. For instance, Robo1 and Robo4 mRNA expression was found up-regulated in a large scale gene expression study on colorectal cancer [236]. Furthermore, increased levels of Slit2 have been observed in a subgroup of hormone refractory prostate cancer [237].

Despite these exceptions, Slit2-Robo downregulation and epigenetic inactivation have frequently been linked to reduced survival in various cancers, including prostate, breast and lung cancer [231], underscoring the potential tumor suppressor function.

1.3.6 Slit and its Robo receptors - implications in neural invasion of PDAC?

Slit-Robo signaling has been implicated in development, physiology and pathologies of a number of epithelial organs. Nevertheless, there are no comprehensive studies that specify a physiological function for Slit2-Robo in the adult pancreas. However, several lines of evidence strongly suggest that the Slit2-Robo system has retained a function in the adult pancreas:

First, the adult pancreas is densely innervated [238]. Slit2-Robo have been shown to regulate the spatial and timely recruitment of those neural crest cells from the dorsal tube, which give rise to the innervation of the developing pancreas [220, 239]. Mechanistically, expression of both, Slit and Robo receptors keep pre-migratory neural crest cells in a low-motile state [220, 239]. In turn, migrating neural crest cells, only express Robo receptors, but are repelled from regions with high Slit expression, thus guiding these cells towards their correct target in the developing pancreas [220, 239].

Second, in good agreement of such a coordinated guidance function in organ innervation, autocrine and/or juxtacrine Slit2-Robo1/2 signaling has been found to stimulate motor axon fasciculation during muscle innervation [240]. It is thus conceivable that Slit2-Robo have preserved a regulatory function on chemokine-mediated guidance of pancreatic nerve-fascicles in the adult pancreas.

Third, Slit and Robo expression is not restricted to the developing nervous system, but has recently been implicated in the neuroplasticity of the adult nervous system. It was shown that the migration of immature neurons from the subventricular zone (SVZ) to the olfactory bulb (OB) within the adult brain is controlled by secreted Slit1 [241]. The secretion of Slit1 by immature neurons, in turn, induces morphological changes in astrocytes, which express Robo receptors, leading to the formation of astrocytic tunnels, “glial tubes”, that constitute ideal pathways for rapid neuronal migration within the adult brain [241]. Thus, Slit-Robo signaling not only interferes with cell motility directly in the migrating cell, but is also able to reorganize the microenvironment to provide the infrastructure essential for cell migration within the adult brain.

It is thus conceivable that Slit2-Robo have preserved a regulatory function on the mutual interplay and interdependence between tumor cells and nerves in the adult pancreas. Consequently, modification of Slit2-Robo signaling in PDAC might in turn lead to aberrant axonal growth and might therefore contribute to neuronal hypertrophy in chronic pancreatitis or facilitate neural invasion in PDAC.

Similar to Slit2-Robo, a recent study identified GDNF as an important guidance cue for neural crest cells during pancreas innervation [238]. In mice, the conditional knockout of GDNF in the pancreatic epithelium ($GDNF^{-/-}$) was associated with reduced infiltration of neurons and glial cells and impaired parasympathetic innervation of the pancreas [238]. Of interest, experimental models have suggested a functional role for GDNF in neural invasion of pancreatic cancer cells [104], and a clinical association between elevated GDNF-RET protein expression and intrapancreatic neural invasion [242]. In analogy to GDNF-RET, one could speculate that Slit2-Robo signaling might hence be involved in neural invasion of PDAC.

1.4 Work hypothesis: Slit-Robo and PDAC

Invasion, metastasis and in particular neural invasion, limit curative treatment options in PDAC. Axon guidance factors regulate the directed motility of epithelial cells, endothelial cells and neurons during epithelial morphogenesis, angiogenesis and neurogenesis. Changes in the expression of axon guidance factors and their receptors occur in several types of cancers and have been linked to metastasis and patient survival. Hence, we decided to study the expression and function of Slit2 for growth, invasion, metastasis, angiogenesis and neural invasion of PDAC.

Here we hypothesized that the axon guidance factor Slit2 and its Robo receptors could be relevant for the dissemination of PDAC via their effects on the (directed) motility of the tumor cells and/or via their interaction with stromal structures, such as vessels and nerves, that function as routes of invasion and metastasis.

The following three experimental approaches aim to answer our research questions:

(1) expression analysis of Slit2 in clinical samples and subsequent correlation with clinicopathological parameters

(2) experimental gain- and loss-of-function studies in appropriate *in vitro* and *in vivo* models to evaluate the role of Slit2-Robo for pancreatic cancer cell motility, metastasis, growth and angiogenesis

(3) assessment of the potential function for Slit2-Robo on tumor cell-nerve-interactions in suitable *in vitro* and *ex vivo* models of neural invasion

2. Materials and methods

2.1 Materials

2.1.1 Chemicals and consumables

Chemicals and reagents were purchased from the following distributors, listed alphabetically: Abcam (Cambridge, UK), Affymetrix (Cleveland, OH, USA), AppliChem GmbH (Darmstadt, Germany), Applied Biosystems (Foster City, CA, USA), Becton Dickinson, Franklin Lakes, NJ, USA, Bethyl Laboratories (Montgomery, TX, USA), Biochrom AG (Berlin, Germany), BioRad Laboratories GmbH (Munich, Germany), Boehringer Ingelheim GmbH (Ingelheim am Rhein, Germany), DAKO (Hamburg, Germany), Dianova (Hamburg, Germany), GE Healthcare (Little Chalfont, UK), Herbeta Arzneimittel (Berlin, Germany), Invitrogen Life Technologies (Carlsbad, CA, USA), Merck (Darmstadt, Germany), Millipore (Billerica, MA, USA), Pan-Biotech GmbH (Aidenbach, Germany), PeproTech (Hamburg, Germany), PolyPlus (Illkirch, France), Promega (Fitchburg, WI, USA), Qiagen (Hilden, Germany), R&D Systems, Minneapolis, MN, USA), Roche (Basel, Switzerland), Roth (Karlsruhe, Germany), Serva Electrophoresis GmbH (Heidelberg, Germany), Sigma-Aldrich Chemie GmbH (Steinheim, Germany), Thermo Fisher Scientific (Waltham, MA, USA), Vector Laboratories (Wertheim-Bettingen, Germany)

Consumables were delivered by: Ansell (Yarra City, Australia), Becton Dickinson (Franklin Lakes, NJ, USA), Braun (Tuttlingen, Germany), Charité (Berlin, Germany), Corning (Lowell, MA, USA), Fine Science Tools GmbH (Heidelberg, Germany), Gebrüder Martin GmbH (Tuttlingen, Germany), Gerhard Menzel GmbH (Braunschweig, Germany), Ibidi GmbH (Martinsried, Germany), Leica Microsystems GmbH (Nussloch, Germany), MP Biomedicals (Santa Ana, CA, USA), Roth (Karlsruhe, Germany), Sarstedt (Nümbrecht, Germany), Thermo Fisher Scientific (Waltham, Ma, USA), VWR International (Radnor, CA, USA).

2.1.2 Media, solutions and buffers

Cell culture media and additives were purchased from: Becton Dickinson (Franklin Lakes, NJ, USA), Biochrom AG (Berlin, Germany), EMD Chemicals, Inc. (San Diego, CA, USA), Invitrogen Life Technologies (Carlsbad, CA, USA), Lonza Group (Basel, Switzerland), PAA Laboratories GmbH (Pasching, Austria), R&D Systems, Inc. (Minneapolis, MN, USA), Roche (Basel, Switzerland), Sigma-Aldrich Chemie GmbH (Steinheim, Germany).

Standard-media, -solutions and -buffers were prepared according to Sambrook *et al.* [243]. All solutions have been prepared with Milli-Q purified water and autoclaved if required (121 °C/ 1 bar/ 25 min). Unstable ingredients have been sterile-filtered and added before usage. The composition of special solutions and buffers are mentioned in the respective methods.

2.1.3 Equipment

A listing of the equipment used is provided below and suppliers are indicated. Suppliers were: CAWO Photochemisches Werk (Schrobenhausen, Germany), Eppendorf AG (Hamburg, Germany), Leica (Wetzlar, Germany), Nikon (Tokyo, Japan), Thermo Fischer Scientific (Waltham, USA), VWR International (Radnor, CA, USA), Zeiss (Jena, Germany)

Microscopes

The following microscopes were used for cell culture, isolation of tissues, histology and time lapse experiments.

Table 1: Microscopes

Device	Company
Primo Vert (Cell culture microscope)	Zeiss
Axiovert 40 CFL + AxioCam MRC (Histology microscope)	Zeiss
DMI6000 B (Microscope for time-lapse imaging)	Leica
SMZ645 (Stereomicroscope)	Nikon

Centrifuges

For cell culture and molecular biological experiments, the following centrifuges were used.

Table 2: Centrifuges

Device	Company
Heraeus labofuge 400r (Mid bench centrifuge)	Thermo Fischer Scientific
Microcentrifuge 5424R (Microcentrifuge)	Eppendorf AG
MiniStar Silverline (Microcentrifuge)	VWR International
Microcentrifuge 5424 (Microcentrifuge)	Eppendorf AG
Microcentrifuge 5810R (Microcentrifuge)	Eppendorf AG

2.1.4 Enzymes and reaction kits

Enzymes and reaction kits were purchased from the following distributors: Agilent (Santa Clara, USA), Applied Biosystems (Foster City, CA, USA), BioRad Laboratories GmbH (Munich, Germany), Invitrogen Life Technologies (Carlsbad, CA, USA), Qiagen (Hilden, Germany), Vector Laboratories (Wertheim-Bettingen, Germany). Protocols were followed according to the manufacturers' instructions.

Table 3: Reaction kits

Kit	Company
High Capacity cDNA Reverse Transcription Kit	Applied Biosystems
iScript cDNA Synthesis Kit	BioRad
One-Step RT-PCR Kit	Invitrogen Life
Plasmid MAXI Kit	Qiagen
RNA-6000-Nano Kit	Agilent
RNeasy Lipid Tissue Mini Kit	Qiagen
RNeasy Mini Kit	Qiagen
Vectastain-Elite-ABC kit	Vector Laboratories

2.1.5 Antibodies and recombinant proteins

The following antibodies were used in immunoblots, immunofluorescence microscopy and immunohistochemistry:

Table 4: Primary antibodies

Target	Antibody
Anti-Actin	Polyclonal rabbit antibody (Sigma-Aldrich); WB: 1 µg/ml
Anti-CD31 (PECAM-1)	Purified rat antibody (Becton Dickinson); IHC: 1/50
Anti-Cortactin (p80/p85) [4F11]	Monoclonal mouse antibody (Millipore); IF: 1/200
Anti-Flag (clone M2)	Monoclonal mouse antibody (Sigma-Aldrich); WB: 10 µg/ml
Anti-Flag	Polyclonal rabbit antibody (Sigma-Aldrich); WB: 10 µg/ml
Anti-Myc [9E10]	Monoclonal mouse antibody (Invitrogen Life Technologies); WB: 10 µg/ml
Anti-Neurofilament (ab8135)	Polyclonal rabbit antibody (Abcam); IF: 1/500
Anti-Robo1	Polyclonal rabbit antibody (Bethyl Laboratories); WB: 10 µg/ml; IHC: 1/50
Anti-Robo1 (ab7279)	Polyclonal rabbit antibody (Abcam); IHC: 1/50
Anti-Robo4 (ab10547)	Polyclonal rabbit antibody (Abcam); IHC: 1/50
Anti-S100 (Ab-2)	Polyclonal rabbit antibody (Dianova); IHC: 1/100
Anti-Slit2 (AB5701)	Polyclonal rabbit antibody (Millipore); IHC: 1/200
Anti-Slit2 (HPA023088)	Polyclonal rabbit antibody (Sigma-Aldrich); IHC: 1/25

Table 5: Secondary antibodies

Target	Antibody
Anti-Mouse IgG	Polyclonal rat antibody; biotinylated (DAKO); IHC 1/200
Anti-Mouse IgG	Polyclonal goat antibody; FITC-conjugated (Dianova); IF: 1/200
Anti-Mouse IgG	Polyclonal goat antibody; HRP-conjugated (Dianova); WB: 1/10000
Anti-Rabbit IgG	Polyclonal goat antibody; biotinylated (Vector Laboratories); IHC 1/200
Anti-Rabbit IgG	Polyclonal goat antibody; FITC-conjugated (Dianova); IF: 1/200
Anti-Rabbit IgG	Polyclonal goat antibody; HRP-conjugated (Dianova); WB: 1/10000
Anti-Rat IgG	Polyclonal rabbit antibody; biotinylated (DAKO); IHC 1/200

Table 6: Fluorescent dyes

Dye	Company
DAPI (Nucleic acid stain)	Sigma-Aldrich; IF: 2 µg/ml
Phalloidin-Tetramethyl-rhodamine-B-isothio-cyanate (TRITC) (Staining of actin filaments)	Sigma-Aldrich; IF: 100 µg/ml

Table 7: Recombinant proteins

Recombinant protein	Details
Robo1-Fc	Recombinant rat Robo1-Fc chimera (R&D Systems). Cell culture assays: 5-10 µg/ml; *in vivo*: 45 µg/ml
huSlit2N	Recombinant human Slit2N (1093 aa), (Sigma-Aldrich). Cell culture assays: 200 ng/ml
huSlit2N	Recombinant human Slit2N (1093 aa), (PeproTech). Cell culture assays: 200 ng/ml
VEGF	Recombinant human VEGF-165(R&D Systems). Cell culture assays: 50 ng/ml

2.1.6 Microbial strains

The following bacteria strain was used for the amplification and isolation of plasmid DNA: XL10-Gold® Ultracompetent E. coli (Stratagene Technical Services, La Jolla, CA, USA). Genotype and background: TetrD(mcrA)183 D(mcrCB-hsdSMR-mrr)173 endA1 supE44 thi-1 recA1 gyrA96 relA1 lac Hte [F´ proAB laclqZDM15 Tn10 (Tetr) Amy Camr]. After transformation with plasmid-DNA, bacteria were cultured in LB growth medium (Roth) and plated on agar plates containing the appropriate antibiotic (ampicillin, kanamycin). Agar plates were incubated at 37 °C for 24 h. Individual colonies were picked and propagated in 250 ml Erlenmeyer flasks.

Growth medium was autoclaved and unstable additives were sterile filtered and added just before usage. Glycerol stocks were prepared as back-up for each transformed cloned.

2.1.7 Eukaryotic cell lines

Specific information on the individual cell lines were obtained from the American Type Culture Collection (ATCC) or the Leibniz-Institut DSMZ. Cells were seeded in the indicated media and cultivated in an incubator at 37 °C and 5 % CO_2-atmopshere and 90 % air humidity. For each cell type or transfected cell line frozen stocks of early passages were prepared and stored at -80 °C and liquid nitrogen. The following cell lines and primary cells were used for *in vitro* and *in vivo* assays.

Tumor cell lines:

ASPC-1: Purchased from ATCC (Manassas, USA). Description: Human pancreatic cancer cell line; derived from ascites inoculated xenograft. Media: RPMI 1640/ 10 % FBS/ P+S/ Glu.

BXPC3: Purchased from ATCC (Manassas, USA). Description: Adherent, epithelioid pancreatic cancer cell line; derived from human adenocarcinoma. Media: DMEM / 10 % FBS/ P+S/ Glu.

Capan-1: Purchased from DSMZ (Braunschweig, Germany). Description: Adherent, epithelioid pancreatic cancer cell line; derived from human carcinoma. Media: RPMI 1640/ 10 % FBS/ P+S/ Glu.

Capan-2: Purchased from DSMZ (Braunschweig, Germany). Description: Adherent, epithelioid pancreatic cancer cell line; derived from human carcinoma. Media: RPMI 1640/ 10 % FBS/ P+S/ Glu.

DANG: Purchased from DSMZ (Braunschweig, Germany). Description: Adherent, epithelioid pancreatic cancer cell line; derived from human carcinoma. Media: RPMI 1640/ 10 % FBS/ P+S/ Glu

MiaPaCa-2: Purchased from DSMZ (Braunschweig, Germany). Description: Adherent, epithelioid pancreatic cancer cell line; derived from human carcinoma. Media: DMEM / 10 % FBS/ P+S/ Glu.

MiaPaCa-2^{TR}: Kindly provided by Petra Schulz (formerly Department of Hepatology and Gastroenterology, Charité-Universitätsmedizin Berlin, Campus Virchow-Klinikum). Description: Stable cell clone generated by stable transfection of pcDNA6/TR into MiaPaCa-2 cells, resulting in expression of the Tet repressor [244]. Recipient for pcDNA4/TO-SP-3xFLAG-Slit2-myc-His for inducible expression of Slit2. Media: DMEM / 10 % FBS/ P+S/ Glu.

Panc1: Purchased from ATCC (Manassas, USA). Description: Adherent, epithelioid pancreatic cancer cell line; derived from human carcinoma. Media: DMEM / 10 % FBS/ P+S/ Glu.

Panc1^{TR}: Kindly provided by Petra Schulz (formerly Department of Hepatology and Gastroenterology, Charité-Universitätsmedizin Berlin, Campus Virchow-Klinikum). Description: Stable cell clone generated by stable transfection of pcDNA6/TR into Panc1 cells, resulting in expression of the Tet repressor. Recipient for pcDNA4/TO-SP-3xFLAG-Slit2-myc-His for inducible expression of Slit2. Media: DMEM / 10 % FBS/ P+S/ Glu.

Panc02: Kindly provided by V. Schmitz (Department of Internal Medicine I, University of Bonn). Description: Adherent, murine pancreatic cancer cell line. Derived from mice with C57/Bl-6 background. Media: DMEM / 10 % FBS/ P+S/ Glu.

Permanent cell lines:

Human Embryonic Kidney 293 cells **(HEK293):** Purchased from ATCC (Manassas, USA). Description: Human embryonic kidney cells (transformed by adenovirus); derived from human embryonic kidney. Media: RPMI 1640/ 10 % FBS/ P+S/ Glu.

Human pancreatic duct epithelial cells (**HPDE,** H6c7): Kindly provided by Dr. M. Tsao (Princess Margaret Cancer Center, UHN, Toronto, Canada). Description: Adherent, immortalized epithelial cells from

normal adult human pancreatic ducts. Media: Keratinocyte Basal Medium + supplements (Lonza). [245, 246]

Primary endothelial cells:

Human Umbilical Vein Endothelial Cells **(HUVEC):** Lonza (Basel, Switzerland). Description: Primary endothelial cells derived from human umbilical veins. Media: EGM-2 Bullet + supplements (Lonza). Cell culture ware were coated with 3 % Collagen.

Human Dermal Microvascular Endothelial Cells **(HDMEC):** PromoCell (Heidelberg, Germany). Description: Primary endothelial cells derived from human dermis. Media: EGM-2 Bullet + supplements (Lonza). Cell culture ware were coated with 3 % Collagen.

Primary neuronal cells:

Rat Schwann cells **(SWC):** Source: Kindly provided by C. Birchmeier (MDC, Berlin, Germany). Description: Primary rat Schwann cells. Media (full): DMEM/ F12 (1x)/ 10 % FBS/ NRG-1 (R&D Systems)/ Forskolin (EMD Chemicals, Inc.). Cell culture ware were coated with Poly-L-Lysine (SIGMA-Aldrich) and laminin (Roche).

2.2 Genetic and molecular biological methods

2.2.1 Molecular cloning of Slit2 expression constructs

Human Slit2 full-length cDNA (clone: Hs.29802; imaGenes, Berlin, Germany) was cloned into pcDNA4/TO-mycHis (Invitrogen; Darmstadt, Germany), resulting in pcDNA4/TO-SP-3xFLAG-Slit2-mycHis (Figure 3 A, B). Cloning strategy and the implementation of the various cloning steps were done by SINA Science Services GmbH (Berlin, Germany) according to the following protocol. In a first step human Slit2 full-length cDNA (without leader sequence) was amplified and then cloned into the pcDNA4/TO-mycHis vector (Invitrogen) via the restriction sites *NotI* and *XbaI*. The second step comprised the insertion of the Slit2 leader sequence followed by a 3xFLAG-sequence. The leader sequence of Slit2 was therefore elongated with primers in such a way that it results in a triple FLAG-tag. This fragment was again cloned into the pcDNA4/TO-SP-Slit2-mycHis before the Slit2 cDNA via *BamHI* and *NotI*.

The final product was pcDNA4/TO-SP-3xFLAG-Slit2-mycHis leading to secreted Slit2 with an N-terminal triple FLAG-tag (from here on FLAG-tag) and a C-terminal myc-His-tag (from here on myc-tag). The product was sequenced and analyzed by SINA Science Services GmbH (Berlin, Germany). SINA Science Services GmbH (Berlin, Germany) provided the plasmid DNA and glycerol stocks with transformed bacteria (*E. coli* DH5alpha) as well as sequence documentation.

A special feature of the pcDNA4/TO-mycHis vector is that it contains two tetracycline operator 2 ($TetO_2$) sites within the promoter region. This allows for regulated gene expression, if cells are co-transfected with pcDNA4/TO-mycHis vector and the pcDNA6/TR vector [please refer to user manual and vector maps provided by Invitrogen]. The pcDNA6/TR vector expresses high levels of the tetracycline (Tet) repressor, which binds to the $TetO_2$ sites and thus inhibits gene expression from the pcDNA4/TO-mycHis vector. Gene expression can be induced by adding doxycycline, a stable tetracycline analogue, which induces conformational changes within the Tet repressor and thereby preventing the binding of the Tet repressor to the promoter of the pcDNA4/TO-mycHis vector. If cells are transfected with the pcDNA4/TO-mycHis vector alone, the gene of interest is continuously expressed.

2.2.2 Transformation – heat shock method

A frozen stock of competent *E. coli* DH5α was put on ice for 10 min. 50 µl of bacteria were then transferred into a 1.5 ml Eppendorf reaction tube and mixed with 2 µl ß-Mercaptoethanol followed by another incubation step on ice for 10 min. Then 1 to 2 µg of plasmid-DNA were added mixed and incubated on ice for 30 min. Hereafter, the cells were heat shocked for 30 sec in a water bath (42 °C) and placed on ice for 2 min. Afterwards 950 µl of preheated LB media (37 °C) was added. The bacteria were incubated for 1 h at 37 °C on a shaker. 100 to 200 µl were plated on agar containing the appropriate antibiotic and incubated overnight at 37 °C.

2.2.3 Maxi preparation of plasmid DNA

In order to obtain sufficient starting material, a pre-/starter culture was prepared by transferring a single colony from a previously inoculated agar plate to a 15 ml Falcon tube containing 5 ml LB medium supplemented with the appropriate antibiotic. The culture was incubated overnight at 37 °C under agitation (incubator hood TH 30, Edmund Bühler GmbH). The pre-culture was then added to 200 ml LB media containing the appropriate antibiotic. The cells were incubated overnight at 37 °C and 225 rpm. In some cases glycerol stocks were prepared by mixing 600 µl glycerol with the same volume of bacteria solution. The stocks were stored at -80 °C until usage. For isolation of plasmid DNA the Plasmid MAXI Kit (Qiagen) was used. Therefore 100 to 200 ml of the overnight culture was centrifuged (15 min/ 1000 rpm/ 4 °C). The bacteria pellet was further prepared according to the manufacturer's instructions (Qiagen). The precipitated plasmid was air dried and solved in 100-300 µl double-distilled (nuclease-free) water.

2.2.4 Analytical agarose gel electrophoresis

A horizontal gel electrophoresis system (BioRad) was used to separate DNA fragments according to their molecular size. Standard protocols were followed [243]. Electrophoresis was carried out in 1x TAE buffer (40 mM Tris, 20 mM glacial acetic acid, 20 mM EDTA) and a 1-2.5 % (w/v) agarose gel containing ethidium bromide (EtBr). For size determination a size marker (GeneRuler 50 or 100 bp DNA Ladder, Thermo Fisher Scientific) was loaded to the gel together with the sample probes. After electrophoresis, separated DNA bands were visualized using a UV-transilluminator and subsequent image documentation (Biometra, Germany).

2.2.5 Isolation of RNA from tissue extracts and eukaryotic cells

For the isolation of total RNA from eukaryotic cell lines the RNeasy Mini Kit (Qiagen) was used. Buffers and reagents were applied according to the manufacturer's protocol. Cells were cultured in 6-well plates or 10 cm dishes until a confluence of about 70 % was reached. For DNA demethylation assays $3x10^5$ tumor cells were seeded in 6-well plates and incubated for 72 h with 10 µM 5-AZA-2'Deoxycytidine

(Merck). The cells were trypsinized and centrifuged (5 min/ 1500 rpm/ RT). The cell pellet was washed twice with PBS and centrifuged again (5 min/ 1500 rpm/ RT). Thereafter, the pellet was dissolved in RLT-lysis-buffer. Cell lysis was facilitated by pipetting up and down with a 29 gauge (G) syringe (repeated five times).

Isolation of total RNA from tissue was done with the RNeasy Lipid Tissue Mini Kit (Qiagen). This kit is recommended for tissue that is aliphatic and rich in stroma. A small piece of tissue was transferred to a Lysing Matrix D tube (MP Biomedicals). Carefully 700 µl of QIAzol lysis reagent were added to the reaction tube and homogenized (15 sec/ 5500 rpm) with the FastPrep-24 homogenizer (MP Biomedicals). The mixture was left for 5 min at room temperature. After the incubation time 140 µl of chloroform was added, mixed vigorously for 15 sec and incubated again for 2 to 3 min at RT. The subsequent centrifugation step (15 min/ 12000 rpm/ 4 °C) resulted in three phases, an aqueous, inter- and organic phase. The aqueous phase contained the RNA (about 320 µl) and was transferred into a new Eppendorf reaction tube.

From here on all steps were equal for RNA isolation from cells and tissue. The on-column DN*ase* digestion, the several washing steps and elution of total RNA were done according to the manufacturer's protocol. RNA was eluted with 30 µl RN*ase*-free water. RNA samples were kept on ice and concentration was determined with a NanoDrop ND 1000.

2.2.6 Complementary cDNA synthesis (RT-PCR)

Isolated total RNA from tissue extracts or eukaryotic cells was transcribed into cDNA with the reverse transcriptase enzyme. A single reverse transcription PCR (from here on simple referred as RT-PCR) reaction contained the following buffers and reagents from the iScript cDNA Synthesis Kit (BioRad): 2 µl of RT buffer, 0.8 µl of deoxynucleotide triphosphates (dNTPs), 2 µl RT random primers and 1 µl of MultiScribe Reverse Transcriptase. 1-2 µg of total RNA was added to the mixture and filled up with RN*ase*-free water up to 20 µl.

Table 8: PCR program for cDNA synthesis

PCR reaction was carried out in a RT-PCR cycler (Perkin Elmer, USA) by using the following program

Step	Operation	Temperature	Time
	Lid	99 °C	-
1	Annealing	25 °C	10 min
2	Elongation	37 °C	120 min
3	Inactivation	85 °C	5 sec
4	-	4 °C	∞

The following primers were used for qualitative PCR:

Table 9: Primers for qualitative PCR

Primer	Sequence
huSlit2 forward:	5'-TCC TAA CTC CAA AGG GAT TCA AAT GT-3'
huSlit2 reverse	5'-GGC TCC GTT TTT ACA CTT GTT GTC T-3'
huRobo1 forward	5'-GCA TCG CTG GAA GTA GCC ATA CT-3'
huRobo1 reverse	5'-CAT GAA ATG GTG GGC TCA GGA T-3'

Table 10: PCR program for qualitative PCR

Step	Operation	Temperature	Time	Annotation
	Lid	99 °C	-	
1	Denaturation	95 °C	30 sec	Iteration loop: step 2-5 35 cycles
2	Annealing	55 °C	30 sec	
3	Elongation	72 °C	30 sec	
		72 °C	10 min	
4		4 °C	∞	

2.2.7 Quantitative polymerase chain reaction (qRT-PCR)

For analysis of Slit2 gene expression in cell culture systems ready to use primers and probes were purchased from Applied Biosystems and 18S was utilized as housekeeping gene. Triplicates were prepared for every sample each containing 10 ng of cDNA. A master mix was prepared for a single reaction as follows: 5 µl 2x uni MM buffer, 0.3 µl of each primer (10 µM) and 0.3 µl probe (5 µM). The ready to use mix from Applied Biosystems was used according to the manufacturer's instructions. Amplification of the target gene and the housekeeping gene were measured with the 7500 Fast Real-Time PCR system (Applied Biosystems). Each experiment was repeated at least three times.

mRNA expression analysis in patient samples was done in cooperation with Jan L. Körner (Department of Hepatology and Gastroenterology, Charité-Universitätsmedizin Berlin, Campus Virchow-Klinikum), who conducted the mRNA isolation and qRT-PCR reactions, but had no part in the patho-morphologic evaluation of patients material and data analysis. Isolation of total RNA from patient tissue material was carried out with the RNeasy mini kit (Qiagen). RNA quality was validated with the Agilent's 2100 Bioanalyzer in combination with the RNA-6000-Nano Kit (Agilent). For quantification of Slit2 gene expression ready to use primers and probes were purchased from Applied Biosystems and GAPDH was utilized as housekeeping gene. Quantitative qRT-PCR was conducted in triplicates using the CFX96 thermo-cycler (BioRad). Each experiment was done in triplicates. Primer sequences are indicated below (Table 11).

Equation 1: Quantification of gene expression

Samples were analyzed using the Livak-method [247], a relative quantification method ("ΔΔCT").

a) $\Delta C_{T,Target} = C_{T,Target} - C_{T,Reference}$

b) $\Delta C_{T,Calibrator} = C_{T,Calibrator} - C_{T,Reference}$

c) $\Delta\Delta C_T = \Delta C_{T,Target} - \Delta C_{T,Calibrator}$

d) $X = 2^{-\Delta\Delta CT}$

Table 11: Primers for quantitative PCR

Name	Primer/ Probe	Dyes	Company
Slit2	Hs00191193_m1	Fam/ TAMRA	Applied Biosystems
18s fw	ACA TCC AAG GAA GGC AGC AG		Biotez
18s rev	TTT TCG TCA CTA CCT CCC CG		Biotez
18s probe	CGC GCA AAT TAC CCA CTC CCG AC	Fam/ TAMRA	Biotez
GAPDH fw	CCA CTC CTC CAC CTT TGA C		Biotez
GAPDH rev	ACC CTG TTG CTG TAG CCA		Biotez
GAPDH probe	TTG CCC TCA ACG ACC ACT TTG TC	Fam/ TAMRA	Biotez

Table 12: qRT-PCR program

PCR program for gene expression analysis in cell culture systems (7500 Fast Real-Time PCR system):

Step	Temperature	Time
1	95 °C	2 min
2	95 °C	3 sec
3	60 °C	20 sec
		40 Cycles

2.3 Protein-analytical methods

2.3.1 Preparation of cell extracts and tissue lysates

For preparation of protein extracts from cell cultures, cells were grown until a confluence of 70 % was reached.

Cells were either scraped into 100-500 µl RIPA lysis buffer (150 mM NaCl, 50 mM TRIS (pH8), 0.1 % SDS, 1 % NP-40, 0.5 % DOC, protease inhibitors were added freshly) or collected by trypsinization, washed twice in PBS and then RIPA buffer was added on ice. Cells were lysed by sonication (80 %/ 10 sec) or by shearing the lysates with a 29G syringe. The lysate was incubated on ice for 20 min and centrifuged (15 min/ 15000 rpm/ 4 °C). The supernatant was transferred to a new reaction tube and stored at -80 °C if not used immediately.

For tissue extracts (e.g. xenograft tumors), a small amount of tissue was prepared on dry ice. The frozen sample was added to a Lysing Matrix D tube (MP Biomedicals) together with 200 µl RIPA lysis buffer (2.3.1). The tissue was homogenized using Fast-Prep-24 homogenizer (20 sec/ 4 M/S). Remaining pieces of tissue were removed by pipetting up and down with a 29G syringe. The homogenate was transferred to a new reaction tube and centrifuged (15 min/ 15000 rpm/ 4 °C). The supernatant was collected and stored at -80 °C if not used immediately.

The Lowry protein assay was used according to manufacturer's protocol (DC Protein Assay Instruction Manual, BioRad) to determine total protein concentration with BSA as a protein standard.

2.3.2 Trichloroacetic Acid (TCA) Precipitation of Proteins

For precipitation of proteins from cell culture supernatants, $1x10^6$ cells were seeded in a 10 cm dish for 24 h in medium (10 % FBS/ P+S/ Glu). The media was discarded and the cells were washed twice with PBS. Fresh media without FBS was added and the cells were incubated for another 48 h. After this period, the supernatant was collected and centrifuged (5 min/ 1500 rpm/ 4 °C) to remove cell debris. The supernatant was mixed with half the volume of TCA-solution (final TCA concentration, 21 %) in a 15 ml falcon tube. The mixture was placed in an overhead rotator for uniform protein precipitation at 4 °C for 24 h. The supernatant was then centrifuged (Swinging bucket rotor/ 10 min/

4000 rpm/ 4 °C). The supernatant was discarded and the pellet washed with 1 ml acetone followed by another centrifugation step (10 min/ 5000 rpm/ 4 °C). The pellet was allowed to dry and redissolved in 50-100 µl TCA buffer (50 mM Tris pH 8.0, 100 mM DTT, 2 % SDS, 10 % glycerol).

2.3.3 Sodium Dodecyl Sulfate-Polyacrylamide Gel Electrophoresis (SDS-PAGE)

For the separation of proteins from cell lysates or tissue extracts, the discontinuous gel electrophoresis under denaturing conditions was used as first described by Laemmli [248]. According to the protein size, gels with 5-10 % Acrylamide/ Bisacrylamide were used. Protein lysates were adjusted to equal concentration of total protein and mixed with 5x SDS-PAA-loading buffer (62.5 mM TrisHCl, 20 % Glycerol, 2 % SDS, 5 % β-Mercaptoethanol, pH 6.8). Samples were heated for 5 min (100 °C), kept on ice for 10 sec. and loaded into the gel wells. For later estimates of molecular size a pre-stained protein marker was also loaded (Thermo Fisher Scientific). SDS-PAGE was performed with the Mini-PROTEAN® Tetra Cell (BioRad) according to the manufacturer's instructions. After the separation, the gel was either stained with Coomassie or further analyzed by immunoblotting.

2.3.4 Immunoblotting

For specific protein detection an immunoblot analysis was performed. The proteins separated during SDS-PAGE were therefore transferred to a nitrocellulose membrane via a wet electro-blotting system (BioRad) according to the manufacturer's protocol (Protein Blotting Guide, BioRad). Unspecific binding was blocked with blocking buffer (PBS, 5 % dry milk, 0.1 % TWEEN-20) for 30 min at RT. Immobilized proteins were detected with specific antibodies diluted in blocking buffer for 1 h 30 min at RT or overnight at 4 °C. The membrane was washed three times with washing buffer (PBS, 0.1 % TWEEN-20) and incubated with the secondary antibody conjugated to horse radish peroxidase (HRP) enzyme in blocking buffer for 30 min to 1 h at RT. Finally, the membrane was washed again and incubated with ECL solution for chemiluminescent protein detection for 3 min. Chemiluminescence signals were detected with CAWOMAT 2000 IR automatic film documentation system (CAWO Photochemisches Werk).

2.4 Cell biological methods and *in vitro* assays

2.4.1 General cell culture

General cell culture work was performed under sterile conditions under a clean bench using sterile disposable plastic ware. For cell culture only sterile, disposable consumables were used. Unsterile culture ware was sterilized before usage. Cells were cultivated in an incubator at 37 °C, 5 % CO_2 and >95 % air humidity until a confluence of about 70 % was reached. Standard culture medium contained 10 % FBS and 0.05 µg/ml penicillin-streptomycin (complete medium) unless otherwise stated. Confluent cells were washed twice with PBS and detached with trypsin. Trypsin reaction was stopped with medium containing 10 % FBS or soybean trypsin inhibitor (Invitrogen). Cells were centrifuged (5 min/ 1000-1500 rpm/ RT) and washed twice with PBS before they were reseeded in fresh culture ware. Cells in culture were replaced frequently by a stock of frozen cells and tested periodically for mycoplasma. Aliquots from early passages of newly acquired cells or transfectants were prepared for long term storage. Thereby, $1x10^6$ cells were mixed with 500 µl of cryo-conservation medium (90 % FBS, 10 % DMSO), slowly freezed in a padded envelope at minus 80 °C and transferred to a container with liquid oxygen for long-term storage.

For cell number determination, cells were stained with Trypan blue, diluted and applied to a Neubauer counting chamber. Cells in all four squares were counted and cell number was calculated.

2.4.2 Transfection of MiaPaCa and Panc1 human pancreatic cancer cells with the inducible Slit2-vector system

For inducible expression, full-length Slit2-cDNA (Hs.29802; imaGenes, Berlin, Germany) was cloned into pcDNA4/TO-3xflag-mycHIS (T-Rex™; Invitrogen, Carlsbad, CA, USA), resulting in pcDNA4/TO-SP-3xflag-Slit2-mycHis as described in 2.2.1 (Figure 3A, B). MiaPaCa and Panc1 cell clones transfected with pcDNA6/ TR had previously been established and kindly provided by Dr. Petra Schulz (please refer to 2.1.7) [100, 244].

The expression capacity after doxycycline administration was tested for each clone. The clones were therefore transiently transfected with

pcDNA4/TO-Luc (Invitrogen) using Effectene transfection reagent (Qiagen) according to the manufacturer's protocol. The transfection with pcDNA4/TO-Luc vector would normally lead to a constant expression of the firefly luciferase enzyme but if co-transfected with pcDNA6/ TR, the expression is repressed through binding of the Tet repressor to the $TetO_2$ sites in the promoter region of pcDNA4/TO-Luc. In order to induce the expression of luciferase in the cells, they were incubated for 48 h with 1 µg/ml Doxycycline (tetracycline analogue), which prevents the binding of the Tet repressor to the $TetO_2$ sites and therefore releases its breaks on the expression of the luciferase gene. Cell lysis and subsequent measurement of luciferase activity was done with a reporter assay system according to the manufacturer's protocol (Promega). Both, MiaPaCa^{TR} and Panc1^{TR} clones, showed sufficient luciferase gene expression and a concomitant low basal expression (data not shown).

Both clones were further used for stable transfection with pcDNA4/TO-SP-3xflag-Slit2-mycHis using Effectene (Qiagen, Hilden, Germany) and subsequent selection of cell clones with 500 µg/ml Zeocin. In a pilot set of experiments one MiaPaCa$^{TR\text{-}Slit2}$ clone with inducible Slit2 expression was generated with technical support from M. Welzel, to obtain proof of principle for the feasibility of the planned experiments of this thesis. In order to exclude clone specific effects, further MiaPaCa$^{TR\text{-}Slit2}$ and also Panc1$^{TR\text{-}Slit2}$ clones were generated and characterized in the course of this thesis. Slit2 expression was induced via addition of 1 µg/ml doxycycline (Figure 3C). Vehicle treated cells served as control cells in immunoblots, cell culture assays and *in vivo* experiments. MiaPaCa$^{TR\text{-}Slit2}$ and Panc1$^{TR\text{-}Slit2}$ clones, with sufficient Slit expression and a concomitant low basal expression (data not shown) were selected for experimental assays.

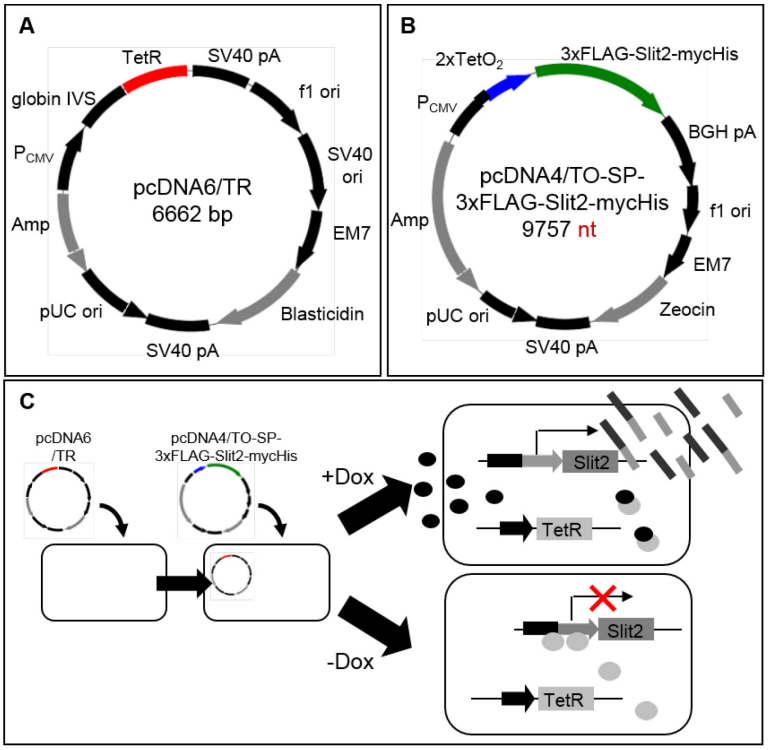

Figure 3: Tetracycline-inducible vector system for inducible expression of Slit2 in MiaPaCa and Panc1 human pancreatic cancer cells

(A, B) The inducible expression system is based on the sequential transfection of cells with the regulatory plasmid pcDNA6/TR (A) and the vector pcDNA4/TO-SP-3xFLAG-Slit2-mycHis (B), which contains the Slit2 gene. The regulatory plasmid pcDNA6/TR codes for the Tet-Repressor (TetR) that binds to the 2xTetO2 element within the promoter region of the pcDNA4/TO-mycHis vector. **(C)** After sequential transfection with both plasmids, individual clones are selected and tested for high protein expression and low basal expression. Administration of doxycycline a stable tetracycline analogue to the cell culture media causes allosteric modification within the TetR protein, preventing its binding to the promoter, and thereby initiating gene expression [249, 250]. Under doxycycline-free conditions, the TetR expressed from pcDNA6 gene binds to the promoter region in pcDNA4/TO-mycHis, thereby preventing expression of the target gene of interest.

2.4.3 Stable transfection of murine Panc02 cancer cells with Slit2-vector

Murine Panc02 cells were transfected exclusively with pcDNA4/TO-SP-3xflag-Slit2-mycHis using jetPei® (PolyPlus) according to the manufacturer's protocol. Individual clones with high constitutive expression of Slit2 were selected and expanded in medium supplemented with 400 µg/ml Zeocin. For use *in vivo*, mixed populations of 6 Mock- and Slit2-transfected clones each were generated.

2.4.4 shRNA-mediated knockdown of Robo1 in DANG cells

For assessment of Robo1 function in DANG pancreatic cancer cells, DANG cells were incubated with MISSION® lentiviral-transduction particles (Sigma-Aldrich) for shRNA-mediated Robo1 knockdown, and non-target control particles were used according to the manufacturer at a MOI of 10. Stable clones were selected in puromycin-containing medium (0.6 µg/ml) and successful knockdown was tested via immunoblot.

2.4.5 Stable transfection of HEK293 cells with soluble RoboN

HEK293 cells were stably transfected with a plasmid encoding HA-tagged RoboN provided by Jane Wu (Northwestern University, IL, USA) and as previously described [251]. HEK293 were transfected using jetPei® (PolyPlus) according to the manufacturer's protocol, and stable clones were selected and expanded in medium supplemented with 400 µg/ml Zeocin. RoboN-containing supernatant from HEK293 cells was used in *in vitro* assays to functionally inhibit Slit2. HEK293 cells were therefore seeded in complete medium and cultured for 24 h in an incubator. Afterwards, cells were washed twice with PBS and medium containing no FBS was added. Supernatant was collected after 48 h from RoboN and Mock transfected cells and separated from cell debris by centrifugation.

Table 13: Overview of stable transfectants:

Vector	Background Cells	Transfectants	Annotation
Vector (1) pcDNA6/TR	MiaPaCa Panc1	MiaPaCa^{TR} Panc1^{TR}	Inducible expression system. Expression of Slit2 is under the control of the Tet repressor. Slit2 expression is induced by administration of doxycycline. Vehicle treated cells served as controls.
Vector (2) pcDNA4/TO-SP-3xflag-Slit2-mycHis	MiaPaCa^{TR} Panc1^{TR}	MiaPaCa$^{TR\text{-}Slit2}$ Panc1$^{TR\text{-}Slit2}$	
Vector (2) pcDNA4/TO-SP-3xflag-Slit2N-mycHis	MiaPaCa^{TR} Panc1^{TR}	MiaPaCa$^{TR\text{-}Slit2N}$ Panc1$^{TR\text{-}Slit2N}$	Inducible expression system. Expression of Slit2N is under the control of the Tet repressor. Slit2 expression is induced by administration of doxycycline. Vehicle treated cells served as controls.
pcDNA4/TO-SP-3xflag-Slit2-mycHis	MiaPaCa	MiaPaCa^{Slit2}	Stable expression of Slit2. Mock transfected cells served as controls
pcDNA4/TO-SP-3xflag-Slit2-mycHis	Panc1	Panc1^{Slit2}	Stable expression of Slit2. Mock transfected cells served as controls
pcDNA4/TO-SP-3xflag-Slit2-mycHis	Panc02	Panc02^{Slit2}	Stable expression of Slit2. Mock transfected cells served as controls
pSecTag-RoboN	HEK293	HEK293^{RoboN}	Kindly provided by J. Y. Wu (Northwestern University, IL, USA) [251]. Overexpression of HA-tagged RoboN (extracellular domain of rat Robo1, aa 1-718). Cells were used to generate RoboN-enriched supernatant
pSecTag	HEK293	HEK293^{MockN}	Kindly provided by J. Y. Wu. Mock-control cells for HEK293^{RoboN}
MISSION® lentiviral-transduction (Robo1 Transduction Particles)	DANG	DANG$^{Robo1\text{-}KD}$	shRNA-mediated Robo1 knockdown.

Vector	Background Cells	Transfectants	Annotation
MISSION® lentiviral-transduction (Control Transduction Particles)	DANG	$DANG^{Scr}$	Control cells for $DANG^{Robo1\text{-}KD}$

2.4.6 Proliferation assay

For *in vitro* proliferation assay $1x10^3$ - $2x10^4$ cells (depending on the cell line) were plated in 24-well-dishes and cultured for 24, 48, 72 and 96 h (doxycycline-pretreated, if applicable). Cell numbers were counted at each time point with a Neubauer counting chamber as described in 2.4.1. Each experiment was done in triplicates and repeated three times.

2.4.7 Wound healing assay

IBIDI silicone cell culture inserts were used for wound healing assay and applied as advised by the manufacturer. The culture inserts were placed in a 35 mm well of a 6-well plate, and $3.5x10^4$ cells were added per chamber. Cells were incubated for 24 h in DMEM (10 % FBS) with or without 1 µg/ml doxycycline to induce Slit2 expression. Cells were washed twice with PBS and serum starved for 5 h. Media was changed to DMEM (1 % FBS) and gap closure was monitored for 20 h via time-lapse microscopy. Videos were analyzed using open source TScratch software® (ETH Zurich, Switzerland) as described [252].

2.4.8 Random migration assay

For random migration assays $2x10^4$ cells were seeded per well in a 12-well plate and incubated with or without 1 µg/ml doxycycline for 24 h. Cells were then serum-starved for another 4 h. Subsequently media was changed to DMEM (1 % FBS; 0.1 % BSA) and random migration was monitored via time-lapse microscopy. Cell tracks were analyzed with WimTaxis® software (WIMASIS GmbH; Munich, Germany).

2.4.9 Migration and invasion assays

For migration assays, $2x10^5$ cells/insert (doxycycline-pretreated, if applicable) were placed in serum-free medium in the upper chamber of 8 µm-Transwells (Corning) and allowed to migrate for 8-12 h towards 1 % FBS (2 % FBS for HUVEC) added to the lower chamber. Migrated cells were stained with crystal-violet or DAPI and quantified by counting 5 standardized fields at 100x magnification as described [98, 253].

Tumor cell migration towards gradients from Schwann cells, cultured in the lower chamber for 16 h in DMEM (0.1 % BSA), and vice versa, was determined. Therefore, $1x10^5$ cells were seeded per well in a 24-well plate containing growth media. Media was changed to DMEM (0.1 % FBS) and incubated for another 24 h (administration of doxycycline, if applicable). Migration assay was done as described above.

For HUVEC cell migration towards gradients from $MiaPaCa^{TR\text{-}Slit2}$ and $MiaPaCa^{TR\text{-}Slit2N}$, cultured in the lower chamber, $8x10^4$ cells of the respective MiaPaCa clone were seeded in growth medium. Slit2 expression was induced with doxycycline. Vehicle treated cells served as controls. Media was changed to DMEM (0.1 % FBS) and cells were cultivated for another 24 h. For HUVEC migration $2x10^5$ cells were applied to transwell inserts coated with 3 % collagen and allowed to migrate towards gradients released from the tumor cells in the lower chamber for 20 h.

2.4.10 Lamellipodia formation of endothelial cells

Serum-starved HUVEC were stimulated with 50 ng/ml VEGF on collagen-coated cover-slides in Slit2- or Vehicle-conditioned medium. After 1 h cells were fixed with 70 % ethanol and stained with α-cortactin, phalloidin-TRITC and DAPI. Quantification of lamellipodia was done using AxioVision® (Zeiss) and ImageJ® software (NIH; Bethesda, USA).

2.4.11 Dorsal root ganglion (DRG)-tumor cell co-culture assay

4-5 weeks old C57Bl6 mice (Charles River) were used for the isolation of DRGs. The spine was totally dissected from the mouse body and freed from surrounding tissue as best as possible (Figure 19). The spine was divided in half with a scalpel and the spinal cord was removed to expose the cavities containing the DRGs. The overlaying dorsal layer was removed with forceps under a stereomicroscope. The DRGs were carefully isolated with forceps and placed in a 6-well culture dish containing PBS (10 % FBS/ 0.05 µg/ml Pen-Strep) on ice. Subsequent remaining roots (dorsal root, ventral root, posterior root), were carefully removed from ganglia. Such prepared ganglia were transferred to DMEM (10 % FBS/ 0.05 µg/ml Pen-Strep) and incubated overnight.

For DRG-tumor cell co-cultures, the DRGs were placed in 12-well culture plates in a growth-factor-reduced Matrigel drop (20 µl). Tumor cells ($4x10^4$) were placed in a separate Matrigel drop at 1 mm distance from the DRG. Both Matrigel drops harboring DRG or tumor cells were connected with a Matrigel bridge, allowing outgrowth and elongation of neurites, and tumor cell migration along contacted neurites. An empty Matrigel drop at the opposite site served as control for random tumor cell migration. Co-cultures were incubated in DMEM (10 % FBS) with doxycycline or vehicle. Medium was replaced by medium containing 1 % FBS as soon as neurite outgrowth occurred. Tile-scan images were taken every day of co-culture. For assessment of neural invasion, the area covered by tumor cells was quantified using AxioVision Rel. 4.8 Software (Zeiss Microscopy GmbH, Jena, Germany). The dynamic process by which cancer cells migrated along neurites was evaluated using time-lapse imaging (Leica DMI6000-B) in a chamber with closed environment at 37 °C and 5 % CO2. Images were taken on days 9-15 every 30 min for up to 20 h to follow cell locomotion. Using automated acquisition software (Leica LAS AF6000), up to 20 individual tumor cells were simultaneously imaged in each experiment. Travel distances, velocity and directness were calculated using ImageJ®, Manual Tracking plug-in, and IBIDI chemotaxis software.

2.5 Xenograft tumor models

2.5.1 Orthotopic mouse models of PDAC

All animal experiments were approved by local authorities and guidelines for proper conduct of animal experiments were followed. The laboratory animals were housed in the animal facility at the Max Delbrück Center MDC under standardized, nearly sterile conditions.

2.5.2 Laboratory animals

For the orthotopic xenograft tumor model 6-8 weeks old female SCID beige mice (20-24 g) were obtained from Charles River Laboratories (Sulzfeld, Germany). The Fox Chase SCID beige mice are deficient for T- and B-cells and bear an impaired natural killer (NK) cell development. This immunodeficiency allows the engraftment of human pancreatic cancer cells. For the subcutaneous xenograft tumor model 8 week old NMRI nu/nu (athymic) mice were obtained from Taconic (Hudson, NY, USA). The athymic BomTac:NMRI-Foxn1^{nu} mice have only few T-cells resulting in a reduced reaction to T-cell dependent antigens and a compensatory increase in NK cells. For the syngeneic tumor model with murine Panc02 pancreatic cancer cells, 8 week old C57BL/6 mice were obtained from Charles River Laboratories (Sulzfeld, Germany).

2.5.3 Orthotopic pancreatic xenograft mouse model

For *in vivo* experiments the earliest available passages of MiaPaCa$^{TR\text{-}Slit2}$ or DANG$^{Robo1\text{-}KD/Scr}$ cells were expanded for application *in vivo*. At the day of the experiment cell density reached a confluence of 70 %. Cells were washed twice with PBS and detached with trypsin. Cell detachment was observed with a cell culture microscope. The trypsin reaction was stopped with complete medium (DMEM/ 10 % FBS/ Pen-Strep) and centrifuged (5 min/ 1500 rpm/ RT). Subsequent cells were washed twice with PBS to remove residual FBS and cell concentration was determined. 10^6 MiaPaCa$^{TR\text{-}Slit2}$ cells or DANG$^{Robo1\text{-}KD/scr}$ in 500 µl PBS were aliquoted per 1.5 ml reaction tube and centrifuged again (5 min/ 1100 rpm/ RT). The cell aliquots were left on ice until usage. The surgical intervention was carried out under

a laminar airflow cabinet and only sterile materials were used. For implantation, mice were anesthetized with a mixture of 100 µg/g ketamine and 10 µg/g Xylazine. The anesthetized mice were fixed on the back and the hair on the abdomen was removed with a razor. The skin at the surgical site was disinfected and a 1 cm incision was made to open the abdomen. The stomach was carefully placed extraperitoneal to expose the pancreas. For cell injection supernatant were discarded, the cell pellet resuspended in 20 µl PBS and injected into the pancreatic head with a fine needle (29G) [98, 100]. Successful implantation was easily monitored by the formation of a small bubble in the pancreas. After 7 (MiaPaCa$^{TR\text{-}Slit2}$) or 3 (DANG$^{Robo1\text{-}KD/Scr}$) weeks, mice were sacrificed, primary tumors harvested, and enlarged lymph nodes as well as livers collected for histology [30, 31]. The mesentery was excised and metastatic nodules were counted as described [98]. All excised tissues were cryo-preserved in liquid nitrogen and stored at -80 °C until usage.

For syngeneic tumors, 2x10^5 Panc02^{Slit2} or Panc02^{Mock} cells, respectively, were injected into the head of the pancreas of 8 week old female C57/Bl-6 mice. The procedure for preparation and implantation of the tumor cells were the same as for the xenograft model. Mice were sacrificed on day 13 and primary tumors as well as metastatic spread in the abdominal cavity were evaluated. For quantitative assessment of mesenteric metastasis, metastatic nodules were counted. Additionally, the mesentery was carefully excised and mesenteric weight was determined, based on the observation that mesenteric weight correlates with mesenteric metastasis in this model. Incidence of ascites was recorded.

2.5.4 Subcutaneous DANG tumor model

Female NMRI$^{nu/nu}$ mice (20-24 g) were from Charles River Laboratories (Sulzfeld, Germany). 8x10^6 DANG$^{Robo1\text{-}KD}$ and respective scrambled control DANG cells were mixed with 150 µl growth-factor-reduced Matrigel® (BD Pharmingen) and injected subcutaneously into the dorsal flank of mice. For sequestration of endogenous Slit2 released by DANG cells, Robo1-Fc (45 µg/ml) or vehicle was added to the tumor cell-Matrigel mixture prior to implantation. Mice were sacrificed after 10 days and primary tumors harvested.

2.6 Immunohistochemical analysis

2.6.1 Preparation of cryosections

Cryopreserved material was embedded in Tissue TEK O.C.T Compound to provide a matrix for orientation and stabilization. From the embedded tissue 5 to 10 µm frozen sections were prepared with a cryo-microtome and sequential sections were mounted on a microscope slide. The slides were stored at -80 °C.

2.6.2 Immunohistochemical staining of frozen sections

Cryo-sections were fixed in PFA (4 % in PBS) and washed three times for 5 min followed by a blocking step with H_2O_2 (0.3 % in PBS) for 10 min to reduce background staining resulting from endogenous peroxidases. Cells were permeabilized with Triton X (0.1 % in PBS) for 30 min followed by another washing step with PBS. The tissue sections were then incubated with the primary antibody (in 0.3 % Triton X/ PBS) and washed again before the biotinylated secondary antibody was applied (for further information on the antibodies please refer to chapter 2.1.5). Immunoperoxidase-staining was performed using Vectastain-Elite-ABC kit and AEC as substrate chromogen (Vector Laboratories, Wertheim-Bettingen, Germany) according to the manufacturer's protocol. Nuclei were counterstained with hematoxylin and eosin (HE) staining solution. Thereafter, the sections were mounted with Kaiser's glycerol gelatine and carefully sealed with a cover slip.

2.6.3 Vessel density

In order to quantify differences in tumor angiogenesis from xenograft tumors, the average number of CD31-positive vessels was determined from three regions of maximal vascular density at 200x magnification as described [254].

2.7 Patient samples

Pancreatic cancer specimens

Tissue samples were from PDAC patients undergoing surgery at Charité-Universitätsmedizin from 1996-2013. Patients gave written informed consent. Data on TNM classification and tumor infiltration of lymph nodes were retrieved from pathology reports.

Table 14: Patients baseline characteristics

Parameters	PDAC
Sex (female/male)	9/19
Age, median (range)	64 (41-82)
TNM-stage:	
Stage I	0
Stage II (A/B)	3
Stage III (A/B)	21
Stage IV	4
Grading	
G1	1
G2	19
G3	8

2.8 Statistical analysis

Data are presented as Means±SEM, unless indicated otherwise. Statistical significance was determined by t-test/Anova and Fisher's exact test using GraphPad® Prism (San-Diego, CA). (*) $P<0.05$ values were considered significant. ROC (Receiver Operating Characteristic) curves were calculated using GraphPad® Prism (San-Diego, CA).

3. Results

3.1 Expression analysis of Slit2 and its receptors Robo1 and Robo4

Expression of Slits and their Robo receptors is tightly controlled in many physiological processes during embryogenesis and adulthood. Changes in the expression of Slit and Robo occur in a variety of diseases including cancer. Available data however suggest that alterations of Slit2 and Robo expression in cancer occur in a tumor-type dependent manner with Slit2 expression being increased in some tumors and reduced or lost in other tumor entities. To date, Slit2 and Robo expression in PDAC has not yet been delineated.

3.1.1 Differential expression of the Slit receptors Robo1 and Robo4 in human PDAC

In order to determine the relevance of the Slit2-Robo system in PDAC, we first assessed the expression of the ligand, Slit2, and its Robo receptors in a panel of human clinical specimens of PDAC and respective healthy control tissues obtained from patients who underwent surgery due to ductal adenocarcinoma of the pancreas.

Utilizing immunohistochemistry, we localized the expression of the Slit2 receptor Robo1 in ductal epithelial cells of healthy pancreas and pancreatic cancer tissues (Figure 4A, B). By comparison, we found that Robo4 was almost exclusively expressed in the pancreatic vasculature and tumor vessels, which is in accordance with previous reports of Robo4 expression primarily by endothelial cells (Figure 4D, E) [198, 200]. In addition, a more detailed immunohistochemical analysis of serial cryo-sections stained with antibodies against Robo1, Robo4 and the neuronal marker S100, revealed expression of Robo1, but not Robo4 in pancreatic nerves (Figure 4C-H). Hence, we identified functionally distinct compartments within the pancreas and PDAC that express Robo receptors and thus have the capacity to respond to secreted Slit2 ligands.

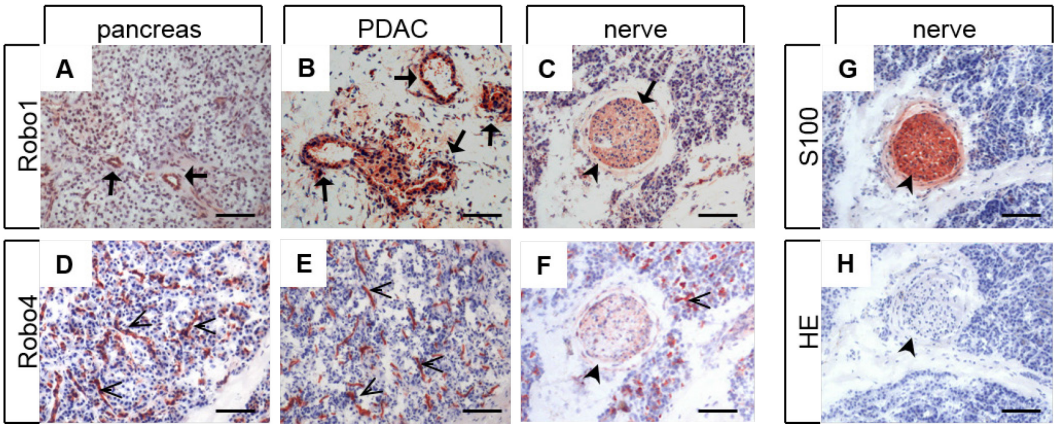

Figure 4: Differential expression of Robo1 and Robo4 in the tumor cell, vascular and neuronal compartments of human PDAC

(A-F) Representative Immunohistochemical staining for the Slit2 receptors Robo1 (A, B, and C) and Robo4 (D, E, and F) on cryosections of clinical specimens from non-transformed pancreatic tissue (A, D) and PDAC (B, E), and intrapancreatic nerves (C, F). **(G-H)** Immunohistochemical staining for the neural marker S100 (G) and HE-counterstaining (H). Arrows depict Robo1 staining in duct epithelial cells and intrapancreatic nerves, arrowheads indicate Robo4 expression in the vasculature, and filled arrowheads point to pancreatic nerves. Bar graph is 100 μm.[I]

3.1.2 Expression of Slit2 is reduced in pancreatic cancer and inversely correlates with enhanced lymphatic metastasis

In an analogous approach, we tried to establish the immunohistochemical detection of Slit2, both on cryosections as well as formalin fixed and paraffin-embedded tissue (the latter in collaboration with Dr. Ruza Arsenic, Department of Pathology, Charité; please refer to supplementary information in 7.1 and Suppl. Figure 1-3). However, although several commercially available antibodies against Slit2 were tested, none of these antibodies revealed convincing patterns of immunoreactivity, when evaluated in parallel on either monolayers or formalin-fixed and paraffin-embedded pellets of cells deficient of or competent for Slit2 expression.

As we could not satisfactorily validate the immunohistochemical approach, we quantitatively determined the expression of Slit2 mRNA by qRT-PCR. A prospective collection of patient samples with confirmed PDAC and non-transformed pancreatic tissues (n=28 PDAC

[I] Histological stainings in figure 4 were partly provided by M. Schröder

and n=29 non-transformed pancreas) was available for mRNA preparation.

Quantitative RT-PCR analysis revealed substantial mRNA expression of Slit2 in tissues of healthy pancreas (Figure 5A), which is in line with published expression profiling data that indicated Slit2 mRNA expression in ductal epithelial cells of the pancreas [255, 256]. In contrast, Slit2 mRNA expression was found distinctly reduced in PDAC tissues (Figure 5A). Furthermore, we conducted a subgroup analysis of matched tumor pairs and non-transformed pancreatic tissue from the same patient (n=8 matched-pairs). Again Slit2 mRNA expression in the tumor was found significantly reduced compared to the exact corresponding non-transformed tissue (Figure 5B).

The determination of Slit2 mRNA expression in healthy and malignant tissues now enabled the compilation of ROC curves in order to define a cut-off value for pathologic Slit2 mRNA levels based on the maximum likelihood ratio (Figure 5C). Notably, in patients allocated to the group with pathological Slit2 expression, Slit2 mRNA expression correlated with lymph node metastasis. Thus, patients with Slit2 levels <median (low Slit2, n=9) had a higher incidence of lymph node metastasis (stage N1; Figure 5D), and furthermore exhibited a higher fraction of tumor-infiltrated lymph nodes as compared to patients with Slit2 levels >median (high Slit2, n=9; Figure 5E). Conversely, patients with lymph node metastasis (N1 tumors) exhibited lower overall Slit2 mRNA levels as compared to patients without lymph node metastasis (N0 tumors), (Figure 5F).

Taken together our expression analyses indicated the presence of the Slit2-Robo signaling pathway in healthy pancreas, whereas Slit2 expression was reduced in PDAC. Reduced Slit2 mRNA expression furthermore correlated with both a higher incidence and higher extent of lymph node metastasis, suggesting that loss of Slit2 in PDAC may be associated with an increased ability of tumor cells to metastasize.

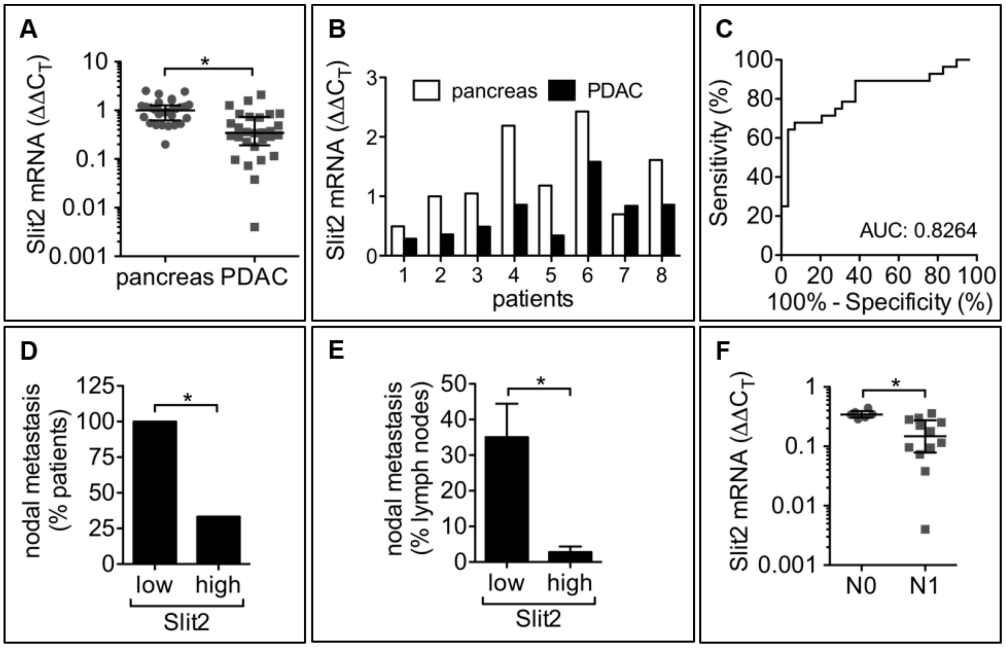

Figure 5: Slit2 mRNA expression is reduced in human PDAC and inversely correlates with increased metastasis

(A) Slit2 mRNA expression in PDAC (n=28) and non-transformed pancreas (n=29) was determined using qRT-PCR and normalized to GAPDH. Shown is the scatter dot plot with median and interquartile range ($p<0.0001$, Mann Whitney test). **(B)** Slit2 mRNA expression in human paired tumor and non-neoplastic tissues from the same patients was determined using qRT-PCR and normalized based on GAPDH as internal control ($p=0.0156$; Wilcoxon matched-pairs signed rank test). **(C)** ROC-analysis for determination of a cut-off level, which best discriminates PDAC from non-transformed pancreas (cut-off < 0.458; likelihood ratio: 18.64). Further analysis was restricted to tumors exhibiting pathologic Slit2-mRNA levels (n=18). **(D, E)** Incidence of nodal metastasis (D; $p=0.009$; Fisher's exact test) and percentage of tumor-infiltrated lymph nodes (E; $p=0.005$; Mann Whitney test) in patients with low (< median, n=9) or high (> median, n=9) tumoral Slit2-mRNA levels. **(F)** Tumoral Slit2-mRNA levels in patients without (N0) and with nodal metastasis (N1); ($p=0.0043$, Mann Whitney test). Shown is the scatter dot plot with Median and the interquartile range.

3.1.3 Expression analysis of the Slit2 and Robo receptor-ligand system in human pancreatic cancer cell lines

In order to experimentally address the functional role of Slit2-Robo in PDAC, we then aimed to identify appropriate cell systems. We therefore determined the expression of Slit2 and Robo1 in a panel of well characterized human PDAC cell lines [257] using qRT-PCR and immunoblotting.

Consistent with the observed strong Robo1 immunoreactivity in ductal epithelial cells of PDAC specimens, immunoblotting indicated the presence of Robo1 in all PDAC cell lines examined, except for ASPC1 cells (Figure 6A). In contrast, Slit2 mRNA expression was variable. High levels of Slit2 mRNA, comparable to those in non-transformed pancreatic tissue, were observed in the immortalized pancreatic epithelial cell line HPDE and the well-differentiated cell line DANG (Figure 6B). In contrast, Slit2 expression was either substantially reduced in Capan-1 and Capan-2 cells, or entirely lost in the poorly-differentiated MiaPaCa and Panc1 cell lines [257] (Figure 6B), which is in line with the observed reduction of Slit2 in human PDAC samples.

Reduction of Slit2 has been attributed to epigenetic silencing due to promoter hypermethylation in some cancer types, such as prostate, breast and lung cancer [231]. We consequently analyzed whether such epigenetic alterations may underlie the loss of Slit2 expression in the respective pancreatic cancer cell lines. We therefore treated Slit2-deficient Panc1 and MiaPaCa cells with the azacitidine derivate decitabine (5-AZA-2'deoxycytidine or 5-AZA-dC), which constitutes a demethylating agent widely used for epigenetic studies [Reviewed in 258, 259]. Indeed, 5-AZA-dC treatment restored Slit2 expression in Panc1 cells (Figure 6C), identifying epigenetic modifications as one potential cause of aberrant Slit2-Robo signaling in PDAC cell lines. In contrast, treatment of MiaPaCa with 5-AZA-dC had no effect on the expression of Slit2 (Figure 6C), indicating that different mechanisms of Slit2 gene inactivation are present in PDAC cell lines.

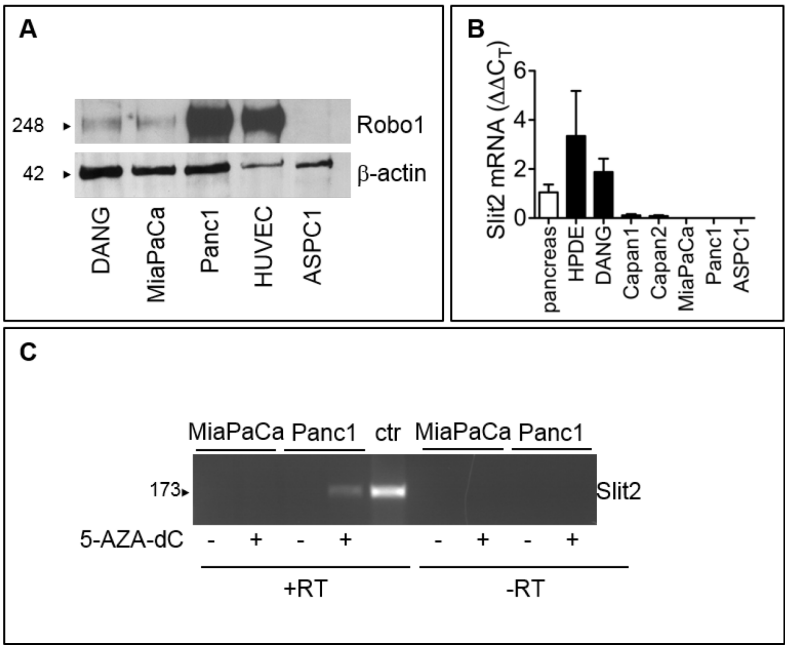

Figure 6: Expression analysis of Slit2 and Robo1 in PDAC cell lines and specimens

(A) Protein expression analysis of Robo1 in lysates of PDAC cell lines and HUVEC using immunoblotting[II]. Sizes of expected bands are given in kDa. **(B)** Relative quantification of Slit2 mRNA expression levels in a panel of human PDAC cell lines and healthy pancreatic tissue using quantitative RT-PCR. Normalization was based on 18S RNA as endogenous control. **(C)** Panc1 cells were incubated with 10 μM 5-AZA-dC for 72 h, and subsequently Slit2 mRNA expression determined using qualitative PCR. Reactivation of Slit2 expression in Panc1 cells by 5-AZA-dC suggests silencing of Slit2 gene due to promoter hypermethylation. As control (ctr), cDNA from Slit2 expressing DANG cells was used. Marker is a 100 bp ladder. Size of the expected PCR gene-product is given in bp.

3.2 Functional characterization of Slit2-mediated auto-/paracrine effects on PDAC cells *in Vitro*

In order to investigate the biological function of the Slit2-Robo system in PDAC, we used different methodological approaches. We first aimed at ectopic re-expression of Slit2 in cell lines, which lack endogenous Slit2. Since Slit2 is secreted by tumor cells, this approach would allow to determine autocrine and/or paracrine effects of Slit2 on the tumor cells themselves and other cell types present in the PDAC stromal compartment, such as endothelial and neuronal cells. Conversely, we

[II] Robo1 immunoblot in figure 6A was kindly provided by M. Welzel

also decided to investigate the effects of functional inactivation of Slit2-Robo signaling by lentiviral-mediated knockdown of endogenous Robo1 in Slit2 competent PDAC cells.

3.2.1 Generation of PDAC cell lines with inducible Slit2 re-expression

MiaPaCa and Panc1 cells, both lack endogenous Slit2, and hence represented cell models suitable to experimentally address the consequences of a Slit2 gain-of-function approach. Accordingly, we generated cell clones with inducible Slit2 expression using the tetracycline-inducible TRex^{TM} vector system, which allows for the regulated induction of Slit2 upon treatment of cells with the tetracycline analogue doxycycline (for detailed information, please refer to 2.2.1 and 2.4.2) [249, 250, 260].

Human full-length Slit2, comprising the nucleotides 1-1469, was subcloned into the pcDNA4/TO vector (for detailed information, please refer to 2.2.1). For convenient detection of full-length Slit2 protein as well as cleavage fragments, an N-terminal 3xFlag-tag and a C-terminal myc-HIS tag have been added, resulting in the generation of the pcDNA4/TO-SP-3xFLAG-Slit2-mycHis plasmid. MiaPaCa and Panc1 cell clones with stable insertion of the regulatory plasmid pcDNA6/TR have previously been generated and characterized in our lab [244], and were available for sequential transfection with the pcDNA4/TO-SP-3xFLAG-Slit2-mycHis plasmid.

From out of 6 and 8 double-transfected MiaPaCa$^{TR\text{-}Slit2}$ and Panc1$^{TR\text{-}Slit2}$ clones, respectively, those were selected, which featured lowest basal expression and strongest inducibility of the Slit2 protein as assessed by immunoblotting. These clones are from here on referred to as MiaPaCa$^{TR\text{-}Slit2}$ and Panc1$^{TR\text{-}Slit2}$ (for detailed information, please refer to 2.4.2). Following stimulation with doxycycline, successful induction and secretion of myc- and Flag-tagged Slit2 in lysates and culture supernatants from double-transfected MiaPaCa$^{TR\text{-}Slit2}$ and Panc1$^{TR\text{-}Slit2}$ cells was confirmed using immunoblotting (Figure 7A, B). We also explored the dose-dependence of Slit2-induction and secretion as assessed by immunoblotting of TCA precipitates of cell culture supernatant. Slit2 induction was accomplished by treatment of cells with increasing doses of doxycycline from 0.001 to 1 mg/ml for 48 h. A dose of 0.001 mg/ml doxycycline resulted in maximal induction of Slit2 expression, and was hence selected for further *in vitro* cell studies.

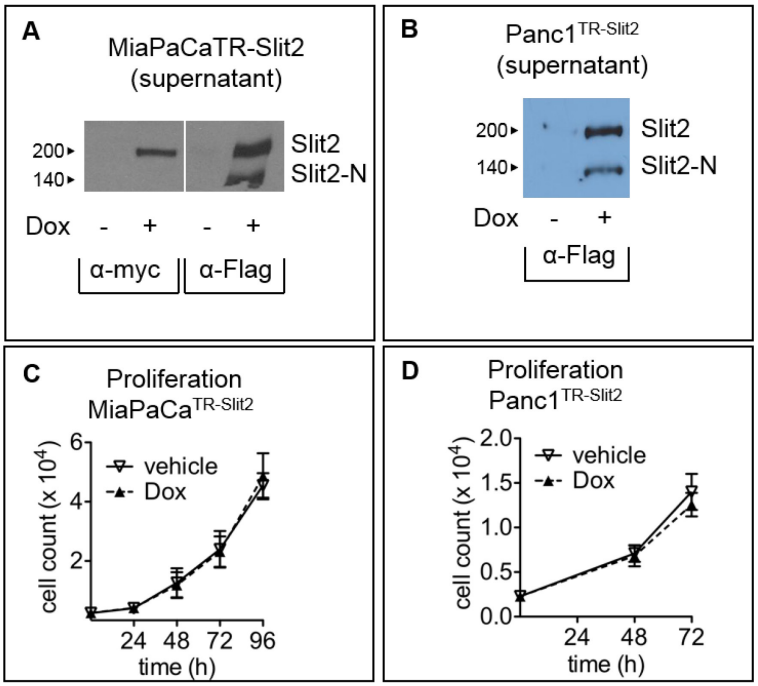

Figure 7: Inducible re-expression of Slit2 in MiaPaCa$^{TR\text{-}Slit2}$ and Panc1$^{TR\text{-}Slit2}$ cells does not affect tumor cell proliferation

(A, B) Using the doxycycline-inducible T-Rex^{TM} vector system, MiaPaCa$^{TR\text{-}Slit2}$ and Panc1$^{TR\text{-}Slit2}$ cells with inducible expression of full-length human Slit2 were generated by transfection with a Slit2-cDNA construct that comprises the nucleotides 1-1469. For detection of Slit2, an N-terminal Flag-tag and a C-terminal myc-HIS-tag flank the Slit2-cDNA. Inducible expression and secretion of the myc- and Flag-tagged Slit2 protein was confirmed using immunoblotting of TCA-precipitates from MiaPaCa$^{TR\text{-}Slit2}$ and Panc1$^{TR\text{-}Slit2}$ cell culture supernatants following treatment with doxycycline (Dox: 1 µg/ml for 48 h) as compared to vehicle treated controls. Proteolytic cleavage of full-length Slit2 (200 kDa) resulted in the generation of the N-terminal Slit2 fragment (Slit2N, 140 kDa). **(C, D)** MiaPaCa$^{TR\text{-}Slit2}$ and Panc1$^{TR\text{-}Slit2}$ cells with inducible Slit2 expression were pretreated with 1 µg/ml doxycycline or vehicle for 48 h, and cell numbers were counted after 24, 48, 72 and 96 hours at indicated time points. Experiments were conducted three times, each in duplicates (MiaPaCa$^{TR\text{-}Slit2}$: n=3, p=0.89; Panc1$^{TR\text{-}Slit2}$: n=4, p=0.55; both Anova).

Notably, MiaPaCa$^{TR\text{-}Slit2}$ and Panc1$^{TR\text{-}Slit2}$ PDAC cell clones not only expressed and secreted Slit2 (200 kDa) but also proteolytically cleaved the full-length protein resulting in a 140 kDa fragment recognized by the anti-Flag antibody in the conditioned media (Figure 7A, B). The molecular weight of the cleavage product is consistent with the N-terminal fragment of Slit2 (Slit2N; AA1110-1118; Suppl. Figure 4A, B), which binds to Robo receptors and mediates a variety of biological functions [162].

3.2.2 Slit2 re-expression does not affect proliferation or random motility of PDAC cells

MiaPaCa and Panc1 cells express the receptor Robo1 (Figure 6A), and may therefore be subjected to auto-/paracrine Slit2 stimulation. Therefore, we determined the consequences of Slit2 induction for cell anchorage-dependent growth and motility of these cells *in vitro*. First, we tested whether induction of Slit2 affected proliferation of MiaPaCa and Panc1 cells. When MiaPaCa$^{TR\text{-}Slit2}$ and Panc1$^{TR\text{-}Slit2}$ cells were pretreated with doxycycline for 48 h to induce Slit2 expression and subsequently cultured over 96 hours, Slit2 did not affect proliferation of these cells (Figure 7C, D).

Next, we determined the consequences of Slit2 gain-of-function on tumor cell properties that are required for metastasis, such as the ability to disengage, to migrate and to invade. First experiments studied random tumor cell migration using time-lapse microscopy, which enabled us to monitor specific parameters of cell movement, such as velocity as well as travelled Euclidean and accumulated distances (Figure 8A-E). Notably, Slit2 did not change any of these parameters when tumor cells were seeded on culture-dishes and allowed to randomly migrate in the presence of 1 % FBS. Similarly, re-expression of Slit2 had no effect on the gap closure of MiaPaCa$^{TR\text{-}Slit2}$ cells in a model assay of wound healing (Figure 8F-J). Taken together, restored expression of Slit2 in tumor cells did not alter tumor cell proliferation or random migration under the experimental conditions studied.

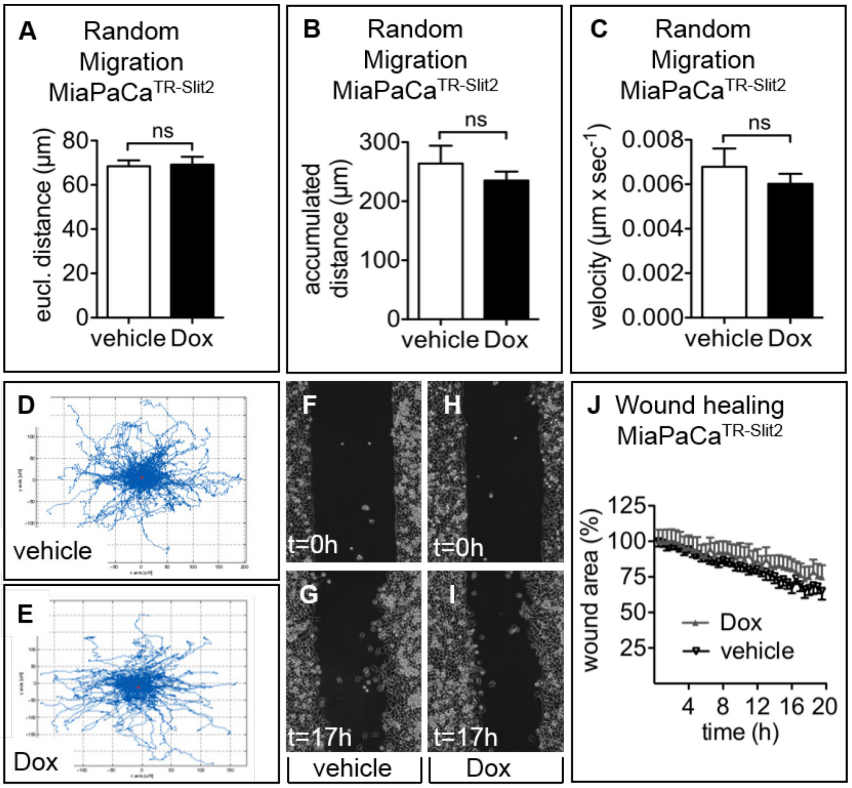

Figure 8: Re-expression of Slit2 does not affect random migration of MiaPaCa cells

(A-C) MiaPaCa$^{TR\text{-}Slit2}$ cells were seeded on culture plates, and random migration assessed using time-lapse microscopy over 12 h. Induction of Slit2 expression did not affect Euclidean distance (A), accumulated distance (B) and velocity (C) in random migration assays as quantified using WimTaxis® software (n=3, p=0.87, p=0.42 and p=0.44, respectively). **(D, E)** Representative plot data images show summary of individual tumor cell trajectories in random migration assays of MiaPaCa$^{TR\text{-}Slit2}$ cells with Slit2 induction as compared to vehicle control cells. **(F-J)** Confluent MiaPaCa$^{TR\text{-}Slit2}$ cell layers were subjected to wound healing assays. Reduction of the open wound area was evaluated using time-lapse microscopy over a period of 20 h in vehicle and doxycycline-treated cell cultures. Experiments were conducted three times, each in duplicates. Data are presented as percent of open wound area at t=0 h and represent means ±SEM (n=3, p=0.37; Anova).

3.2.3 Slit2 re-expression inhibits directed migration and invasion of PDAC cells

In addition to random migration, tumor cells exhibit directed movement towards chemoattractive gradients. Therefore, we examined the effects of Slit2 on directed migration of MiaPaCa$^{TR\text{-}Slit2}$ and Panc1$^{TR\text{-}Slit2}$ tumor cells towards a chemogradient of 1 % FBS *in vitro* using transwell assays. Indeed, doxycycline-dependent induction of Slit2 inhibited directed migration of MiaPaCa$^{TR\text{-}Slit2}$ and Panc1$^{TR\text{-}Slit2}$ by 49 % and 38 %, respectively, compared to the vehicle-treated controls (Figure 9A, B). Importantly, MiaPaCa^{TR} cells, which only received the regulatory pcDNA6-TR plasmid showed no differences in the migratory behavior upon doxycycline treatment (Figure 9C), thus excluding off-target effects of doxycycline in these assays.

We also generated MiaPaCa^{Slit2} and Panc1^{Slit2} clones with stable overexpression of Slit2. Again the presence of Slit2 inhibited the migration of MiaPaCa^{Slit2} and Panc1^{Slit2} cells by 72 % and 52 %, respectively (not shown), indicating that the observed Slit2 effects did not depend on the mode of ectopic Slit2 expression.

To test whether the observed reduction of migration was indeed due to ectopically expressed and secreted Slit2, we aimed to functionally neutralize the secreted Slit2 ligand by addition of RoboN. RoboN comprises the N-terminal extracellular domains of Robo1 and serves as a soluble-decoy receptor competing with membrane-bound Robo1 for the binding to Slit2. Supernatants from stably transfected HEK cell clones were used as a source for RoboN. Supernatants from RoboN-expressing HEK cells, but not from Mock-transfected control cells almost abrogated the inhibition of directed migration by Slit2 in MiaPaCa$^{TR\text{-}Slit2}$ cells (Figure 9D).

In order to confirm these findings we also utilized commercially available purified human Slit2N (huSlit2N; corresponding to the N-terminal cleavage product of full-length Slit2) and a soluble Fc-coupled Robo1 receptor fragment (Robo1-Fc). The latter sequesters and thereby antagonizes Slit2. Addition of purified huSlit2N reduced the directed migration of wildtype MiaPaCa cells by 59 %, an effect that was prevented by co-incubation with Robo1-Fc (Figure 9G, H). Similarly, huSlit2N reduced the directed migration of Panc1 cells by 36 %. Thus these additional tools confirmed the observations in our PDAC cell variants with Slit2 overexpression.

We also tested the ability of Slit2-conditioned media from MiaPaCa$^{TR\text{-}Slit2}$ clones to regulate the directed migration of cell lines competent or deficient for Robo1. Addition of Slit2-conditioned media into the lower chamber of the transwells reduced the migration of

wildtype (Robo1-competent) MiaPaCa cells by 50 %, but had no effect on Robo1-deficient ASPC1 cells (Figure 9E, F).

These results on directed tumor cell migration suggest a Robo1-mediated effect of Slit2, but cannot exclude that another secondary Slit2 regulated factor is involved. To clarify this aspect, we used supernatants from MiaPaCa cells with stable Slit2 overexpression (MiaPaCa^{Slit2}), which should contain both Slit2 and such a putative secondary factor. Sequestration of Slit2 by Robo1-Fc in these supernatants would block Slit2 effects without affecting the function of this putative indirect factor. Indeed, addition of Robo1-Fc to the conditioned media from MiaPaCa^{Slit2} cells counteracted their capacity to inhibit the directed migration of MiaPaCa cells in transwell assays (Figure 9I). Experiments with supernatants from MiaPaCa^{Mock} served as controls. These results indicate that Slit2 rather than a secondary mediator suppressed MiaPaCa cell migration.

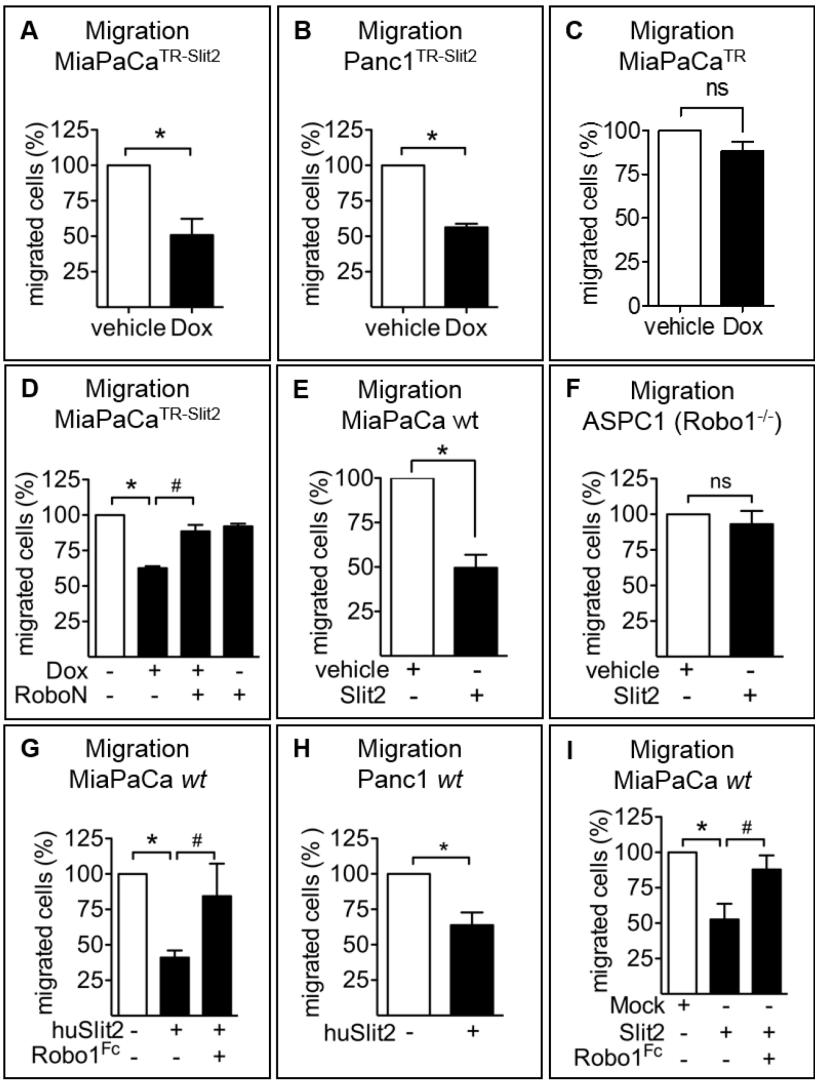

Figure 9: Inducible re-expression of Slit2 inhibits directed migration of PDAC cell lines

(A, B) MiaPaCa$^{TR\text{-}Slit2}$ and Panc1$^{TR\text{-}Slit2}$ cells with inducible Slit2 expression were pretreated with 1 µg/ml doxycycline or vehicle for 48 h and subjected to transwell migration assays. Inducible expression of Slit2 inhibited directed migration of MiaPaCa$^{TR\text{-}Slit2}$ and Panc1$^{TR\text{-}Slit2}$ cells, as compared to vehicle treated controls (MiaPaCa$^{TR\text{-}Slit2}$: n=4, p=0.023; Panc1$^{TR\text{-}Slit2}$: n=3, p=0.016). **(C)** Treatment of MiaPaCa^{TR} with doxycycline had no effect on the directed migration of MiaPaCa^{TR} cells (n=3, p=0.154). **(D)** Conditioned media from HEK293 cells with stable expression of the soluble Robo1 receptor, RoboN, and respective Mock-control were generated. RoboN-conditioned medium abrogated the inhibitory effect of Slit2 on tumor cell migration as compared to Mock-control medium (n=3, *p<0.001, #p<0.05). **(E, F)** Slit2 conditioned medium from doxycycline treated MiaPaCa$^{TR\text{-}Slit2}$ cells inhibited the migration of wildtype, Robo1-competent MiaPaCa cells (E; n=4, p=0.0066), but not of ASPC1 cells deficient for Robo1 (F; n=3, p=0.51)[III]. **(G)** Recombinant human Slit2 (200 ng/mL) inhibited the migration of MiaPaCa and Panc1 wildtype cells. This effect was abrogated by soluble Robo1-Fc (2.5 µg/mL Robo1^{Fc}; n=5, *p=0.0003; #p=0.013). **(H)** Recombinant human Slit2 (200 ng/mL) inhibited the migration of Panc1 wildtype cells (n=4; p=0.022). **(I)** Conditioned media from MiaPaCa cells with stable expression of Slit2 and respective Mock-control media were generated. Slit2-conditioned media inhibited the migration of MiaPaCa cells compared to Mock-control medium (n=5, *p=0.013). Sequestration of Slit2 in conditioned media by addition of recombinant soluble Robo1-Fc to neutralize secreted Slit2 just before the migration assay prevented this inhibitory effect (n=5, #p=0.032).

Tumor cell motility also depends on their capacity to degrade and invade the extracellular matrix. Furthermore, migration of cells within a 3D-cellular matrix more closely resembles the phenotype of migrating cells in tissues compared to 2D cultures [261]. Therefore, we analyzed the consequences of Slit2 expression on the invasive capacity of MiaPaCa$^{TR\text{-}Slit2}$ and Panc1$^{TR\text{-}Slit2}$ cells, using Matrigel coated transwell membranes. Notably, Slit2 induction resulted in a marked inhibition of MiaPaCa$^{TR\text{-}Slit2}$ and Panc1$^{TR\text{-}Slit2}$ tumor cell invasion by 45 % and 55 %, respectively (Figure 10A, B).

[III] ASPC1 migration experiment in figure 9F was kindly provided by M. Welzel

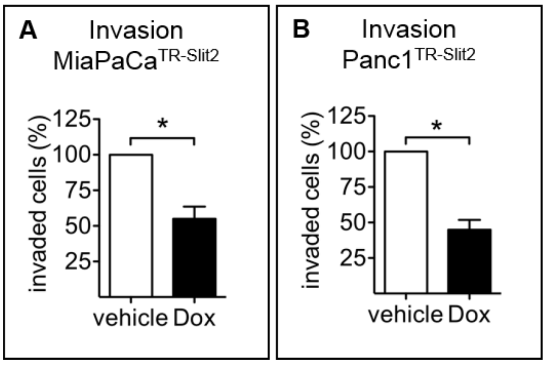

Figure 10: Inducible re-expression of Slit2 inhibits invasion of PDAC cell lines

(A, B) MiaPaCa$^{TR\text{-}Slit2}$ and Panc1$^{TR\text{-}Slit2}$ cells with inducible Slit2 expression were pretreated with 1 µg/ml doxycycline or vehicle for 48 h and subjected to transwell invasion assays. Inducible expression of Slit2 inhibited invasion of MiaPaCa$^{TR\text{-}Slit2}$ (A) and Panc1$^{TR\text{-}Slit2}$ (B) cells, as compared to vehicle treated controls (n=3, p=0.034; n=4, p=0.0042).

Our functional data so far revealed that restored Slit2 expression has the capacity to reduce directed tumor cell migration and invasion. Moreover, differences in the response to Slit2 stimulation between Robo1-competent and Robo1-deficient cells, and the fact that Slit2-mediated effects could be abrogated via a soluble neutralizing Robo1-decoy receptor and soluble Robo1-Fc strongly suggested that the observed Slit2 effects are mediated via direct auto-/paracrine Robo-dependent mechanisms.

3.2.4 Robo1 knockdown stimulates directed migration of PDAC cells

Following these gain-of-function studies, we used a complementary strategy, i.e. functional disruption of Slit-Robo signaling by inactivation of endogenous Robo1. DANG cells express both the Slit2 ligand and the Robo1 receptor and hence represent a suitable model for a functional inactivation of Slit2-Robo1 signaling via lentiviral-mediated knockdown of Robo1. Immunoblot assays confirmed that lentiviral transduction of DANG cells with shRNA against Robo1 led to a marked reduction of Robo1 as compared to scrambled shRNA (Figure 11A). The knockdown of Robo1 receptor in DANG cells had no effect on tumor cell proliferation (Figure 11B), which is consistent with our observation that re-expression of Slit2 did not alter proliferation of MiaPaCa and Panc1 cells. However, Robo1 knockdown in DANG cells doubled the directed migration in transwell assays (Figure 11C), which again is in

good agreement with the inhibitory effect observed upon Slit2 re-expression.

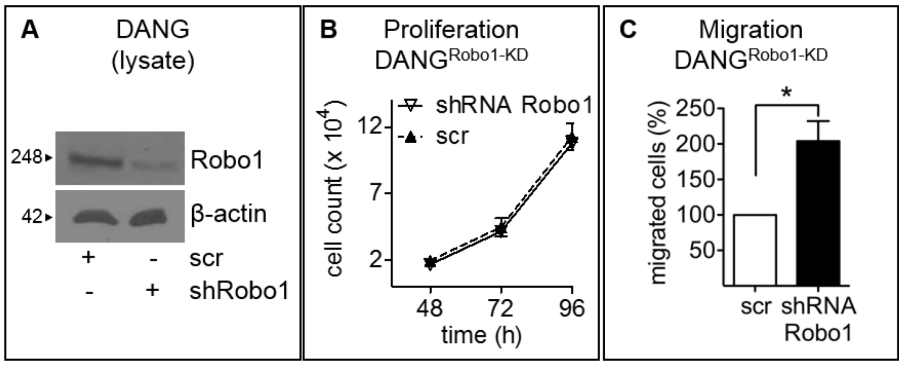

Figure 11: Knockdown of Robo1 enhances directed migration of PDAC cell lines

(A) Lentiviral shRNA-mediated knockdown of endogenous Robo1 in DANG cells was confirmed using immunoblotting of whole cell lysates. **(B)** DANG$^{Robo1\text{-}KD}$ cells with lentiviral-mediated Robo1 knockdown or scrambled-controls (scr) were plated on cell culture dishes and cell numbers were counted at the indicated time points. Experiments were conducted three times, each in duplicates (n=3, p=0.984, Anova). **(C)** Robo1 knockdown enhanced directed migration of DANG$^{Robo1\text{-}KD}$ cells in transwell assays as compared to scrambled-control (n=4, p=0.035; Anova).

Together, these gain- and loss-of-function studies provide compelling support for a functional role of Slit-Robo1-signaling in the control of pancreatic cancer cell motility via autocrine and/or paracrine mechanisms.

3.2.5 Tumor cell derived Slit2 inhibits migration and lamellipodia formation of endothelial cells

Slit2 is a secreted and diffusible factor that may also act on other cell types present within the tumor microenvironment in addition to its effects on epithelial tumor cells. Among these are endothelial cells, inflammatory cells, fibroblasts and neuronal cells, which express Robo receptors and thus might respond to secreted Slit2 [173, 262-265]. Slit2 secreted from pancreatic tumor cells is presented to stromal cells in the PDAC cell-specific context of other growth factors, cytokines and matrix components, which may modify the overall response to Slit2. Therefore, we decided to study the effect of MiaPaCa-derived Slit2 on the motility of HUVEC cells, which express Robo1 and Robo4, and are

hence suitable to study angioregulatory effects of Slit2 on endothelial cells *in vitro*.

Endothelial cell migration in response to chemotactic gradients requires cytoskeletal rearrangements resulting in the formation of lamellipodia and filopodia. In order to determine whether Slit2 interferes with growth factor mediated cytoskeletal rearrangement, we measured the effect of Slit2 on the abundance of lamellipodia formation of individual HUVEC cells stimulated with VEGF. Tumor cell-derived Slit2 impaired VEGF-induced lamellipodia formation of HUVEC as illustrated by F-actin polymerization and spatial redistribution of cortactin (Figure 12A-C).

Next, we evaluated whether tumor-derived Slit2 affects the directed migration of endothelial cells in transwell assays using FBS as a chemoattractant. Consistent with a repulsive effect of tumor cell derived Slit2 on pancreatic cancer cell migration, Slit2-conditioned media from stably transfected MiaPaCa^{Slit2} cell cultures, but not Mock-control medium impaired directed HUVEC migration by 36 % (Figure 12D).

Again, we aimed to assess whether Slit2 directly exerts repulsive effects on HUVEC or whether an indirect mechanism accounted for decreased migration. Hence, tumor cell supernatants were incubated with Robo1-Fc, which neutralizes Slit2, and applied in HUVEC transwell migration assays. Sequestration of Slit2 with soluble Robo1-Fc in the tumor cell supernatant abrogated the repulsive effects on endothelial cell migration (Figure 12D), indicating that Slit2-Robo is indeed responsible for the observed inhibitory functions.

As our data obtained with tumor cell derived Slit2 on the motility of endothelial cells contrasts with some studies that used recombinant Slit2, we also determined the effects of purified Slit2 in our system. In contrast to the observed inhibitory effect on pancreatic tumor cell migration, purified recombinant Slit2N increased the directed migration of HUVEC by 43 % (Figure 12E). Thus, discrepant direct effects on endothelial motility were observed with purified Slit2 and pancreatic cancer cell-derived full-length Slit2, with the latter exhibiting inhibitory effects.

As full-length recombinant Slit2 is difficult to purify (personal communication with Prof. J. Wu; Northwestern University, Chicago, IL, USA), commercially available recombinant Slit2 proteins from commercial sources correspond to the N-terminal cleavage product. In contrast, our tumor cell derived Slit2 supernatant consisted of full-length Slit2 and a certain proportion of Slit2N. Both, full-length Slit2

and the N-terminal fragment were shown to bind to Robo1 and Robo2 with similar Kd values but may have diverging biological effects [162].

In order to further elucidate discrepant results with different Slit2 preparations, we generated MiaPaCa$^{TR\text{-}Slit2N}$ clones with inducible expression of Slit2N. Expression and secretion of the N-terminal fragment upon doxycycline administration were confirmed in the supernatant of the respective cell clones [please refer to Suppl. Figure 4]. Currently, we were able to characterize one MiaPaCa$^{TR\text{-}Slit2N}$ clone with confirmed expression of the N-terminal cleavage product and compared it with the MiaPaCa$^{TR\text{-}Slit2}$ clone. We utilized an endothelial cell transwell migration assay with modified experimental protocol, in which a stable gradient of Slit2 is established by culturing MiaPaCa$^{TR\text{-}Slit2}$ or MiaPaCa$^{TR\text{-}Slit2N}$ in the lower compartment (Figure 12F, G). Interestingly, Slit2N more than doubled the migration of HUVEC cells under these experimental conditions (Figure 12G) in contrast to the consistent and previously observed inhibitory effect of the full-length protein (Figure 12F). Again administration of Robo1-Fc abrogated the inhibitory effect of full-length Slit2 (Figure 12F).

Hence, these data indicate divergent effects of Slit2 on endothelial cells and suggest processing of Slit proteins as an important modifier of Slit2 function.

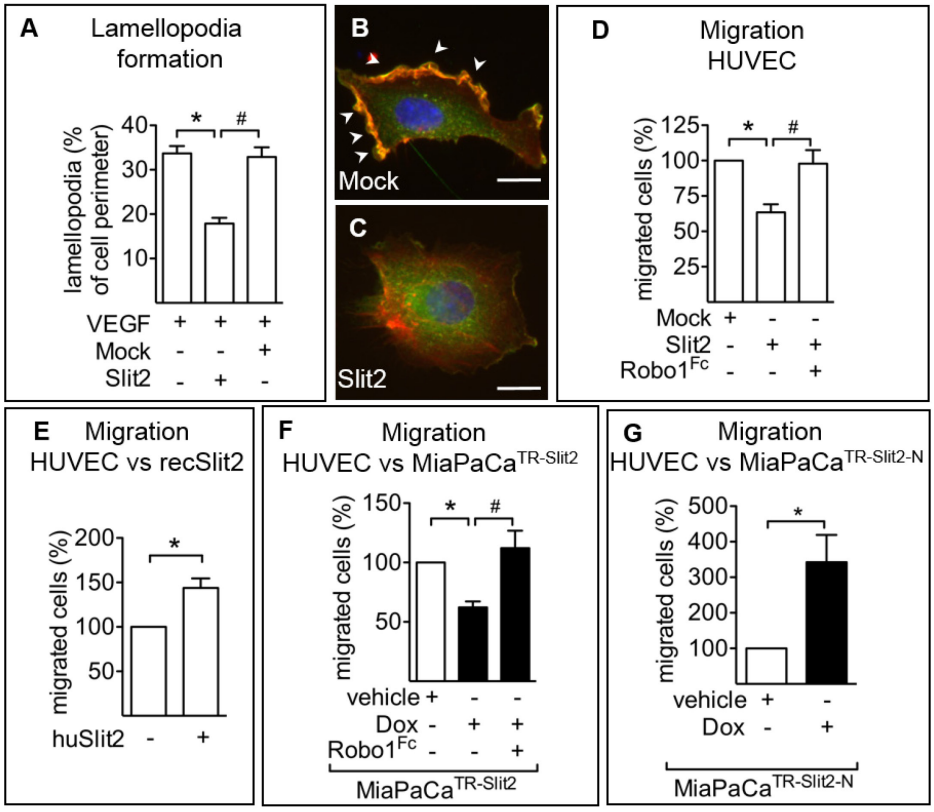

Figure 12: Tumor derived Slit2 inhibits lamellipodia formation and migration of endothelial cells *in vitro*

(A-C) Slit2 conditioned medium from MiaPaCa^{Slit2} cells abrogated VEGF-induced lamellipodia formation, F-actin polymerization and spatial redistribution of cortactin. Arrowheads depict lamellipodia. Abundance of lamellipodia was quantified as percent of total HUVEC cell perimeter. A total of n=95-120 individual endothelial cells out of three independent experiments were analyzed ($p<0.0001$, Anova). Scale bar is 10 μm. Cortactin (green) and phalloidin (red) immunofluorescence staining displayed formation of lamellipodia in HUVEC following VEGF stimulation (50 ng/ml). **(D)** HUVEC were subjected to transwell assays, and migration towards a chemoattractant gradient (2 % FBS) was evaluated in the presence of Slit2 or Mock conditioned media derived from stably transfected MiaPaCa^{Slit2} or MiaPaCa^{Mock} clones, respectively, and added in the lower chamber. Slit2 conditioned medium repelled HUVEC migration (n=4, *p=0.0076). Administration of Robo1-Fc abrogated the effects of Slit2-conditioned medium (n=4, #p=0.021). **(E)** Administration of recombinant huSlit2N enhanced directed migration of HUVEC cells, compared to control cells (n=4, p=0.027). **(F, G)** MiaPaCa cell clones with doxycycline-inducible expression of either full-length Slit2 (A; MiaPaCa$^{TR\text{-}Slit2}$) or the N-terminal Slit2 fragment, Slit2N (B; MiaPaCa$^{TR\text{-}Slit2N}$), were cultured in the lower chamber of transwells during the migration experiment to provide a steady supply of Slit2. HUVEC were subjected to the upper transwell chamber, and migration towards chemoattractant gradients (2 % FBS) was evaluated in the presence of tumor cell released Slit2 or Slit2N, respectively. Of note, continuous expression of Slit2N in the lower chamber substantially stimulated HUVEC migration (G; n=5, *p=0.034) whereas production of full-length Slit2 protein led to inhibition of HUVEC migration (F; n=7, *p=0.0003). Adding Robo1-Fc (10 μg/mL) abrogated this effect (F; n=3, #p=0.017).

3.3 Functional characterization of Slit2 mediated effects on PDAC *in vivo*

So far, our gain- and loss-of-function experiments demonstrated that Slit-Robo signaling is able to regulate tumor cell migration and invasion *in vitro*, suggesting that Slit2-Robo may also control metastatic capacity *in vivo*. Moreover, our *in vitro* experiments using tumor-derived Slit2 also support an angioregulatory effect of the Slit2-Robo system.

To evaluate the role of Slit2-Robo *in vivo*, we performed orthotopic pancreatic tumor studies in mice. In these orthotopic mouse models, tumor cells are injected directly into the physiological environment of the pancreas allowing tumor cell-host interactions, invasion into adjacent organs and the development of distant metastases [53, 266]. Hence, the orthotopic xenograft model is suitable to evaluate the

function of the Slit2-Robo system in the organ-specific context of the pancreas.

3.3.1 Inducible expression of Slit2 in orthotopic xenografts

To experimentally address Slit2 effects on PDAC growth and progression *in vivo*, MiaPaCa$^{TR\text{-}Slit2}$ cells were implanted in the head of the pancreas of SCID beige mice (for detailed information, please refer to 2.5.3). Mice were randomized and treated either with doxycycline administered via the drinking water to induce Slit2 expression or with sucrose as control. At the end of the experiment, protein lysates were prepared from primary tumors, and induction of Slit2 was confirmed by immunoblotting. Indeed, antibodies against the myc-tag detected bands at the expected size of 200 kDa in tumors from doxycycline treated animals, whereas no bands were detected in the control group (Figure 14A).

3.3.2 Re-expression of Slit2 in PDAC cells inhibits growth invasion and metastasis

49 days following tumor cell implantation all mice exhibited tumor growth at the site of tumor cell injection indicating successful tumor cell engraftment of MiaPaCa$^{TR\text{-}Slit2}$ (Figure 13A, B). Quantification of tumor growth revealed that mean weight±SEM of control tumors was 1148.8 mg ± 93 as compared to 859.8 mg ± 55 in tumors with induction of Slit2 expression (Figure 13C). Thus, evaluation of tumor weight revealed a moderate but significant reduction of primary tumor growth by Slit2.

Characteristic for the progress of pancreatic cancer is the local invasion into adjacent organs and early lymphatic metastasis of tumor cells. Therefore, we investigated the effect of Slit2 on these pathologic parameters *in vivo*. In the group with induced Slit2 expression, we noted a reduction of invasion into duodenum by 80 % and invasion into the stomach was absent (Figure 13J, K).

The occurrence of lymphatic and hematogenous metastasis contributes to disease recurrence in patients who underwent surgery. To assess the incidence of metastasis in the orthotopic xenograft model we removed the whole colon along with the mesentery in such a way that we could easily count macroscopically visible tumor nodules (Figure

13D, E). The quantification of tumor nodules indicated substantial reduced abdominal metastasis of tumors with Slit2 expression by 57 % (Figure 13F). Furthermore, an analysis of retroperitoneal lymph nodes in our orthotopic tumor model revealed a reduced incidence of metastasis in xenografts with induction of Slit2 expression compared to the controls by 72 % (Figure 13L).

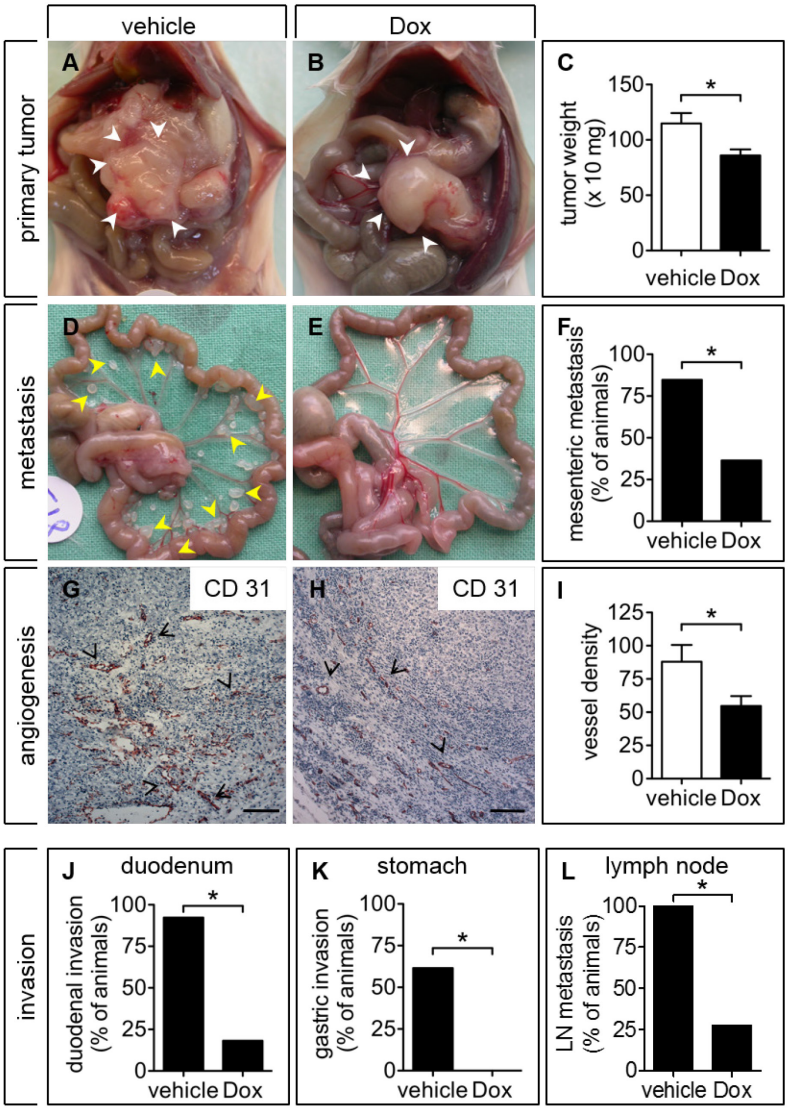

Figure 13: Inducible re-expression of Slit2 inhibits metastatic spread, invasion and angiogenesis of orthotopic PDAC tumors *in vivo*

(A-F) Mice were orthotopically implanted in the head of the pancreas with doxycycline-inducible MiaPaCa$^{TR\text{-}Slit2}$ clones and treated with vehicle (A, D, G; vehicle), or doxycycline (B, E, H; Dox: 2 mg/ml via drinking water). Induction of Slit2 in tumors was confirmed by detecting the abundance of Flag-tagged Slit2 in immunoblots of tumor lysates (**Figure 14**A). Shown are representative pictures with primary pancreatic tumors *in situ* (A, B; white arrowheads) and the excised mesenteries (D, E) with mesenteric metastasis (D; yellow arrowheads) from vehicle (n=13) or doxycycline-treated mice (n=11), respectively. **(C)** Evaluation of primary tumor weight (p=0.018,

Mann-Whitney test). **(F, J-L)** Bar graphs summarize the incidence of histologically confirmed mesenteric metastasis (F; p=0.033), tumor invasion into duodenum (J; p=0.0005) and stomach (K; p=0.002), and metastatic spread into retroperitoneal lymph nodes (L; p=0.0002); all Fisher's exact test. **(G, H)** Representative Immunohistochemical staining on primary tumor sections for CD31 from a vehicle and doxycycline treated animal. Arrowheads depict tumor vessels. Scale bar is 200 μm. **(I)** Bar graph represents quantification of microvessel densities in primary tumors based on CD31 immunoreactivity in vehicle (G) and doxycycline (H) treated tumor-bearing animals (n=12, vehicle-treated; n=11, Dox-treated; p=0.036).

As differences in the extent of metastasis might be secondary to differences in primary tumor growth, we performed analysis on size-matched tumors. Thus n=7 doxycycline- and n=7 vehicle-treated MiaPaCa$^{TR\text{-}Slit2}$ tumors were paired according to tumor weight and subsequently examined for abdominal metastasis and nodal spread (Figure 14B, C). Even in size-matched tumors, the incidence of abdominal metastasis was significantly reduced by 83 % (Figure 14D). Likewise, incidence of nodal spread in the doxycycline-treated mice decreased to 14.3 %, whereas all vehicle treated animals displayed lymphatic nodal spread (Figure 14E).

These data demonstrate that the Slit2-Robo system has a significant effect on the invasion and metastasis of pancreatic cancer cells and thus decisively influences those factors that are mainly responsible for the poor prognosis in this tumor entity.

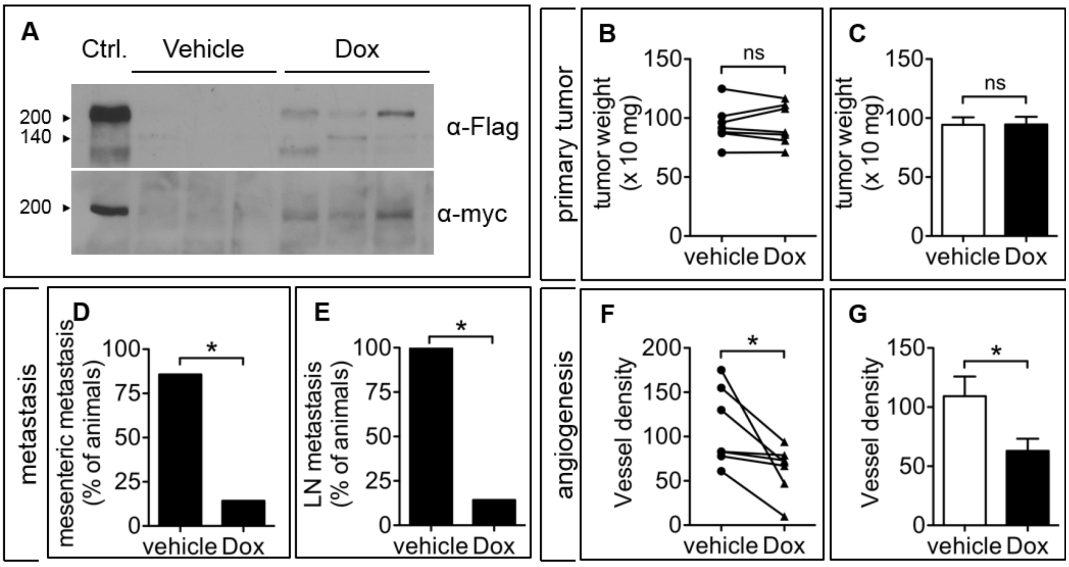

Figure 14: Inducible re-expression of Slit2 inhibits invasion, metastasis and angiogenesis in size-matched orthotopic pancreatic tumors

(A) Immunoblot detects Flag- and myc-tagged Slit2 protein in lysates of MiaPaCa$^{TR\text{-}Slit2}$ tumors from mice treated with 2 mg/ml doxycycline via drinking water (Dox), but not from vehicle-treated control mice. β-actin reactivity was determined from the same lysates. Lysates from doxycycline-treated MiaPaCa$^{TR\text{-}Slit2}$ cells served as positive control (ctr.). **(B, C)** Vehicle- and doxycycline-treated tumors were size-matched according to tumor weight. Shown is the representation of tumor weight of n=7 size-matched vehicle- and doxycycline-treated tumor pairs (B) and respective tumor weight in the paired vehicle- and doxycycline-treated group (C; p=0.947; paired t-test). **(D, E)** Metastasis to the mesentery and lymph nodes were evaluated in size-matched tumors. Shown are contingency graphs of the incidence of mesenteric metastasis (D; p=0.029) and metastatic spread to retroperitoneal lymph nodes (E; p=0.0047); all Fisher's exact test. **(F, G)** CD31-positive micro-vessel densities in paired vehicle- and doxycycline-treated tumors were quantified and represented for each tumor pair (F) and as means±SEM per group (G; n=7, p=0.016; paired t-test).

3.3.3 Re-expression of Slit2 in PDAC cells impairs tumor angiogenesis

Our expression data confirmed the presence of Robo4 in blood vessels of non-transformed pancreas and pancreatic cancer specimens. Furthermore, our *in vitro* experiments suggested a context-dependent functional role of Slit2-Robo signaling in endothelial cells.

For evaluation of tumor angiogenesis in our orthotopic PDAC models, we stained sections of frozen tissue with endothelial specific CD31 and quantified blood vessels based on micro-vessel densities (vehicle-treated: n=12; Dox-treated: n=11). Quantification of angiogenesis revealed that micro-vessel densities were reduced in MiaPaCa$^{TR\text{-}Slit2}$ tumors with Slit2 induction by 37 % (Figure 13G-I).

Since tumor size might have an impact on angiogenesis, we analyzed whether the reduction in micro-vessel densities reached significance in size-matched tumors (n=7, vehicle-treated; n=7, Dox-treated). Indeed, even in the size-matched analysis, microvessel densities were diminished by 42 % in xenografts with induction of Slit2 (Figure 14F, G), thus supporting an inhibitory effect of Slit2 on tumor angiogenesis *in vivo*.

3.3.4 Knockdown of Robo1 in PDAC cells promotes invasion and metastasis

So far we evaluated the role of Slit-Robo in pancreatic cancer using cells with ectopic Slit2 expression. In order to study orthotopic xenografts with endogenous Slit2 expression, we used DANG cells with lentiviral-mediated Robo1 knockdown (for detailed information, please refer to 2.5.3). These DANG cells express endogenous Slit2, thus providing physiologic Slit2 levels. Consequently, Robo1 knockdown in these cells disrupted an autocrine/ paracrine Slit2-Robo1 signaling loop.

For tumor cell injection into the pancreas of SCID beige mice, the same $DANG^{Robo1\text{-}KD}$ cell population with confirmed Robo1 knockdown was used, which had been already characterized *in vitro*. DANG cells treated with scrambled shRNA served as controls ($DANG^{Scr}$). Tumors were harvested after 23 days, and tumor growth, local invasion into adjacent organs, and metastasis were evaluated (n=11, $DANG^{Robo1\text{-}KD}$; n=10, $DANG^{Scr}$; Figure 15).

Disruption of Slit2-Robo signaling in DANG cells did not significantly increase tumor growth (Figure 15A-C) but enhanced local invasion of $DANG^{Robo1\text{-}KD}$ cells into duodenum and stomach by 70 % and 84 %, respectively (Figure 15J,K). Furthermore, the incidence and the extent of metastasis were substantially increased by functional inactivation of Slit2 signaling via Robo1 receptor knockdown in $DANG^{Robo1\text{-}KD}$ cells by 33 % and 70 %, respectively, as compared to scrambled controls (Figure 15F, L).

Since the expression of Slit2 in this experimental approach remained unchanged in both conditions, a systemic effect on stromal cells in the tumor microenvironment was not expected. In good agreement with this notion, the loss of Robo1 in $DANG^{Robo1\text{-}KD}$ cells had no effect on angiogenesis as was evident by unchanged microvessel densities (Figure 15G-I).

Taken together, both experimental gain- and loss-of-function studies strongly support the notion of Slit2-Robo1 as a suppressive ligand-receptor system with repulsive function for invasion and metastasis of pancreatic cancer cells *in vivo*.

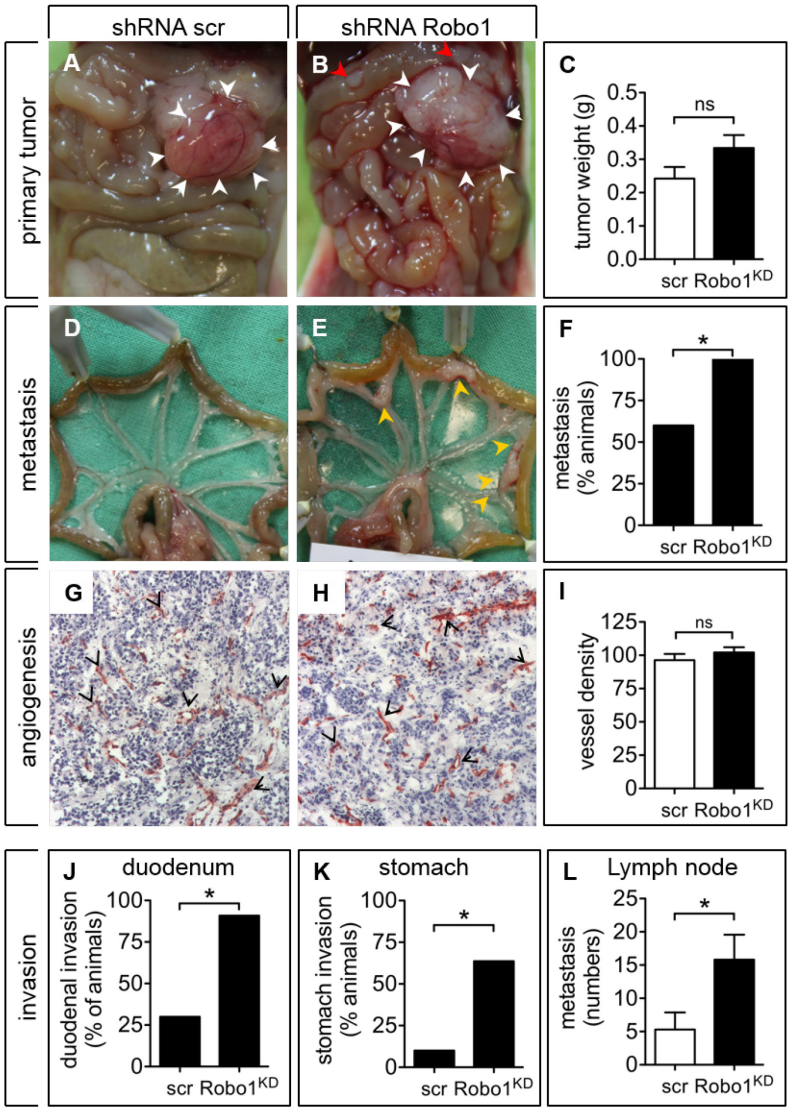

Figure 15: Robo1-knockdown enhances invasion and metastasis, but does not affect angiogenesis of orthotopic pancreatic tumors

(A-F) Orthotopic tumors derived from DANG$^{Robo1\text{-}KD}$ clones with lentiviral-shRNA mediated Robo1 receptor knockdown (n=11, shRNA Robo1) and respective shRNA-scrambled control clones (n=10, shRNA scrambled) were grown orthotopically in mice. Shown are representative illustrations of pancreatic tumors *in situ* (A, B; white arrowheads) and excised mesenteries with mesenteric metastasis from mice bearing scrambled control tumors (D, E) or Robo1 knockdown DANG$^{Robo1\text{-}KD}$ tumors (B,D; yellow arrowheads in D and red arrowheads in B). **(C, F)** Orthotopic tumors were evaluated for tumor weight (C; p=0.170) and metastasis to mesenteries (F; p=0.035). **(J-L)** Contingency graphs show incidence of tumor invasion into duodenum (J; p=0.0075) and stomach (K; p=0.024); all Fisher's exact test. **(L)** Numbers of abdominal metastases increased in DANG$^{Robo1\text{-}KD}$ tumor-bearing animals (L; p=0.016; Mann-Whitney test). **(G-I)** Tumors sections were stained for CD31 to analyze micro-vessel densities, and representative pictures are shown. Arrowheads depict tumor vessels. **(F)** CD31-positive micro-vessel density in DANG$^{Robo1\text{-}KD}$ tumors versus scrambled-controls (p=0.323).

3.3.5 Sequestration of Slit2 in subcutaneous DANG$^{Robo1\text{-}KD}$ xenografts enhances tumor angiogenesis

DANG$^{Robo1\text{-}KD}$ xenografts as used in 3.3.4 did not provide insights on regulation of angiogenesis by endogenous Slit2, as Slit2 levels remained unchanged under the conditions examined. Sequestration of Slit2 by Robo1-Fc in this setting would provide a suitable experimental tool to address this issue but was not feasible in the orthotopic tumor model due to lack of data on the bioavailability and stability of Robo1-Fc and due to high costs following intraperitoneal injection. Consequently, we decided on a subcutaneous xenograft model as a feasible alternative, in which endogenous Slit2 could be neutralized by soluble Robo1-Fc at the time of injection.

Moreover, we choose to use DANG$^{Robo1\text{-}KD}$ cells to ensure that an indirect effect, initiated by the binding of Slit2 to Robo1-competent tumor cells (autocrine loop), does not mask the direct influence of Slit2 on tumor angiogenesis. More precisely, DANG$^{Robo1\text{-}KD}$ cells with confirmed Robo1 knockdown (Figure 11) were pre-incubated with Robo1-Fc or vehicle and injected together with Matrigel in the flank of athymic nude mice (Figure 16; for detailed information, please refer to 2.5.4). As controls, we also implanted DANG^{Scr} cells together with Matrigel and Robo1-Fc or vehicle respectively. Tumors were harvested after 10 days, and micro-vessel density was determined based on CD31 staining of tumor sections. In all conditions, neither tumor weight nor tumor size were significantly changed (Figure 16E, F). Moreover, vascularization was not altered in vehicle-treated DANG^{Scr} and DANG$^{Robo1\text{-}KD}$ tumors confirming the results obtained in the orthotopic DANG model (Figure 16G-I). However, neutralization of Slit2 in DANG$^{Robo1\text{-}KD}$ by Robo1-Fc substantially enhanced microvessel densities by 18 %.

Consequently, our DANG$^{Robo1\text{-}KD}$ xenografts confirmed the capacity of Slit2 to regulate angiogenesis in the more physiologic setting of endogenously produced Slit2. Our results moreover indicated that autocrine Slit-Robo signals were not required for effects on angiogenesis arguing against the possibility that anti-angioregulatory effects were mediated indirectly via a co-factor from the tumor cells.

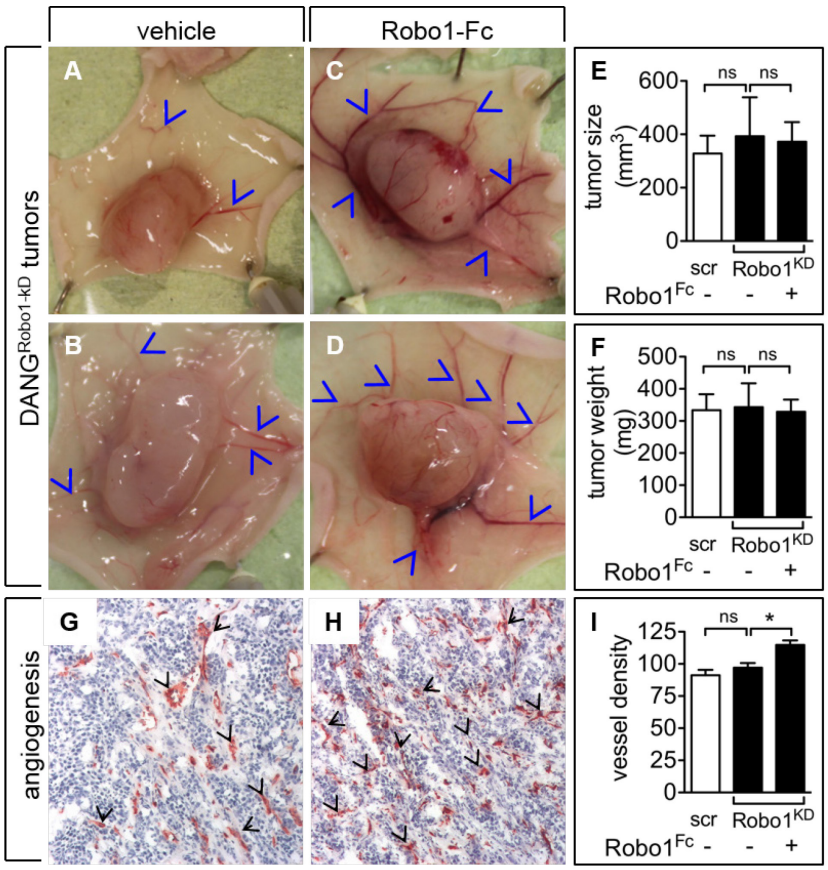

Figure 16: Functional inhibition of Slit2 via Robo1-Fc stimulates angiogenesis in DANG$^{Robo1\text{-}KD}$ tumors subjected to Robo1 receptor knockdown

(A-F) DANG$^{Robo1\text{-}KD}$ cell clones with stable Robo1 receptor knockdown (n= 8, shRNA Robo1^{KD}) and scrambled control clones (n=8, scrambled) were grown as subcutaneous tumors. DANG$^{Robo1\text{-}KD}$ cell populations with confirmed Robo1 receptor knockdown were used to exclude major contribution of indirect effects elicited by autocrine Slit2 stimulation of tumor cells. To functionally inactivate Slit2 released by tumor cells, DANG$^{Robo1\text{-}KD}$ cells were co-incubated with Robo1-Fc (n=5) or vehicle (n=5) prior to subcutaneous implantation in Matrigel plugs. Tumors were harvested after 10 days, and representative illustrations of pancreatic tumors with feeding blood vessels (blue arrowheads) *in situ* are shown. Tumor size (E) and tumor weight (F) were evaluated (all ns). **(G-I)** Micro-vessel densities were determined based on CD31 staining on tumor section. Tumors that had grown in the presence of Robo1-Fc elicited increased micro-vessel density (I; n=8 for scr-control; n=5 for DANG$^{Robo1\text{-}KD}$ in the presence of vehicle or Robo1-Fc, respectively; p=0.0079; Mann Whitney). Arrowheads depict tumor vessels.

3.3.6 *In vivo* syngeneic orthotopic Panc02 Model of PDAC

In order to corroborate the *in vivo* tumor suppressive action of Slit2 in an independent and immunocompetent model, syngeneic orthotopic Panc02$^{Slit2/Mock}$ tumors were evaluated in C57BL/6 mice (Figure 17). Panc02^{Slit2} cells with stable Slit2 expression were done by transfection of wildtype Panc02 cells with pcDNA4/TO-SP-3xflag-Slit2-mycHis vector (for detailed information, please refer to 2.5.3). Panc02 cells transfected with the empty pcDNA4/TO-SP-mycHis served as Mock-control cells.

The syngeneic Panc02 model is highly aggressive and displays advanced tumor growth already after 13 days. Growth of tumors derived from Panc02^{Slit2} cells (n=13) as compared to Panc02^{Mock} control tumors (n=13) was not significantly different (Figure 17A-C), though we noted a trend towards smaller tumor size in Panc02^{Slit2} tumors. Interestingly, and consistent with the idea of Slit2-Robo as inhibitors of invasion and metastasis, we found the incidence of invasive growth into adjacent organs substantially reduced by 72 % in mice with Panc02^{Slit2} tumors compared to Mock-controls (Figure 17D). Due to the aggressive course of the Panc02^{Slit2} model, we could quantify metastasis by counting the malignant nodules in the mesentery despite the short duration (Figure 17E, F). Again the abundance of abdominal metastasis was markedly diminished in Panc02^{Slit2} tumors by 57 % compared to controls (Figure 17G). Moreover, the incidence of ascites was reduced in mice harboring tumors with Slit2 expression by 85 % as compared to mock control tumors (Figure 17H).

Thus, the anti-metastatic and anti-invasive properties assigned to Slit2 in our *in vivo* models were not confined to immunocompromised xenografts.

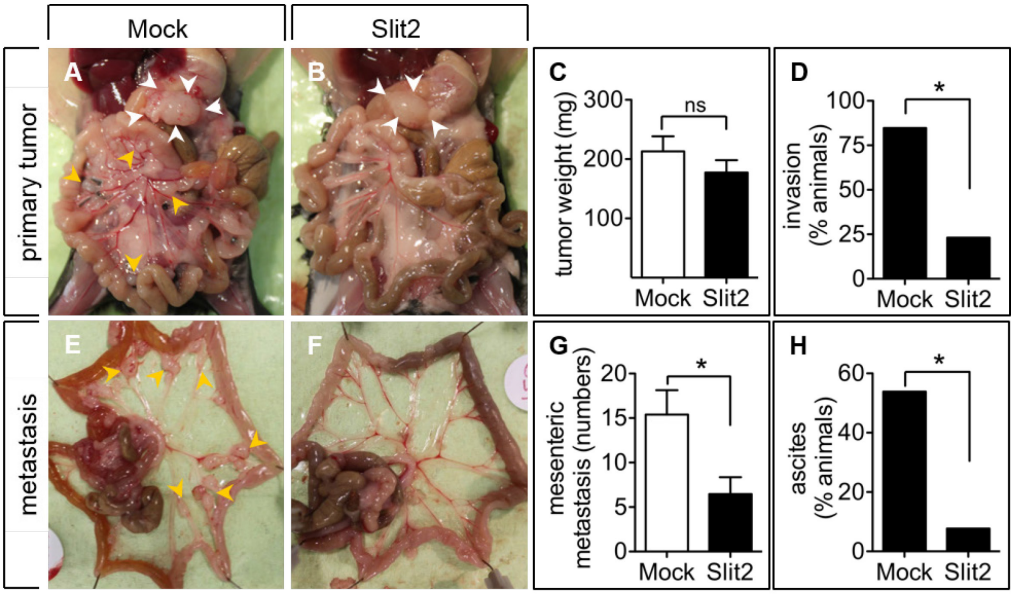

Figure 17: Forced expression of Slit2 inhibits metastasis and invasion in an orthotopic Panc02 syngeneic tumor model

C57/Bl-6 mice were orthotopically implanted in the head of the pancreas with Slit2- or Mock-transfected Panc02 cells. Shown are representative abdominal sites with primary pancreatic tumors (A and B; white arrowheads) and mesenteric metastasis (E and F; yellow arrowheads) from mice bearing $Panc02^{Slit2}$ (n=13) and $Panc02^{Mock}$ (n=13) tumors, respectively, after laparotomy. **(C, D)** Bar graphs show evaluation of primary tumor growth (C; p=0.18) and invasion into adjacent organs (D; p=0.005; Fisher's exact test). **(G, H)** Contingency graphs show abundance of mesenteric metastasis (G; p=0.024; Mann Whitney) and incidence of ascites (H; p=0.03; Fisher's exact test).

3.4 Role of Slit2 for neural invasion of PDAC cells

We next examined the relevance of Slit2-Robo for the mutual interaction of tumor cells with nerves. The underlying hypothesis is based on the well documented influence of Slit2 and its Robo receptors as axon guidance factors on neuronal processes such as axon branching, neural cell migration and differentiation. The fact that we were able to locate Robo1 expression in intrapancreatic nerves reinforced the hypothesis that these neuronal structures are indeed Slit2-responsive and therefore are sensitive to changes in Slit2-Robo signaling. To investigate the reciprocal interaction of tumor and neuronal cells, we thus implemented several *in vitro* and *ex vivo* models with increasing complexity

3.4.1 Slit2 reduces the bidirectional chemoattraction of PDAC cells and neuronal cells

Neural invasion is perceived as mutual interaction of tumor cells and neuronal cells and implicates signaling molecules, such as cell surface bound ligands and their respective receptors as well as soluble chemokines. Thus, chemokine attraction and contact cues provide the mechanistic repertoire for the reciprocal interaction of tumor cells and neuronal cells. Notably, Schwann cells, which constitute the perineural sheaths of nerves, have been implicated in neural invasion as well [267, 268]. In a first approach, we therefore determined the effect of Slit2 on migration of tumor cells towards chemoattractant gradients established by primary Schwann cells. Indeed, tumor cells, seeded in the upper transwell chamber, were attracted by chemogradients released by primary Schwann cell cultures in the lower transwell chamber. Notably, induction of Slit2 in MiaPaCa$^{TR\text{-}Slit2}$ and Panc1$^{TR\text{-}Slit2}$ cells impaired directed tumor cell migration towards the chemogradients established by Schwann cells by 67 % and 42 %, respectively (Figure 18A,B).

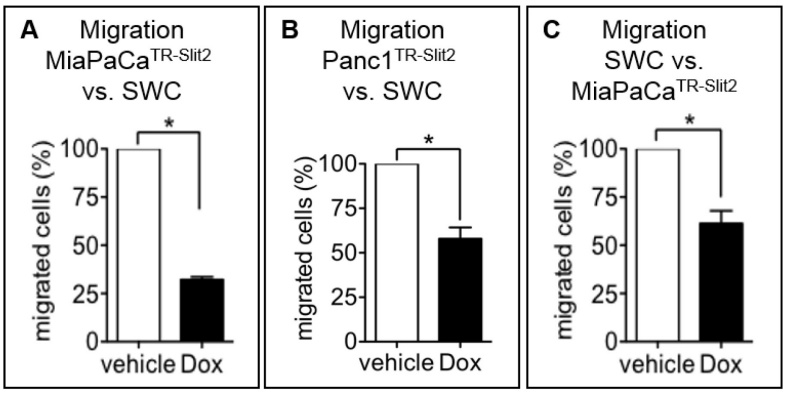

Figure 18: Slit2 impairs bidirectional chemoattraction of tumor and neuronal cells

(A, B) Slit2 inhibited the directed migration of MiaPaCa$^{TR\text{-}Slit2}$ and Panc1$^{TR\text{-}Slit2}$ cells towards chemoattractants released by Schwann cells (SWC) seeded in the lower chamber of transwells (MiaPaCa$^{TR\text{-}Slit2}$: n=3, p=0.014; Panc1$^{TR\text{-}Slit2}$: n=3, p<0.05). **(C)** Slit2 released from MiaPaCa$^{TR\text{-}Slit2}$ cells, which were cultured in the lower chamber of transwells, inhibited the directed migration of Schwann cells (n=3, p=0.027).

Recent published data furthermore suggested that neural invasion also comprise axonal growth in the direction of chemokines released by tumor cells [103, 269]. Accordingly, we modified the experimental configuration and seeded MiaPaCa$^{TR\text{-}Slit2}$ cells in the lower

compartment of the transwell assay, which hence allowed to monitor the migration of Schwann cells towards a chemotactic gradient released by tumor cells. Again we found directed migration of Schwann cells reduced by 38 %, when Slit2-expressing MiaPaCa$^{TR\text{-}Slit2}$ cells were grown in the lower transwell chamber (Figure 18C). Taken together, these data demonstrate that Slit2 counteracted bidirectional chemoattraction between neuronal and PDAC cells.

3.4.2 Slit2 impairs neural invasion in a tumor cell-DRG co-culture model

Studying neural invasion in our *in vivo* model would have been very instructive. However, immunohistochemical analysis using antibodies against the neuronal marker S100 and neurofilament revealed that orthotopic tumors exhibited only poor innervation and hence did not represent reliable models to study neural invasion *in vivo*. To circumvent this problem, we decided to study direct nerve cancer interactions in an *ex vivo* model of neural invasion. Presently, the model that reproduces the processes during neural invasion most accurately is the DRG-tumor cell co-culture model. This model initially introduced by Ayala *et al.* to study nerve-prostate cancer cell interactions [269], is currently used by various research groups to investigate neural invasion and has been modified to meet experimental needs [103, 104, 269].

The steps needed for this *ex vivo* model were implemented according to the current literature, and are documented in detail in the previous chapters of Material and Methods (2.4.11). The first step comprised the isolation of dorsal root ganglions from the murine vertebral column of 3-4 week old C57BL/ 6 mice [270] (Figure 19A-D).

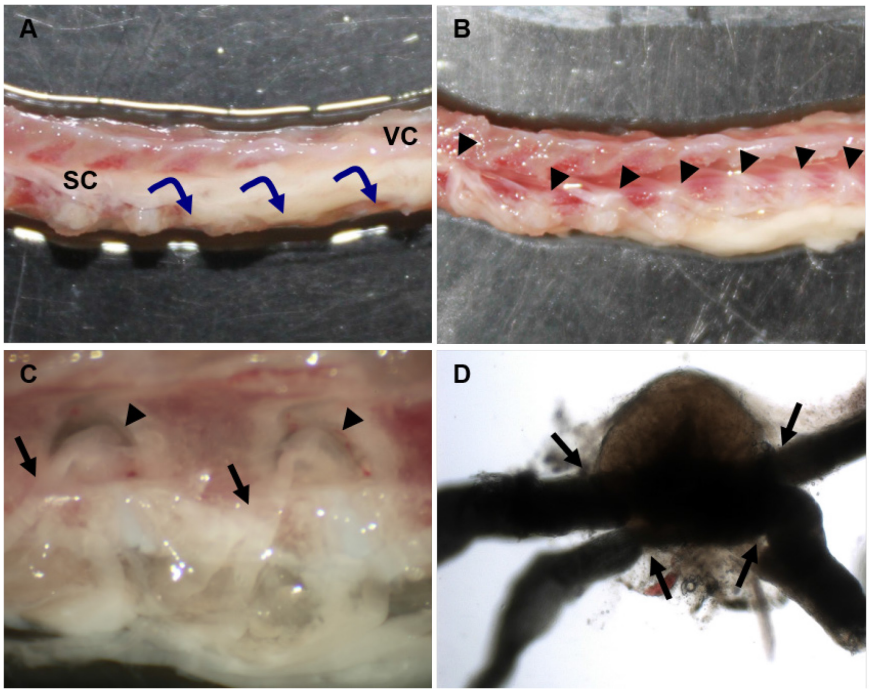

Figure 19: Isolation of dorsal root ganglions from the murine vertebral column.

The entire spine of 3-4 week old C57BL/ 6 mice was isolated and excessive muscle tissue was removed. **(A-B)** The spine was divided along the *vertebrae* into two equal halves and the spinal cord was removed with tweezers (A) to expose the DRGs located within the cavity of the vertebral column (B). **(C)** Higher magnification shows DRGs located within the cavities. **(D)** Isolated DRGs were further processed to remove the remaining dorsal and ventral roots. The isolated DRGs were incubated (37 °C, 5 % CO_2) overnight in complete media (DMEM, 10 % FBS, Pen/Strep) and embedded in 20 µl Matrigel the following day. Viability of DRGs was observed by neurite outgrowth via a cell culture microscope. VC = vertebral column; SC = spinal cord; black arrowhead = DRGs, black arrows = dorsal/ventral roots.

The isolated DRGs were further processed, incubated overnight and placed 1 mm adjacent to MiaPaCa$^{TR\text{-}Slit2}$ cells, both embedded in growth factor reduced Matrigel (Figure 20A). An empty Matrigel drop placed on the opposite site of the tumor cell colony served as control to exclude random tumor cell behavior. These Matrigel droplets were connected via Matrigel bridges ensuring the formation of chemokine-gradients and the exchange of guidance cues. Viability of the DRGs was observed by neurite outgrowth via a cell culture microscope. After approximately 5 days, outgrowth of neurites from the DRG and consecutive elongation of neurites towards the tumor cell colonies were observed (Figure 20B).

Time-lapse microscopy delivered more detailed information, revealing a dynamic process with neurites protruding from the DRG towards chemotactic gradients released from the tumor cells. These neurites then initiated contact with the periphery of the cancer cell colony. Subsequent dissociation of individual tumor cells occurred, which then unidirectionally migrated along the neuronal conduits towards the DRG (Figure 20C, D). Over time more and more tumor cell-nerve-interactions occurred increasing the abundance of tumor cell projections, which in turn invaded the newly formed neuronal structures. We confirmed the identity of those tumor cells by using GFP-labelled MiaPaCa cells (Figure 20E). Based on the area covered by these protrusions, we quantified the extent of *ex vivo* neural invasion and recorded a consistent increase over time. Moreover, as neural invasion increased over time, we observed a consistent and significant reduction of neural invasion after induction of Slit2 in $MiaPaCa^{TR\text{-}Slit2}$ cells at day 9 and day 12 (each by 37 %; Figure 20F).

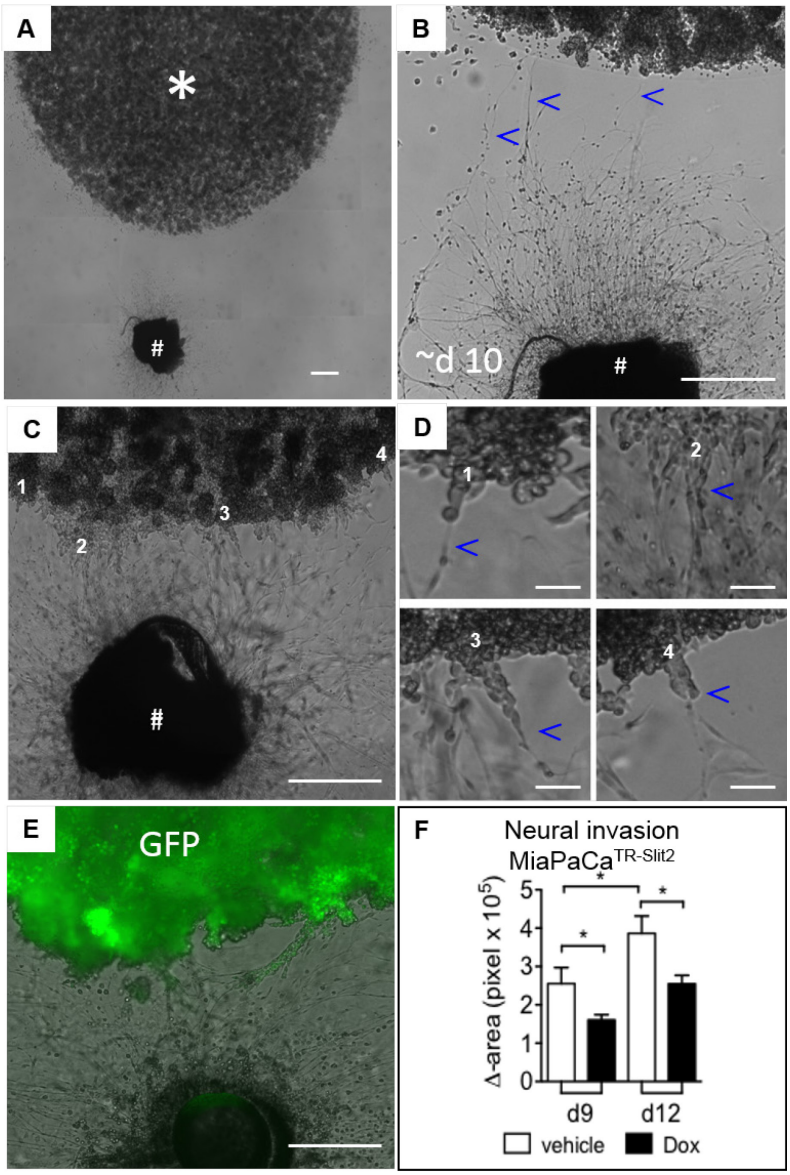

Figure 20: Slit2 reduces neural invasion in a tumor cell, DRG co-culture model

(A) Three-dimensional co-cultures of tumor cells (depicted by asterisk) and dorsal root ganglion (DRG; #) were assembled in Matrigel. **(B)** Outgrowth of neurites from the DRG and extension of neurites (indicated by blue arrowheads) in projection to the tumor cell colony around day 5 were monitored. **(C, D)** Once neurites contact the tumor cell colony, tumor cells disengage from the colony and navigate along the contacted neurite conduits (blue arrowheads) in projection to the ganglia of origin. Numbers indicate sites of neurite-tumor cell contact initiation and refer to the corresponding magnified areas as shown in (D). Blue arrowheads indicate neurites. **(E)** Three-dimensional co-cultures of GFP-labelled MiaPaCa cells and dorsal root ganglion. **(F)** Neural invasion of vehicle or doxycycline treated MiaPaCa$^{TR\text{-}Slit2}$ cells was quantified as the change in area covered by tumor cell projections at day 9 and 12 as compared to the day of co-culture start (day 0; n=3, *p<0.05). Scale bars are 500 µm in A-C, E and 50 µm in D.

3.4.3 Slit2 impairs unidirectional migration of PDAC cells along nerves

A detailed analysis of the high-resolution micrographs revealed that neural invasion of tumor cells occurred particularly in areas with direct nerve contact. To obtain a more precise representation of Slit2 effects on the motility of tumor cells, which are engaged in neurite contact, we used our *ex vivo* DRG co-culture model to monitor the migration of individual tumor cells along neurites via time-lapse microscopy (for detailed information, please refer to 2.4.11). GFP-labelled MiaPaCa cells confirmed that these were actually tumor cells migrating along the neuronal structures and not extravasated stromal cells from the DRG (Figure 21).

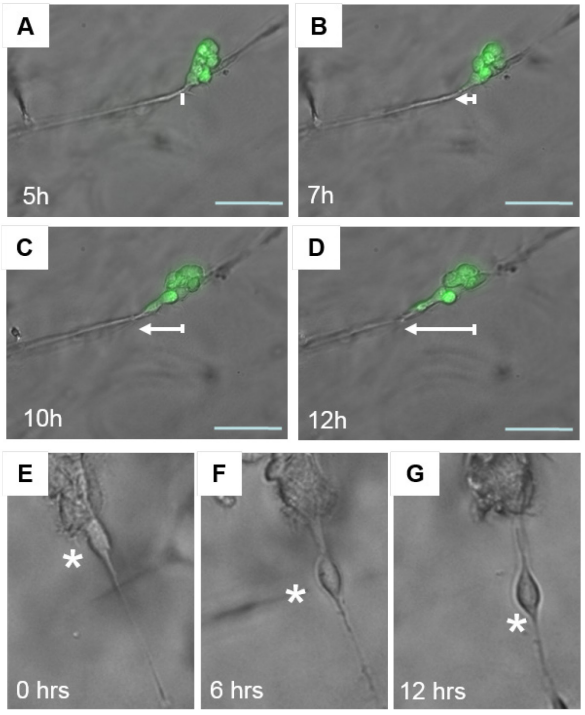

Figure 21: Time-lapse microscopy reveals directional navigation of tumor cells along neurites

(A-D) GFP-expressing MiaPaCa cells (green) migrate along contacted neurites. Pictures show overlay of phase-contrast and immunofluorescence images of individual tumor cells at indicated time points during time-lapse microscopy, starting 5 hours after contact of neurite with tumor cell colony has been established. White arrows indicate Euclidean distance traveled by tumor cells. Scale bar is 100 µm. **(E-G)** Movement of a single MiaPaCa tumor cell, which dissociates from a tumor cell colony and migrates along the contacted nerve as assessed using time-lapse microscopy. Asterisk indicates position of tumor cell at indicated time points.

In order to quantitatively characterize individual tumor cell migration, individual tracks captured from single tumor cells over a time course of 18 h were analyzed by chemotaxis software to determine specific parameters, such as travel distance, velocity and directionality of movement (Figure 22).

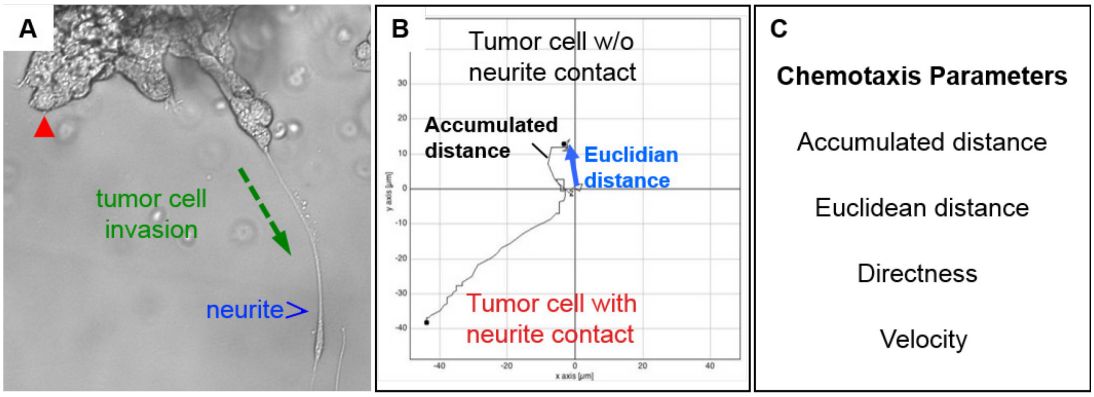

Figure 22: Parameters for individual tumor cell migration

(A-C) Using automated acquisition software (Leica LAS AF6000), up to 20 individual tumor cells were simultaneously imaged in each experiment. Travel distances, velocity and directness were calculated using ImageJ®, Manual Tracking plug-in, and IBIDI chemotaxis software.

A first observation showed differences in the travelled distance between tumor cells with and without nerve contact (Figure 23I, J). Both Euclidean and accumulated distances were significantly increased in tumor cells migrating along neurites by 75 % and 48 %, respectively, compared to those without neuronal contact. Furthermore, the directionality, i.e. the ratio of Euclidean and accumulated distance was increased in cells travelling along the neuronal conduits compared to cells without contact by 52 % (Figure 23K), suggesting juxtacrine signaling between nerves and tumor cells. Notably, induction of Slit2 in MiaPaCa$^{TR\text{-}Slit2}$ cells nearly abrogated the positive effect of the neuronal contact on Euclidean (by 46 %) and accumulated (by 30 %) distance, thereby reducing the directionality of these cells (by 19 %; Figure 23I-K). Similarly, the velocity of MiaPaCa$^{TR\text{-}Slit2}$ cells with nerve contact was increased by 47 %, as compared to controls (Figure 23L). Again induction of Slit2 reduced the velocity of MiaPaCa$^{TR\text{-}Slit2}$ by 31 %.

Under the prevailing experimental conditions, induction of Slit2 did not affect the migratory behavior of tumor cells without neurite contact (Figure 23I-L), indicating that Slit2 specifically functions in the context of tumor cell-nerve-interactions. Hence, the obtained data support a

repulsive function of Slit2 for neural invasion in PDAC by restricting the navigation of tumor cells along attracted neurites.

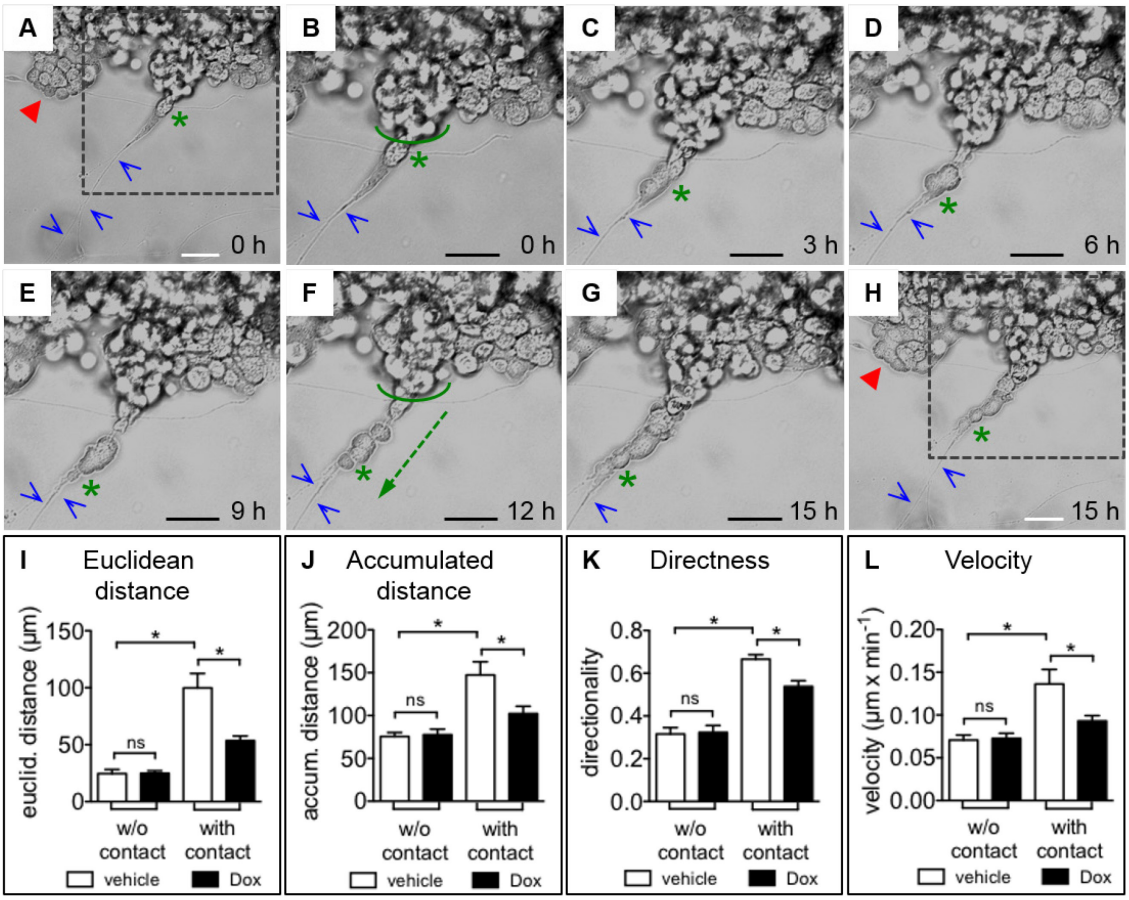

Figure 23: Slit2 inhibits tumor cell migration along neurites in a three-dimensional tumor cell-DRG co-culture model

(A-H) Time-lapse microscopy monitored the migration of individual MiaPaCa$^{TR\text{-}Slit2}$ cells along a contacted DRG neurite over 15 h. Sequential phase-contrast images depict the projection of a DRG neurite (blue arrowheads) into the tumor cell colony, and consecutive unidirectional migration of individual tumor cells (green asterisk) alongside the neurite towards the ganglion of origin. Green arrow (F) indicates the trajectory and migration distance of one individual tumor cell after 12 h. Tumor cells without nerve contact only migrated randomly without directed motility (red arrowheads in A and H). Images (B) and (G) each display magnified views of boxed areas in images (A) and (H), respectively. Scale bar is 50 µm. **(I-L)** Trajectories of individually tracked tumor cells with or without neurite contact were captured by time-lapse microscopy, and Euclidian and accumulated distances, directionality and velocity were quantified. Bar graphs from 10 independent experiments with a total number of n=45-81 individually tracked tumor cells per condition ($p<0.05$; Anova).

4. Discussion

Pancreatic cancer is a devastating and mostly fatal disease. The main reason for the poor prognosis of PDAC, even after curative surgery, is disease recurrence due to early metastatic spread [4]. Independent from lymphatic and vascular metastasis, neural invasion has emerged as a key pathological feature for pancreatic cancer [4], offering tumor cells an alternative route to disseminate into other parts of the body. The elucidation of the molecular mechanisms underlying the various aspects of pancreatic cancer progression and dissemination remains a central point of translational research.

Axon guidance factors were originally discovered as guidance cues during neuronal development, but have since been characterized as regulators of angiogenesis and epithelial morphogenesis in various physiological and pathological processes [Reviewed in 89, 90]. On the basis of these properties, we hypothesized that axon guidance factors could be important regulators of the major metastatic routes in pancreatic cancer. Based on our hypothesis, we investigated the possible role of the axon guidance molecule Slit2 and its receptors Robo1 and Robo4 for tumor progression of pancreatic cancer.

Our data now provide compelling evidence for a tumor suppressor function of Slit2-Robo in PDAC. Taken together, we were able to show that Slit2 mRNA expression is reduced in PDAC, and correlates with lymphatic metastasis in the clinical setting. Furthermore, our gain- and loss-of-function studies provided experimental evidence that Slit2 impairs directed tumor cell migration and invasion *in vitro*, negatively regulates directed migration and lamellipodia formation of endothelial cells, and finally, exerts an inhibitory effect on invasion, metastasis and angiogenesis in orthotopic tumor models *in vivo*.

4.1 Reduced expression of Slit2 mRNA in human PDAC is associated with enhanced lymphatic metastasis

4.1.1 Expression of Slit2 in the healthy pancreas

Our initial experiments intended to confirm the presence of the Slit2-Robo system in the healthy pancreas, and hence provide a potential clinical relevance for PDAC. At the same time, these data provide a framework for functional analysis.

Quantitative RT-PCR revealed substantial expression of Slit2 mRNA in non-transformed pancreas and in immortalized non-transformed human ductal pancreatic epithelial cells (HPDE). These findings are consistent with available data from mRNA expression analyses in pancreatic ductal epithelial cells isolated from healthy pancreas [245, 246, 255, 256]. With respect to Robo receptors, we detected Robo1 in the epithelial compartment and Robo4 in the vascular compartment.

Little is known about the physiological function of Slit2 and its Robo receptors in the pancreas, but more comprehensive data from other epithelial organs are available. For instance, a number of studies reported expression and function of Slit-Robo in the developing and adult lung, gut, kidney, and breast [113, 115, 117, 118, 123, 126, 217, 271-279]. Moreover, these studies indicate that Slits and Robos function as important regulators of epithelial cell proliferation and guide the correct growth and ductal branching during embryonic development of the mammary gland, lung, colon and kidney [113, 115, 278]. Of interest, expression analysis in *xenopus laevis* identified Slit2 among genes with a spatial expression specifically in the ventral bud during pancreas development [280]. Moreover, studies that specifically examined the endocrine pancreas demonstrated a function of Slits (and Netrins) and their receptors for beta-cell survival and insulin secretion under stress-induced conditions in the adult mouse pancreas [281, 282]. Although Slit2 knockout mice have been generated, homozygous deficiency was perinatal lethal, and no pancreatic pathology was reported [283, 284]. Taken together, these results indicate that the Slit2-Robo system is present in the adult pancreas of different species, including humans, and likely contributes to its physiological functions.

4.1.2 Expression of Slit2 mRNA in PDAC and correlation with clinicopathological parameters

In contrast to non-transformed pancreatic tissues, we found that Slit2 mRNA content was distinctly reduced in PDAC samples and lost in most of the epithelial PDAC cell lines analyzed. The latter, we either linked to epigenetic silencing due to promoter hypermethylation, or was reported by others to be a consequence of loss of heterozygosity [45].

Although few PDAC samples retained high Slit2 mRNA levels, compelling evidence for a reduction of Slit2 mRNA expression in PDAC was obtained from matched analysis of paired PDAC and non-transformed tissue, which consistently revealed reduced Slit2 expression in PDAC.

This profound reduction of Slit2 prompted us to test for a correlation with clinicopathological parameters. The key finding was that reduced Slit2 mRNA expression levels in tumors were associated with higher incidence and a higher extent of lymph node metastasis. Similarly, patients with lymph node metastasis exhibited a lower expression of Slit2 mRNA.

Our observations are in line with published microarray data that ranked Slit2 among those genes that were found reduced in clinical samples of PDAC with lymph node metastasis as compared to lymph node negative PDAC samples [285]. The association of reduced Slit2 mRNA expression with an unfavorable course of the disease fits our hypothesis that expression of Slit2 is of clinical relevance for the progression of PDAC. Furthermore, our results are consistent with studies that found a correlation between loss or epigenetic inactivation of Slit2 and poor prognosis in other tumor entities, such as prostate, breast, and lung cancer [221, 231, 286]. In addition, low expression of Slit2 in stromal fibroblasts was associated with enhanced lymph node metastasis in breast cancer [224].

By comparison, Slit2 expression positively correlated with metastatic tumor spread and reduced overall survival in patients with colorectal cancer [236, 287]. Hence, up- or downregulation of Slit2 expression may occur depending on the tissue- and tumor-type.

Notably, relative expression unit distribution in our mRNA expression analysis of clinical samples revealed that Slit2 expression varied considerably between tumor samples. Some tumors exhibited Slit2 expression levels comparable to healthy pancreas, whereas Slit2 levels were severely reduced in others. One potential explanation could come from loss or functional inactivation of other components of a putative Slit2-Robo tumor-suppressive pathway, such as Robo receptors.

Indeed, a recent seminal study by Biankin *et al.* reported that genomic alterations in genes belonging to the Slit2-Robo pathway are prevalent in PDAC samples [45].

There are two other studies reporting a regulation of Robo1 mRNA expression in pancreatic cancer. In the first study, a BXPC3 progeny with high potential for lymphatic metastasis was generated by repeated subcutaneous injection of BXPC3 cells in the left hind footpad of mice, subsequent isolation of tumor cells from collected lymph nodes and cultivation in cell culture [288]. A microarray analysis comparing these two BXPC3 variants revealed reduced expression of Robo1 in the metastatic BXPC3 progeny compared to the wildtype cell line [288]. The other study examined Robo1 because it constitutes a target of miRNA-218 [289]. In this study miRNA-218 was found downregulated in both the metastatic BXPC3 cell line and in pancreatic cancer specimen, and inversely correlated with lymphatic metastasis [289]. Interestingly, miRNA-218 is located at the intron of Slit2 and targets the 3'untranslated region (3'UTR) of the Robo1 gene, thereby negatively regulating Robo1 expression in a feed-back loop mechanism [290]. Consequently, the reduced expression of miRNA-218 was accompanied by an increase of Robo1 mRNA in PDAC [289]. We have now started to quantitatively analyze the expression of the Robo receptors in our tumor samples, results however are still pending.

Alterations of Robo receptor expression have also been reported in other cancer types, and were linked to patients' prognosis. Thus, increased Robo1 expression was found associated with better survival in breast cancer patients [224], whereas increased expression of Robo1 in patients with colorectal cancer correlated with enhanced metastasis and poor survival rate [236, 287]. Clearly, the exact role of Robo receptors in cancer awaits further clarification.

A more comprehensive knowledge of the expression pattern of the Slit-Robo components would perhaps allow us to classify tumors in groups, in which all components of Slit2-Robo signaling are preserved, or in which either the ligand and/or the receptors are affected. Such a comprehensive study could also include expression analysis of other Slit homologous, i.e. Slit1 and in particular Slit3, which may also be affected [153, 291]. Our current analysis did not include Slit1 and Slit3, but focused on Slit2, as it has been reported to be the family member most prominently expressed outside the nervous system and the most frequently affected in human malignancies [291].

Overall, available expression data strongly suggest that Slit2-Robo exert physiological functions in the developing and adult pancreas. Our own data now indicated that Slit2 expression is reduced in PDAC, and that this reduction is associated with a more aggressive tumor phenotype characterized by increased lymphatic metastasis.

With our qRT-PCR approach we cannot localize the source of Slit2 expression; thus the reduction of Slit2 expression in tumor tissues might be caused by a change of Slit2 expression within the stromal compartment or the tumor cells. Indeed, it has been reported that Slit2 derived from stromal fibroblasts can restrain tumor progression in xenografted breast cancer models [224]. Furthermore, low expression of Slit2 in stromal fibroblasts of clinical samples was associated with enhanced lymph node metastasis in breast cancer, providing evidence that inactivation of Slit2 in the stromal compartment can also contribute to cancer pathogenesis [224]. Localizing the source of Slit2 could provide further insights into the distribution and relative abundance of Slit2 expression in the stromal tumor compartment of PDAC, but would have required immunohistochemical analysis. However, several attempts by our groups and others to validate Slit2 immunohistochemistry on tumor sections failed to obtain convincing staining results on human tissues and Slit2-transfected tumor cell lines [292] (for detailed supplementary information, please refer to 7.1 and Suppl. Figure 1-3).

4.2 Experimental studies to analyze the biological function of Slit2-Robo in PDAC *in vitro* and *in vivo*

The qRT-PCR and immunohistological analysis gave us important information about the expression of Slit2 in healthy pancreatic and malignant human PDAC samples and further identified distinct tumor compartments (epithelial cells, nerves and vessels), which express Robo receptors and are thus susceptible to changes in Slit2 expression. We then chose appropriate *in vitro* and *in vivo* models to experimentally address the function of Slit2-Robo in PDAC cell lines, which differentially express Slit2 and hence were suitable for Slit2 overexpression or functional inactivation studies.

4.2.1 The TREx system for inducible expression of Slit2

As our expression data were most consistent with a tumor-suppressive function for Slit2, we decided on re-expression of Slit2 in Slit2-deficient PDAC cell lines. The inducible TREx™ system (Invitrogen) has been used for this gain-of-function experimental approach, as it

provides certain advantages when compared to the generation of individual stable cell clones.

First, the same cell clone serves as a Slit2-overexpressing clone and control by simple administration of doxycycline or vehicle. These properties were especially advantageous for the *in vivo* experiments as the requirement for multiple Slit2-expressing clones and mock-control clones could thus be circumvented, reducing the number of animals and experimental costs. In addition, this strategy precluded any differences in the culture conditions of the cells and adjustment of the cell number at the day of implantation. Second, by delayed administration of doxycycline, it was possible to induce the expression of Slit2 after tumor cell engraftment was completed, providing both populations with the same starting conditions.

Concerning the use of doxycycline, it should be mentioned that very high concentrations (20 µg/ml) of this stable tetracycline analogue were found to induce apoptosis in tumor cells [293, 294]. Yet, the concentrations of doxycycline used were up to 20 times higher than in our *in vitro* experiments (1 µg/ml). Additionally we conducted appropriate control experiments using MiaPaCa^{TR} cells, which only expressed the TetR repressor. Doxycycline had no effect on the directed migration of these MiaPaCa^{TR} control cells. Moreover, biological effects observed using the inducible MiaPaCa$^{TR\text{-}Slit2}$ and Panc1$^{TR\text{-}Slit2}$ clones were reproduced in cell clones with stable Slit2 (no doxycycline treatment) *in vitro* and *in vivo*. All together, the inducible system allowed us to study the biological function of Slit2 under well controlled conditions.

4.2.2 A functional role for Slit2-Robo in tumor cell invasion and metastasis

Our study presents three orthotopic *in vivo* models that address the function of Slit2-Robo in PDAC. The major findings of our functional analyses are that restored expression of Slit2 substantially reduces metastatic spread, local invasion and angiogenesis. These results were corroborated by findings from a complementary experimental approach, i.e. knockdown of Robo1, which in turn promoted tumor invasion and metastasis. Together, these data support our hypothesis that Slit2-Robo functions as a tumor suppressor in PDAC.

Especially, the orthotopic approach with its presentation of metastatic disease, enabled us to demonstrate that re-expression of Slit2 in pancreatic cancer cell lines significantly reduced the capacity of tumor cells to metastasize to lymph nodes. Our data are thus in accordance

with the clinical association of reduced Slit2 expression in PDAC with lymphatic metastasis described above and with published profiling data that listed Slit2 among genes with reduced expression in pancreatic cancer with lymph node metastasis [285]. These data are further supported by the enhanced invasive and metastatic capacity in our DANG$^{Robo1\text{-}KD}$ xenografts with Robo1 knockdown.

Our data fit with previous reports, which provided *in vivo* evidence for an anti-invasive, anti-metastatic and tumor-suppressive function of Slit2 in other tumor entities [221, 286, 292, 295]. Indeed, re-expression of Slit2 has been shown to attenuate lung metastasis of intravenously injected fibrosarcoma cells [292], and to prevent invasive growth of orthotopically injected glioma cells into the brain of mice [295]. The inhibitory effect of Slit2 on glioma cell metastasis in the brain was attributed to the property of recombinant or tumor cell-derived Slit2 to constrain glioma cell migration and invasion *in vitro* via inactivation of CDC42 activity [295].

Mechanistically, Slit2-mediated inhibition of invasion and metastasis that we observed in our *in vivo* models, might be the result of an impaired tumor cell motility, as evidenced by our *in vitro* experiments. Slit2 re-expression indeed inhibited directed migration and invasion of pancreatic cancer cells without affecting proliferation or random migration. Meanwhile, a growing body of studies has highlighted a central role of Slit2 signaling via Robo receptors in the control of cell motility of a variety of different cancer cell lines, such as breast cancer [286, 296-298], lung cancer [221], melanoma [222], medulloblastoma [299], glioma [295, 300], fibrosarcoma, and squamous cell carcinoma [292] cells.

Metastasis may however also depend, at least in part, on tumor size. Hence, the reduced invasion and metastatic spread that we observed in our *in vivo* tumor models might have been the consequence of a reduction in tumor mass. However, only one of our three models revealed a moderate but significant reduction of primary tumor growth (MiaPaCa$^{TR\text{-}Slit2}$ xenografts). Both other approaches showed a trend towards either reduced tumor growth in the case of Slit2 re-expression in Panc02^{Slit2} xenografts or enhanced primary tumor mass in the DANG$^{Robo1\text{-}KD}$ mouse model. Since a significant effect of Slit2-Robo on metastasis was even present in these orthotopic models without altered tumor growth, one may conclude that the role of Slit2-Robo for metastasis is independent from the primary tumor mass. This notion is further supported by our size-matched analysis in the MiaPaCa$^{TR\text{-}Slit2}$ xenograft model, which revealed that metastasis occurred in a tumor size independent manner.

It was interesting to note that Slit2-Robo effects on primary tumor growth varied between our different *in vivo* models. Remarkably, this inconsistence was not observed *in vitro*, where neither MiaPaCa$^{TR\text{-}Slit2}$ cells with Slit2 induction nor the DANG$^{Robo1\text{-}KD}$ cells displayed altered proliferation, when compared to their respective controls. However, the observed reduction in the tumor size of MiaPaCa$^{TR\text{-}Slit2}$ xenografts is consistent with several reports in the literature, e.g. inhibition of tumor growth in orthotopic and subcutaneous *in vivo* models of breast cancer [223, 286, 297]. The divergent effects of Slit2 on MiaPaCa$^{TR\text{-}Slit2}$ proliferation and primary tumor growth are similar to those observed for the breast cancer cell line MDA-MB 231, in which Slit2 had no impact on *in vitro* proliferation [301], but suppressed tumor growth *in vivo* [223]. Differences in the composition or abundance of the tumor stroma, which also participates in Slit2-Robo signaling [224, 286], offers a possible explanation for the divergent effects on primary tumor growth in our *in vivo* models.

Together, our data characterize Slit2-Robo as a suppressor of metastasis and invasive growth. Furthermore, they indicate that this function in the control of metastasis can be separated from effects on primary tumor growth.

4.2.3 Context-dependent Slit2-Robo signaling might mediate diverging functions on tumor metastasis

Our analyses provide convincing evidence for a function of Slit2-Robo in PDAC as a negative regulator of invasion and metastasis, which is in line with the majority of data derived from other tumor entities [Reviewed in 161]. However, some previous reports demonstrated a pro-metastatic function of Slit2. Indeed, knockdown of endogenous Robo1 or functional blockade of Slit2-Robo1 interaction in colorectal epithelial carcinoma cells, resulted in reduced tumor growth and liver metastasis in a subcutaneous athymic mouse model [287]. Furthermore, overexpression of Slit2 stimulated tumor lymphangiogenesis and lymphatic metastasis of pancreatic neuroendocrine islet tumors in the RIP1-Tag model [211].

Reports of a Slit2-Robo mediated stimulation of metastasis *in vivo* are accompanied by studies that demonstrated a pro-migratory function of Slit2-Robo on tumor cells *in vitro* [287, 301-303]. Thus, Slit2-Robo stimulated migration of breast cancer, gastric cancer, colorectal carcinoma and Src-transformed mouse embryonic cells, as well as human mesothelioma cells [287, 301-303].

These divergent findings about the role of Slit2-Robo in different tumor entities and experimental models suggest that the Slit2-Robo function is cell-context and/or organ specific. Several explanations for these discrepancies have emerged, such as modulation of Slit2-Robo signaling by extracellular matrix proteins [304] and proteolytic processing [176, 299, 305-307], as observed for endothelial cells in the current study (as discussed below).

4.2.4 Regulation of angiogenesis and endothelial cell motility by Slit2 in PDAC

To date, there is no consensus on the exact role of Slit2-Robo signaling in angiogenesis, and few studies have addressed this issue in the specific context of tumor neoangiogenesis. Several published reports point towards an inhibitory function of Slit2-Robo in angiogenesis. Thus, Slit2 impaired VEGF induced vessel permeability via Robo4 in mouse models of retinal and choroidal vascular disease [201, 208], and exerted inhibitory effects on basic fibroblast growth factor (bFGF)-mediated neo-vascularization in the rat cornea [209]. However, pro-angiogenic functions of Slit2-Robo signaling have also been observed in a subcutaneous melanoma mouse model [210]. Furthermore, lymphatic vessel length was found increased in pancreatic endocrine tumors from RIP-tag mice with transgenic expression of Slit2 [211]. These variable *in vivo* findings are reflected by contradictory data regarding the function of Slit-Robo for endothelial and mural cells *in vitro*, which either support an anti-angiogenic [175, 197, 201, 208, 209, 264, 286, 308-311] or a pro-angiogenic role [173, 210, 211, 312, 313]. On the one hand, Slit2 activation of Robo4 was found to abrogate VEGF-induced migration, tube formation and permeability of endothelial cells *in vitro* [201, 311]. This inhibitory effect of Slit2-Robo4 on endothelial cell migration was linked to Ras-Raf-Mek-Erk signaling [311], and blockade of Rac by a Robo4-paxillin complex at the cell surface [208, 314]. On the other hand, recombinant Slit2 was found to stimulate endothelial cell migration and tube formation *in vitro* via Robo1 and phosphatidylinositol kinase [210], suggesting that cell- and/or context-specific activation of signaling cascades determine the outcome of Slit2-Robo interactions on endothelial cells.

Results from our *in vivo* PDAC models point to an inhibition of angiogenesis by Slit2-Robo in the context of PDAC, because reduced micro vessel densities were observed *in vivo* in MiaPaCa$^{TR\text{-}Slit2}$ tumors with induction of Slit2. By comparison, the knockdown of Robo1 receptors in xenografted DANG$^{Robo1\text{-}KD}$ tumor cells did not affect micro

vessel densities, which was expected, as the availability of endogenous Slit2 in the vascular compartment had likely remained unchanged. However, the additional functional inactivation of endogenous Slit2 in DANG$^{Robo1\text{-}KD}$ xenografts via Robo1-Fc enhanced microvessel densities, supporting the notion of a Slit2 ligand-dependent effect on endothelial cells, as was seen in the MiaPaCa$^{TR\text{-}Slit2}$ tumors.

Although our *in vivo* models pointed towards an anti-angiogenic function of Slit2, our *in vitro* studies revealed conflicting effects on endothelial cell migration, depending on the Slit2 preparations that were utilized. While Slit2-enriched tumor cell supernatants reduced directed migration and VEGF-induced lamellipodia formation of endothelial cells, purified recombinant Slit2N stimulated endothelial cell migration, suggesting that proteolytic processing of Slit2 might modulate Slit2 activity on endothelial cell motility. The proteolytic procession of Slit2 was previously reported, and distinct functions were assigned to specific Slit2 processing variants [162]. For example, both full-length Slit2 and the N-terminal fragment were found to repel olfactory bulb neurites, whereas only the N-terminal cleavage product was able to induce growth cone collapse and branching, and full-length Slit2 even antagonized these effects [162, 315]. As mentioned before, our tumor derived supernatant contained the entire spectrum of proteolytically processed Slit2 variants, while purified recombinant Slit2N is congruent with the endogenously occurring N-terminal fragment. To be able to directly compare tumor derived supernatants with the N-terminal fragment alone to supernatants with full-length Slit2 and its proteolytic fragment, we generated MiaPaCa$^{TR\text{-}Slit2N}$ cell clones with inducible expression of Slit2N. Results indicated that Slit2N from MiaPaCa$^{TR\text{-}Slit2N}$ cell clones indeed stimulated, whereas full-length Slit2 containing supernatants inhibited the directed migration of endothelial cells *in vitro*. Hence, the ratio of full-length Slit2 versus other fragments produced by cancer cells may shift the effect of Slit2-Robo signaling between stimulation and inhibition of angiogenesis. It is thus possible that the availability and presentation of Slit2 fragments occur in a cell-type specific manner and could therefore offer an explanation for the different Slit effects on angiogenesis reported in the literature.

In contrast to the situation observed with endothelial cells, purified human Slit2N and tumor-derived full-length Slit2 equally inhibited the migration of MiaPaCa and Panc1 pancreatic cancer cells. Currently, we can only speculate on the reasons for this discrepancy. One possible explanation could be differences in the Robo receptor repertoire, for instance the differential expression of Robo4, which was proposed as an endothelial specific receptor [198, 310].

Little is known about the expression and function of Robo4 on non-endothelial cells, though expression of Robo4 in breast cancer cells has previously been reported [301]. Similarly, there is some debate, as to whether Robo4 is able to bind to Slit ligands at all [197, 199]. However, differential expression of Robo4 receptors on pulmonary microvascular endothelial cells (PMECs) versus HUVEC cells were reported, and were linked to differences in Slit2 effects on viral-induced increase of permeability [310]. There is also data providing evidence that different Robo isoforms have varying binding capacities to Slit2 and for ligand-independent functions of the Robo receptors or alternative Slit2-receptors [307, 316-318].

When we first noted the different effects between Slit2-enriched tumor cell supernatants and recombinant purified Slit2N, we also considered the Slit-dependent induction of another angiogenic factor by tumor cells. In more detail, our preparation of tumor cell supernatants could have allowed the autocrine Slit2-Robo1-mediated expression of another factor within the tumor cells, which in turn might be responsible for the observed anti-angiogenic effects *in vitro*. However, Slit2 enriched tumor cell supernatants, in which Slit2 was neutralized by addition of Robo1-Fc, lost their ability to inhibit endothelial cell migration. Hence, we concluded that no such secondary factor but Slit2 itself directly inhibited endothelial cell migration.

These *in vitro* data do not exclude synergistic or antagonistic effects of other factors in the micro-milieu (whether they are modulated by Slit2-Robo or not) in the *in vivo* context. For instance, it was shown that Slit2 acting as a single factor, stimulated angiogenesis via the mTORC2-dependent activation of AKT and Rac GTPases, whereas Slit2 in the presence of ephrinA1 had anti-angiogenic properties *in vitro* and *in vivo* [175]. Rather, we wanted to clarify that Slit2 produced by tumor cells had the capacity to directly inhibit endothelial cell migration and angiogenesis in our PDAC models.

We cannot delineate, whether the observed inhibition of angiogenesis contributed to the reduction of metastasis in the MiaPaCa$^{TR\text{-}Slit2}$ xenograft model. As Slit2 has also been implicated in the regulation of vascular permeability [310], one might speculate however that Slit2 mediated differences in vascular permeability contributed to the decreased incidence of malignant ascites in Panc02 tumors with Slit2 expression. Currently, a contribution of angioregulatory effects of Slit2 to impair metastasis appears plausible but speculative. However, DANG orthotopic tumors with Robo1 receptor knockdown, in which neovascularization was not affected, displayed enhanced metastasis. These data strongly indicate that impairment of tumor angiogenesis by Slit2 may contribute but is not the major cause of Slit2 effects on metastasis.

Taken together, Slit2 inhibited angiogenesis in some of our *in vivo* PDAC models, but this was no requirement for Slit/Robo1 effects on metastasis in PDAC.

4.2.5 Slit2-Robo signaling might alter tumor progression by affecting stromal cells in the tumor microenvironment

Chronic pancreatitis represents a risk factor for pancreatic cancer, suggesting that inflammation contributes to pancreatic carcinogenesis. Moreover, inflammation participates in the formation of a desmoplastic stroma, which is a characteristic feature of PDAC and provides the microenvironment that supports tumor progression.

Interestingly, one of the first functions recognized for Slit and Robos outside of the nervous system was their inhibitory effect on leukocyte chemotaxis [319], providing a first link between Slit2 and inflammatory processes. Specifically, Slit2 impaired SDF-1 induced chemotaxis of leukocytes via Robo1.

Since then, numerous studies have documented a functional role for Slits and Robos on the motility of various immune cells *in vitro* [176, 262, 263, 320, 321]. For instance, Slit2 was shown to negatively regulate the chemotaxis of neutrophils towards N-formyl-methionine-leucine-phenylalanine (fMLP), while leaving random migration unaffected [262]. This is interesting since we also found an effect of Slit2 on directed tumor cell migration, while we observed no effect on random migration. These effects on directed migration were further linked to the inhibitory influence of Slit2 on the activation of CDC42 and Rac2 [262]. Moreover, Slit2 inhibited SDF1-induced migration of neutrophils, but enhanced eosinophil chemotaxis [176, 320]. These differential effects of Slit on the chemotaxis of leukocytes were explained by the differential expression of the Slit-Robo downstream effector srGAP1, which consequently led to differential activation and recruitment of additional intracellular effector proteins [176]. Hence, this study provided a mechanism by which different cell types within the immune system differentially integrate Slit2-Robo signaling into diverging functions.

Several studies delineated a function for Slit2 in the process of immune cell infiltration into the desmoplastic stroma *in vivo*. For example, knockout of Slit2 and Slit3 in the murine mammary anlage induced SDF1 expression in the breast epithelium, and increased infiltration of immune cells into the desmoplastic tumor stroma, when

the mammary anlage was xenografted into the fat pad of nude mice [223]. In addition, Slit2 was found to protect the vasculature from cytokine-induced permeability [314, 322]. Hence, Slit2 may also reduce excessive vascular leakage. The latter might be important for the formation of malignant ascites, tumor cell extravasation, and metastasis in our PDAC models.

Our xenograft *in vivo* models are not ideal to address the role of the immune system for PDAC. Given the importance of Slit2 for inflammatory processes, the question arises, whether the results observed in our immunocompromised xenograft models are representative for the “true” *in vivo* situation or whether immune cell-mediated effects might change the phenotype of our models. Still, similar Slit2 effects were corroborated in the syngeneic, immunocompetent Panc02 tumor model, suggesting that the observed effects of Slit2-Robo signaling on tumor cell invasion and metastasis remain valid in the immune-competent situation.

4.3 Slit2 impairs bidirectional chemoattraction of pancreatic cancer cells and neuronal cells

Based on the function of Slit2-Robo as an established axon guidance factor during development of the nervous system, we hypothesized that Slit2-Robo signaling might be important for organ innervation of the developing pancreas and regulation of the neuronal network in the adult pancreas. We further postulate that a deregulation of these pathways might also have an impact on nerve-cancer interactions in pancreatic cancer.

Beside the effects of Slit2-Robo on tumor metastasis and angiogenesis, our data highlight a novel aspect of Slit2-Robo function in PDAC. Data from *ex vivo* DRG-PDAC cell co-cultures suggest a critical function of Slit2 for the interaction of PDAC cells with peripheral nerves, and hence for a key mechanism underlying neural invasion, i.e. neurotrophic interaction of tumor cells with nerves. Indeed, using time-lapse microscopy, our experiments monitored PDAC cell movement along the conduit provided by outgrowing neurites [103, 104]. Re-expression of Slit2 in PDAC cells impaired their capacity to navigate along contacted neurites by reducing travel distance and directionality. By comparison, Slit2 induction had no effect on the movements of tumor cells that did not engage in neurite contact, suggesting that Slit2 efficiently counteracted mechanisms that facilitate directional motility of tumor cells in the microenvironment, present in the immediate vicinity and/or created by contacting nerves.

Together with the observed strong Robo1 immunoreactivity in pancreatic nerves of human PDAC, our *in vitro* and *ex vivo* data suggest that Slit2-Robo signaling in PDAC encompasses the interaction of tumor cells with pancreatic nerves.

4.3.1 Slit2-Robo - regulators of organ innervation

The adult pancreas is characterized by a dense neuronal network [238]. It consists of parenchymal nerve fibers that are permanently subjected to structural remodeling in order to stimulate blood vessels and pancreatic ducts, thus controlling exocrine and endocrine pancreatic functions [238].

Although the role of Slit2-Robo in neuronal homeostasis of the adult pancreas has not yet been delineated, Slit2-Robo has already been implicated in the innervation of the developing pancreas. Indeed, it has been demonstrated that the spatial-temporal expression of Slit2 and Robo1 guidance cues help to confine the patterned migration of those neural crest cells, which later on initiate pancreatic innervation by enteric and sensory neurons [220]. Mechanistically, Slit2 expressed from tissues adjacent to the trajectory routes provide guidance by repelling Robo1 expressing neural crest cells and preventing them from entering regions with high concentrations of Slit2 molecules. Moreover, GDNF, which has previously been linked to Slit2-Robo signaling during ureteric bud formation, has recently been found to regulate neural colonization and homing of neuronal progenitors in the embryonic pancreas [238]. Thus, it appears conceivable that Slit ligands and Robo receptors have retained a role beyond the control of neural crest cell navigation in development, and contribute to neuronal homeostasis of the adult pancreas by guiding and/or counteracting growth factor and chemokine-mediated attraction of pancreatic nerves [220, 238].

In support of such a function, loss-of-function studies have recently implicated repulsive Slit2-Robo action in the stimulation of motor-neuron axon fasciculation during muscle innervation [151, 240], and hence extended the roles of guidance molecules in brain wiring to the correct growth and patterning of peripheral nerves during organ innervation. Indeed, motor-neurons in mice lacking Slit2, but not Slit1 or Slit3, were defasciculated into abundant individual axons *in vivo*, and $Slit2^{-/-}$ motor explants exhibited excessive axonal outgrowth *in vitro* [240].

4.3.2 Functional analysis of neural invasion *in vivo*

Currently, there is no genetically-modified orthotopic model available, that accurately recapitulates the events that occur during perineural invasion of pancreatic cancer cells *in vivo*. Furthermore, our xenograft models displayed only poor innervation as assessed by immunohistological analysis for neurofilament, and were therefore not suitable to study neural invasion, although few other studies have assessed neural invasion in xenograft models [323].

Due to the insufficient representation of neural invasion in common (orthotopic) tumor models, investigators have turned to alternative *in vivo* and *ex-vivo* models to analyze certain relevant aspects of perineural invasion.

In one of these alternative models, tumor cells were injected adjacent to a subcutaneous transplanted human nerve in nude athymic mice [324] [Reviewed in 65]. By applying this model, pancreatic cancer cell lines with high frequency of perineural invasion were identified and their gene profile correlated to perineural invasion [324] [Reviewed in 65]. Criticism of the model included that the degree of tumor cell line differentiation did not really correlate with the frequency of neural invasion and that the subcutaneous localization of the nerve does not mirror the actual environment of the pancreas [65].

In a second model, the sciatic nerve model applied by Gil and colleagues, tumor cells were implanted directly into the perineurium of the sciatic nerve [104, 105, 325, 326] [Reviewed in 65]. With this approach they could show that systemic treatment with a tyrosine kinase inhibitor against RET resulted in reduced neural invasion [104] [Reviewed in 65]. Gil *et al.* thus demonstrated the potential of this model to evaluate diagnostic tools and therapies [104, 105, 325, 326] [Reviewed in 65].

In both models described above, tumor cells are brought artificially into the vicinity of nerves, which has been a source of criticism [65]. Further studies are needed to evaluate, how accurately neural invasion is recapitulated in these *in vivo* models.

4.3.3 The DRG-tumor cell *ex vivo* neural invasion model accurately recapitulates tumor-cell nerve interactions

Despite varying limitations, these *in vivo* models proved valuable to analyze certain aspects of perineural invasion, and thus extended our knowledge about the underlying molecular processes involved in nerve-cancer interactions. However, they are experimentally complex and labor intensive. Hence, they have been supplemented and/or replaced by a 3D DRG-tumor cell co-culture model, which currently constitutes the best available *ex vivo* approach to model neural invasion. More specifically, they allow to evaluate axonal outgrowth of neurites and unidirectional migration/invasion of tumor cells along the neurites towards the ganglion of origin [103, 104, 269].

First valuable data derived from the *ex vivo* co-culture model came from a study on prostate cancer that investigated the underlying mechanisms of prostate cancer cell-nerve interactions [269]. The data obtained from these experiments demonstrated that human prostate cancer cells (Du-145, LNCaP, PC3) actively attract neurites from co-cultured mouse DRGs in a cell-density dependent-fashion and reciprocally migrate along the established neurite conduits, thus providing first conclusive data on a two-way interaction of tumor cells and nerves [269]. These results were not observed for a prostate stromal cell line (HTS-40F), indicating that these are tumor cell specific properties [269].

Other studies confirmed these findings for the pancreatic cancer cell lines MiaPaCa and T3M4, which stimulated neurite outgrowth from mouse DRGs and displayed an increased colony formation, compared to control cells cultured without DRGs [103, 327].

Microarray data revealed an upregulation of survival genes in prostate and pancreatic cancer cells in close proximity to nerves indicating that nerves provide cancer cells with growth factors (e.g. TGF-alpha, NGF and NCAM) to suppress apoptosis, creating a cancer cell growth promoting microenvironment [327, 328].

A more detailed study on the mutual interaction of pancreatic cancer cells and nerves demonstrated that nerves not only provide growth and survival signals, but also secrete factors to induce morphological changes in tumor cells (so called “cancer-cell spike formations”) in advance to neural invasion [103]. These morphological changes were cell density-dependent and occurred solely in tumor cells in close proximity to nerves, but not in tumor cells on the opposite side of the DRG [103]. Moreover, an increase of the neurotrophic factors NGF and

Artemin was observed in the progress of tumor cell migration towards the ganglion [103]. Hence, this study demonstrated that neural invasion is not just a bystander effect of a more aggressive tumor cell phenotype, but is based on the chemoattraction of tumor cells by a specific set of molecules released from nerves.

A subsequent study supported the hypothesis that tumor cells are specifically attracted by molecules that are secreted by nerves [104]. First, this study identified tumor cells with the capacity to invade nerves (pancreatic cancer cell lines Panc1 and MiaPaCa; cervical cancer cell line HeLa) and cell lines that did not have these properties (head and neck cancer QLL2, SCC25; lung adenocarcinoma H292; salivary gland mucoepidermoid adenocarcinoma H3118) [104].

Key observations from this study were similarly found in our current work. Thus, time-lapse microscopy and analysis revealed that tumor cells migrating along neurites showed an increased directionality and travelled a greater distance in comparison to cells without nerve contact [104], which is consistent with data from our experimental set-up. In contrast to our study no significant differences in the velocity of tumor cells with nerve contact and control cells were observed. This might be the consequence of different experimental conditions and or reagents resulting in a slightly different matrix composition.

In support of such a matrix-effect on cell migration, several studies provide evidence that matrix components and cell surface proteins such as integrins and cadherins, influence the migratory behavior of cells, regulating matrix stiffness and mode of migration (single cell versus collective cell migration) [261, 329-341]. Such cell–cell and cell–substrate adhesion molecules [342] were also shown to regulate directed migration via changes in cell speed [340, 341, 343] and directionality [344]. For instance, the N-cadherin expression level modulated integrin-mediated polarity and strongly impacted on the speed and directionality of glial cell migration [330, 344].

Interestingly, Slit-Robo signaling was previously linked to cadherin regulation [221, 342, 345-347]. Thus Slit and Robo signaling may influence migratory parameters, such as cell speed and directionality via interaction with ECM-proteins or juxtacrine interactions with other surface receptors [334]. This in turn could suggest that Slit2-Robo regulates migratory parameters not only via regulation of intracellular proteins that cause cytoskeletal rearrangements, but also via interaction with other surface or matrix bound proteins. In this regard, it was shown that secreted Slit2 is often bound to the cell surface [151, 348]. For instance, the glycoprotein dystroglycan, which inter alia mediates the interaction between the cytoskeleton of a cell and the extracellular matrix, was found to bind to laminin in the ECM on one side and to the laminin-G module of Slit2-C on the other side, thereby

organizing its distribution and presentation [349, 350]. Furthermore binding of full-length and N-terminal Slits to their Robo receptors on commissural axons is stabilized by syndecan, resulting in growth cone collapse and branching [349, 350].

Slit and Robo might directly regulate cell migration on the surface of adjacent cells via juxtacrine signaling as shown in a study on the migration of *Drosophila* larval sensory neurons [351]. In the proposed model cell-cell contacts are mediated via Slit2 signaling in trans with Robo1 and Robo2 ("Slit sandwich"), directing neuronal migration and correct organ positioning [351]. This example from the nervous system clearly illustrates that Slit2 binding to Robo receptors regulates cell motility not only via intracellular effector pathways, but also via context-specific juxtacrine interactions of neighboring cells. Conceivably, Slit2-Robo can elicit similar juxtacrine interactions between tumor cells, nerves and matrix. A loss of Slit2 and Robo might thus enhance tumor cell motility by relieving such juxtacrine constraints.

There is also data that demonstrate an effect of Slit2-Robo on cell velocity and directionality [352]. Specifically, Slit2 was shown to alter the directionality of neuronal migration *in vitro* and *in vivo* and to impair cell velocity, depending on the prevailing conditions [352]. In addition, soluble Slit2 enhanced the velocity of individual neural crest cells and increased the distance travelled [239]. In an *ex vivo* approach using subventricular zone (SVZ) explants, Slit-conditioned media from transfected HEK cells was shown to reduce the velocity of migrating neurons under these experimental conditions [352]. More interestingly, Slit2-Robo was shown to inhibit directed migration of glioblastoma multiforme-derived brain tumor stem-like cells (BTSC) in transwell assays and to enhance the velocity of these cells, when plated on a nano-patterned surface [353]. Furthermore, the effects of Slit2 on cell migration were associated with a Slit2-induced increase in phosphor-Akt and a reduction of β-catenin expression [353]. However, there is also data showing that Slit2-Robo influences cell migration without affecting cell speed, indicating that the influence of Slit2-Robo on the various aspects of cell migration depends on the cellular and molecular context [215, 262, 354].

4.3.4 Slit2-Robo signaling intersects with pathways that are involved in neural invasion

One of the most promising candidates with an established function for perineural invasion is GDNF, of which its co-receptors RET and GFRα1 are abundantly expressed in tumor specimen of patients with confirmed neural invasion [104]. Mechanistically, GDNF released by nerves induced neural invasion via binding to RET-receptors expressed by pancreatic cancer cells, and thus acts as a potent chemoattractant on PDAC cells [104]. Activation of CDC42 was proposed to mediate the stimulation of neural invasion by GDNF in PDAC cells [355]. Interestingly, Slit2 impaired growth factor mediated CDC42 activation in tumor cells [222] and interferes with GDNF during embryonic development [113]. It is therefore tempting to speculate that Slit2 may have inhibited neural invasion of MiaPaCa cells in our model by suppressing CDC42 activity.

An alternative mode of action for Slit2-Robo to influence the mutual interaction of cancer-cells and nerves might come from their potential to interfere with guidance molecules produced by stromal cells other than neuronal cells [113, 223]. Interestingly, tumor-invaded nerves showed an increased infiltration of endoneurial macrophages, which were further shown to be attracted by tumor-derived SDF1 [105]. Attraction and activation of endoneurial macrophages by tumor cells resulted in an increased secretion of GDNF from endoneurial macrophages and phosphorylation of RET in tumor cells [105]. Furthermore, recruitment of macrophages and neural invasion was reduced in CCR2-deficient mice in the sciatic nerve model [105]. Slit-Robo signaling, which was shown to counteract SDF1-CXCR4 effects [319] might therefore act via multi-layered mechanisms: first, via cytoskeletal rearrangements in the migrating tumor cells that respond to a chemotactic gradient, and second by changing/ antagonizing guidance cues released from specific stromal cells in the microenvironment. One could therefore postulate the following mechanism: neural invasion is negatively affected by the Slit-Robo system by restricting the migration machinery within the malignant cells and by inhibiting the expression or function of guidance molecules in neuronal or other stromal cells.

Future studies should clarify, whether nerve-associated cells, such as mural or immune cells are influenced by Slits and Robos. The contribution of inflammatory processes for neural invasion is the subject of current research [105, 356], and might be another route via which Slit-Robo signaling affects neural plasticity in pancreatic cancer. Literature and data from our laboratory suggest that Slit2 regulation of Schwann cells might be important as well [265, 267, 268, 357].

Regulation of SWCs could be intriguing for specific aspects of neural invasion as they secrete neurotrophic factors, provide the infrastructure for neuronal migration, and guide and promote neurite outgrowth [358-362]. As we could experimentally demonstrate that tumor-derived Slit2 is able to inhibit the directed migration of SWCs, Slit2-Robo signaling might thus influence the supportive function of SWCs for nerves during physiological and pathological processes such as neural invasion. For instance, it was shown that the repulsive effect of Slit2 on Schwann cell migration depends on the modulation of the intracellular Ca^{2+} release in Schwann cells by Slit2, which might be important for peripheral nerve regeneration [265].

Recently, a study was published that showed that low Slit2 expression in patients of intrahepatic cholangiocarcinoma is frequently associated with increased lymph node metastasis and more interestingly, also with perineural invasion [363]. A correlation between Slit2 and neural invasion in clinical samples of pancreatic cancer would give convincing support to the role of Slit2 as a suppressor of neural invasion that we propose. Unfortunately, neural invasion was present in almost all patients from our cohort and a first attempt to define groups based on different grading scores of neural invasion failed as the group sizes were too small to provide statistical significant results. Thus, we were not yet able to correlate Slit2 expression with an abundance of neural invasion in our patient cohort. Current research activities aim to increase our cohort size and to establish such correlations.

Together our data provide evidence for a functional role for the Slit Robo system as tumor suppressors in human pancreatic cancer. Beside its postulated function in tumor angiogenesis, we identified Slit2-Robo as regulators of tumor invasion and metastasis. Furthermore, our data highlight a novel function of these axon guidance members as inhibitors of nerve-cancer interactions that limit therapeutic approaches and determine the poor clinical outcome of PDAC.

5. Perspective/ Outlook

So far, evidence for a clinical relevant function of Slit2-Robo in PDAC as suppressors of tumor cell invasion, metastasis, angiogenesis and nerve-cancer cell interactions could be provided.

Based on our results, we plan the following future studies to extend our knowledge of Slit-Robo function in pancreatic cancer:

First, we are currently collecting more clinical samples in order to address the relation of Slit2 expression levels and neural invasion in clinical samples. Due to the high prevalence of neural invasion in surgical samples, a larger cohort will be required to obtain a representative subgroup without neural invasion for statistical analysis.

Second, quantitative expression analysis of Slit1, Slit3, Robo1 and Robo2 in patient samples with varying Slit2 mRNA levels should provide further information as to what extent other components of the Slit-Robo ligand-receptor system are affected in PDAC.

Third, consistent, with data from other studies, our experiments have yielded different effects of the Slit2 protein and its cleavage products. To further address the biological function of the Slit2 fragments for cancer progression, tumor angiogenesis and neural invasion, we have already generated inducible clones that produce and secrete either Slit2N or Slit2C. From these we hope to dissect the (divergent) functions of Slit2 and its cleavage products and their potential for balancing the final biological outcome of Slit2-Robo signaling, for instance its diverging effects on tumor angiogenesis.

Fourth, we are planning microarray analyses of our pancreatic cancer cell lines with modified Slit2/Robo expression in order to identify novel downstream targets/mediators of Slit2/Robo signaling.

Finally, we are conducting immunohistological analyses of tumors from our syngeneic immunocompetent Panc02 model in order to elucidate, whether Slit2-Robo signaling affects immune cells in the tumor stroma and thus inflammatory processes with impact on PDAC progression. This model would furthermore allow to determine effects of tumor-derived Slit2 on vascular permeability.

6. List of References

1. Stathis, A. and M.J. Moore, *Advanced pancreatic carcinoma: current treatment and future challenges.* Nat Rev Clin Oncol. **7**(3): p. 163-72.
2. Koorstra, J.B., et al., *Morphogenesis of pancreatic cancer: role of pancreatic intraepithelial neoplasia (PanINs).* Langenbecks Arch Surg, 2008. **393**(4): p. 561-70.
3. Korc, M., *Pathways for aberrant angiogenesis in pancreatic cancer.* Mol Cancer, 2003. **2**: p. 8.
4. Perini, M.V., et al., *Clinical and pathologic prognostic factors for curative resection for pancreatic cancer.* HPB (Oxford), 2008. **10**(5): p. 356-62.
5. Seufferlein, T., et al., *[S3-guideline exocrine pancreatic cancer].* Z Gastroenterol, 2013. **51**(12): p. 1395-440.
6. Vincent, A., et al., *Pancreatic cancer.* Lancet. **378**(9791): p. 607-20.
7. Zuo, H.D., et al., *CT and MR imaging patterns for pancreatic carcinoma invading the extrapancreatic neural plexus (Part II): Imaging of pancreatic carcinoma nerve invasion.* World J Radiol. **4**(1): p. 13-20.
8. Zuo, H.D., et al., *CT and MR imaging patterns for pancreatic carcinoma invading the extrapancreatic neural plexus (Part I): Anatomy, imaging of the extrapancreatic nerve.* World J Radiol. **4**(2): p. 36-43.
9. Liu, X., et al., *Enhanced pancreatic cancer gene therapy by combination of adenoviral vector expressing c-erb-B2 (Her-2/neu)-targeted immunotoxin with a replication-competent adenovirus or etoposide.* Hum Gene Ther, 2010. **21**(2): p. 157-70.
10. Motoi, F., et al., *Neoadjuvant Chemotherapy with Gemcitabine and S-1 for Resectable and Borderline Pancreatic Ductal Adenocarcinoma: Results from a Prospective Multi-institutional Phase 2 Trial.* Ann Surg Oncol.
11. Kleeff, J., et al., *Surgery for recurrent pancreatic ductal adenocarcinoma.* Ann Surg, 2007. **245**(4): p. 566-72.
12. Burris, H.A., 3rd, et al., *Improvements in survival and clinical benefit with gemcitabine as first-line therapy for patients with advanced pancreas cancer: a randomized trial.* J Clin Oncol, 1997. **15**(6): p. 2403-13.
13. Chiu, J. and T. Yau, *Metastatic pancreatic cancer: are we making progress in treatment?* Gastroenterol Res Pract, 2012. **2012**: p. 898931.
14. Cunningham, D., et al., *Phase III randomized comparison of gemcitabine versus gemcitabine plus capecitabine in patients with advanced pancreatic cancer.* J Clin Oncol, 2009. **27**(33): p. 5513-8.
15. Hubner, R.A., et al., *Gemcitabine plus capecitabine in unselected patients with advanced pancreatic cancer.* Pancreas, 2013. **42**(3): p. 511-5.
16. Herrmann, R., et al., *Gemcitabine plus capecitabine compared with gemcitabine alone in advanced pancreatic cancer: a randomized, multicenter, phase III trial of the Swiss Group for*

Clinical Cancer Research and the Central European Cooperative Oncology Group. J Clin Oncol, 2007. **25**(16): p. 2212-7.
17. Moore, M.J., et al., *Erlotinib plus gemcitabine compared with gemcitabine alone in patients with advanced pancreatic cancer: a phase III trial of the National Cancer Institute of Canada Clinical Trials Group.* J Clin Oncol, 2007. **25**(15): p. 1960-6.
18. Cinar, P. and M.A. Tempero, *Monoclonal antibodies and other targeted therapies for pancreatic cancer.* Cancer J. **18**(6): p. 653-64.
19. Choi, M., R. Kim, and M.W. Saif, *What options are available for refractory pancreatic cancer?* Jop, 2012. **13**(2): p. 163-5.
20. Conroy, T., et al., *FOLFIRINOX versus gemcitabine for metastatic pancreatic cancer.* N Engl J Med, 2011. **364**(19): p. 1817-25.
21. Heinemann, V., et al., *Meta-analysis of randomized trials: evaluation of benefit from gemcitabine-based combination chemotherapy applied in advanced pancreatic cancer.* BMC Cancer, 2008. **8**: p. 82.
22. Hu, J., et al., *A meta-analysis of gemcitabine containing chemotherapy for locally advanced and metastatic pancreatic adenocarcinoma.* J Hematol Oncol, 2011. **4**: p. 11.
23. Demols, A., et al., *Gemcitabine and oxaliplatin (GEMOX) in gemcitabine refractory advanced pancreatic adenocarcinoma: a phase II study.* Br J Cancer, 2006. **94**(4): p. 481-5.
24. Laurent, S., et al., *Feasibility of radiotherapy with concomitant gemcitabine and oxaliplatin in locally advanced pancreatic cancer and distal cholangiocarcinoma: a prospective dose finding phase I-II study.* Ann Oncol, 2009. **20**(8): p. 1369-74.
25. Petrelli, F., et al., *What else in gemcitabine-pretreated advanced pancreatic cancer? An update of second line therapies.* Rev Recent Clin Trials, 2010. **5**(1): p. 43-56.
26. Louvet, C., et al., *Gemcitabine combined with oxaliplatin in advanced pancreatic adenocarcinoma: final results of a GERCOR multicenter phase II study.* J Clin Oncol, 2002. **20**(6): p. 1512-8.
27. Rivera, F., et al., *Treatment of advanced pancreatic cancer: from gemcitabine single agent to combinations and targeted therapy.* Cancer Treat Rev, 2009. **35**(4): p. 335-9.
28. Silvestris, N., et al., *Target Therapies In Pancreatic Carcinoma.* Curr Med Chem.
29. Von Hoff, D.D., et al., *Gemcitabine plus nab-paclitaxel is an active regimen in patients with advanced pancreatic cancer: a phase I/II trial.* J Clin Oncol, 2011. **29**(34): p. 4548-54.
30. Liss, A.S. and S.P. Thayer, *Therapeutic targeting of pancreatic stroma.*, in *Pancreatic Cancer and Tumor Microenvironment*, P.J. Grippo and H.G. Munshi, Editors. 2012, Transworld Research Network: India.
31. Hirono, S., et al., *Molecular markers associated with lymph node metastasis in pancreatic ductal adenocarcinoma by genome-wide expression profiling.* Cancer Sci. **101**(1): p. 259-66.
32. Chatterjee, D., et al., *Perineural and intraneural invasion in posttherapy pancreaticoduodenectomy specimens predicts poor prognosis in patients with pancreatic ductal adenocarcinoma.* Am J Surg Pathol. **36**(3): p. 409-17.
33. Koorstra, J.B., et al., *Pancreatic carcinogenesis.* Pancreatology, 2008. **8**(2): p. 110-25.

34. Lochan, R., et al., *Genetic susceptibility in pancreatic ductal adenocarcinoma.* Br J Surg, 2008. **95**(1): p. 22-32.
35. Morris, J.P.t., S.C. Wang, and M. Hebrok, *KRAS, Hedgehog, Wnt and the twisted developmental biology of pancreatic ductal adenocarcinoma.* Nat Rev Cancer. **10**(10): p. 683-95.
36. Vitone, L.J., et al., *The inherited genetics of pancreatic cancer and prospects for secondary screening.* Best Pract Res Clin Gastroenterol, 2006. **20**(2): p. 253-83.
37. Raimondi, S., et al., *Pancreatic cancer in chronic pancreatitis; aetiology, incidence, and early detection.* Best Pract Res Clin Gastroenterol, 2010. **24**(3): p. 349-58.
38. Hruban, R.H., R.E. Wilentz, and S.E. Kern, *Genetic progression in the pancreatic ducts.* Am J Pathol, 2000. **156**(6): p. 1821-5.
39. Luttges, J., et al., *Allelic loss is often the first hit in the biallelic inactivation of the p53 and DPC4 genes during pancreatic carcinogenesis.* Am J Pathol, 2001. **158**(5): p. 1677-83.
40. Buchholz, M., et al., *Transcriptome analysis of microdissected pancreatic intraepithelial neoplastic lesions.* Oncogene, 2005. **24**(44): p. 6626-36.
41. Haugk, B., *Pancreatic intraepithelial neoplasia-can we detect early pancreatic cancer?* Histopathology. **57**(4): p. 503-14.
42. Heid, I., et al., *Early requirement of Rac1 in a mouse model of pancreatic cancer.* Gastroenterology. **141**(2): p. 719-30, 730 e1-7.
43. Hezel, A.F., et al., *Genetics and biology of pancreatic ductal adenocarcinoma.* Genes Dev, 2006. **20**(10): p. 1218-49.
44. Downward, J., *Targeting RAS signalling pathways in cancer therapy.* Nat Rev Cancer, 2003. **3**(1): p. 11-22.
45. Biankin, A.V., et al., *Pancreatic cancer genomes reveal aberrations in axon guidance pathway genes.* Nature. **491**(7424): p. 399-405.
46. Singh, S.K. and V. Ellenrieder, *Senescence in pancreatic carcinogenesis: from signalling to chromatin remodelling and epigenetics.* Gut, 2013. **62**(9): p. 1364-72.
47. Lee, K.E. and D. Bar-Sagi, *Oncogenic KRas suppresses inflammation-associated senescence of pancreatic ductal cells.* Cancer Cell, 2010. **18**(5): p. 448-58.
48. Bardeesy, N. and R.A. DePinho, *Pancreatic cancer biology and genetics.* Nat Rev Cancer, 2002. **2**(12): p. 897-909.
49. Delpu, Y., et al., *Genetic and epigenetic alterations in pancreatic carcinogenesis.* Curr Genomics, 2011. **12**(1): p. 15-24.
50. Jones, S., et al., *Core signaling pathways in human pancreatic cancers revealed by global genomic analyses.* Science, 2008. **321**(5897): p. 1801-6.
51. Hruban, R.H., et al., *Pathology of genetically engineered mouse models of pancreatic exocrine cancer: consensus report and recommendations.* Cancer Res, 2006. **66**(1): p. 95-106.
52. Mazur, P.K. and J.T. Siveke, *Genetically engineered mouse models of pancreatic cancer: unravelling tumour biology and progressing translational oncology.* Gut. **61**(10): p. 1488-500.
53. Herreros-Villanueva, M., et al., *Mouse models of pancreatic cancer.* World J Gastroenterol. **18**(12): p. 1286-94.

54. Guerra, C., et al., *Chronic pancreatitis is essential for induction of pancreatic ductal adenocarcinoma by K-Ras oncogenes in adult mice.* Cancer Cell, 2007. **11**(3): p. 291-302.
55. Carriere, C., et al., *Acute pancreatitis markedly accelerates pancreatic cancer progression in mice expressing oncogenic Kras.* Biochem Biophys Res Commun, 2009. **382**(3): p. 561-5.
56. Carriere, C., et al., *Acute pancreatitis accelerates initiation and progression to pancreatic cancer in mice expressing oncogenic Kras in the nestin cell lineage.* PLoS One, 2011. **6**(11): p. e27725.
57. Korc, M., *Pancreatic cancer-associated stroma production.* Am J Surg, 2007. **194**(4 Suppl): p. S84-6.
58. Steele, C.W., et al., *Exploiting inflammation for therapeutic gain in pancreatic cancer.* Br J Cancer, 2013. **108**(5): p. 997-1003.
59. Farrow, B., D. Albo, and D.H. Berger, *The role of the tumor microenvironment in the progression of pancreatic cancer.* J Surg Res, 2008. **149**(2): p. 319-28.
60. Bellone, G., et al., *Cytokine expression profile in human pancreatic carcinoma cells and in surgical specimens: implications for survival.* Cancer Immunol Immunother, 2006. **55**(6): p. 684-98.
61. Mahadevan, D. and D.D. Von Hoff, *Tumor-stroma interactions in pancreatic ductal adenocarcinoma.* Mol Cancer Ther, 2007. **6**(4): p. 1186-97.
62. Ijichi, H., et al., *Inhibiting Cxcr2 disrupts tumor-stromal interactions and improves survival in a mouse model of pancreatic ductal adenocarcinoma.* J Clin Invest, 2011. **121**(10): p. 4106-17.
63. Neesse, A., et al., *Stromal biology and therapy in pancreatic cancer.* Gut, 2011. **60**(6): p. 861-8.
64. Ceyhan, G.O., et al., *Nerve growth factor and artemin are paracrine mediators of pancreatic neuropathy in pancreatic adenocarcinoma.* Ann Surg. **251**(5): p. 923-31.
65. Demir IE, C.G., Liebl F, D'Haese JG, Maak M, Friess H, *Neural invasion in pancreatic cancer: The past, present and future. Cancers.* Cancers, 2010.
66. Ciardiello, F., et al., *Antiangiogenic and antitumor activity of anti-epidermal growth factor receptor C225 monoclonal antibody in combination with vascular endothelial growth factor antisense oligonucleotide in human GEO colon cancer cells.* Clin Cancer Res, 2000. **6**(9): p. 3739-47.
67. Spano, J.P., et al., *Efficacy of gemcitabine plus axitinib compared with gemcitabine alone in patients with advanced pancreatic cancer: an open-label randomised phase II study.* Lancet, 2008. **371**(9630): p. 2101-8.
68. Van Cutsem, E., et al., *Phase III trial of bevacizumab in combination with gemcitabine and erlotinib in patients with metastatic pancreatic cancer.* J Clin Oncol, 2009. **27**(13): p. 2231-7.
69. Kindler, H.L., et al., *Axitinib plus gemcitabine versus placebo plus gemcitabine in patients with advanced pancreatic adenocarcinoma: a double-blind randomised phase 3 study.* Lancet Oncol, 2011. **12**(3): p. 256-62.

70. Bergers, G. and D. Hanahan, *Modes of resistance to anti-angiogenic therapy.* Nat Rev Cancer, 2008. **8**(8): p. 592-603.
71. Liebig, C., et al., *Perineural invasion in cancer: a review of the literature.* Cancer, 2009. **115**(15): p. 3379-91.
72. Carmeliet, P. and M. Tessier-Lavigne, *Common mechanisms of nerve and blood vessel wiring.* Nature, 2005. **436**(7048): p. 193-200.
73. Ward, N.L. and J.C. Lamanna, *The neurovascular unit and its growth factors: coordinated response in the vascular and nervous systems.* Neurol Res, 2004. **26**(8): p. 870-83.
74. Ruhrberg, C., et al., *Spatially restricted patterning cues provided by heparin-binding VEGF-A control blood vessel branching morphogenesis.* Genes Dev, 2002. **16**(20): p. 2684-98.
75. Gerhardt, H., et al., *VEGF guides angiogenic sprouting utilizing endothelial tip cell filopodia.* J Cell Biol, 2003. **161**(6): p. 1163-77.
76. Hellstrom, M., et al., *Dll4 signalling through Notch1 regulates formation of tip cells during angiogenesis.* Nature, 2007. **445**(7129): p. 776-80.
77. Betsholtz, C., P. Lindblom, and H. Gerhardt, *Role of pericytes in vascular morphogenesis.* Exs, 2005(94): p. 115-25.
78. Gaengel, K., et al., *Endothelial-mural cell signaling in vascular development and angiogenesis.* Arterioscler Thromb Vasc Biol, 2009. **29**(5): p. 630-8.
79. Rymo, S.F., et al., *A two-way communication between microglial cells and angiogenic sprouts regulates angiogenesis in aortic ring cultures.* PLoS One. **6**(1): p. e15846.
80. Nicosia, R.F., et al., *Paracrine regulation of angiogenesis by different cell types in the aorta ring model.* Int J Dev Biol. **55**(4-5): p. 447-53.
81. Unoki, N., et al., *SDF-1/CXCR4 contributes to the activation of tip cells and microglia in retinal angiogenesis.* Invest Ophthalmol Vis Sci. **51**(7): p. 3362-71.
82. Fantin, A., et al., *Tissue macrophages act as cellular chaperones for vascular anastomosis downstream of VEGF-mediated endothelial tip cell induction.* Blood. **116**(5): p. 829-40.
83. Wessells, N.K. and R.P. Nuttall, *Normal branching, induced branching, and steering of cultured parasympathetic motor neurons.* Exp Cell Res, 1978. **115**(1): p. 111-22.
84. Carmeliet, P., *Blood vessels and nerves: common signals, pathways and diseases.* Nat Rev Genet, 2003. **4**(9): p. 710-20.
85. Geudens, I. and H. Gerhardt, *Coordinating cell behaviour during blood vessel formation.* Development. **138**(21): p. 4569-83.
86. Mukouyama, Y.S., et al., *Sensory nerves determine the pattern of arterial differentiation and blood vessel branching in the skin.* Cell, 2002. **109**(6): p. 693-705.
87. Gerhardt, H., et al., *Neuropilin-1 is required for endothelial tip cell guidance in the developing central nervous system.* Dev Dyn, 2004. **231**(3): p. 503-9.
88. Melani, M. and B.M. Weinstein, *Common factors regulating patterning of the nervous and vascular systems.* Annu Rev Cell Dev Biol. **26**: p. 639-65.
89. Segura, I., et al., *The neurovascular link in health and disease: an update.* Trends Mol Med, 2009. **15**(10): p. 439-51.

90. Quaegebeur, A., C. Lange, and P. Carmeliet, *The neurovascular link in health and disease: molecular mechanisms and therapeutic implications.* Neuron. **71**(3): p. 406-24.
91. Adams, R.H. and A. Eichmann, *Axon guidance molecules in vascular patterning.* Cold Spring Harb Perspect Biol. **2**(5): p. a001875.
92. De Smet, F., et al., *Mechanisms of vessel branching: filopodia on endothelial tip cells lead the way.* Arterioscler Thromb Vasc Biol, 2009. **29**(5): p. 639-49.
93. Wey, J.S., et al., *Overexpression of neuropilin-1 promotes constitutive MAPK signalling and chemoresistance in pancreatic cancer cells.* Br J Cancer, 2005. **93**(2): p. 233-41.
94. Larrivee, B., et al., *Activation of the UNC5B receptor by Netrin-1 inhibits sprouting angiogenesis.* Genes Dev, 2007. **21**(19): p. 2433-47.
95. Berge, M., et al., *Neuropilin-1 is upregulated in hepatocellular carcinoma and contributes to tumour growth and vascular remodelling.* J Hepatol. **55**(4): p. 866-75.
96. Jia, H., et al., *Neuropilin-1 antagonism in human carcinoma cells inhibits migration and enhances chemosensitivity.* Br J Cancer. **102**(3): p. 541-52.
97. Bapat, A.A., et al., *Perineural invasion and associated pain in pancreatic cancer.* Nat Rev Cancer. **11**(10): p. 695-707.
98. Fischer, C., et al., *Anti-PlGF inhibits growth of VEGF(R)-inhibitor-resistant tumors without affecting healthy vessels.* Cell, 2007. **131**(3): p. 463-75.
99. Fischer, C., et al., *FLT1 and its ligands VEGFB and PlGF: drug targets for anti-angiogenic therapy?* Nat Rev Cancer, 2008. **8**(12): p. 942-56.
100. Schulz, P., et al., *Angiopoietin-2 drives lymphatic metastasis of pancreatic cancer.* Faseb J. **25**(10): p. 3325-35.
101. Lu, X., et al., *The netrin receptor UNC5B mediates guidance events controlling morphogenesis of the vascular system.* Nature, 2004. **432**(7014): p. 179-86.
102. Mitsunaga, S., et al., *Detail histologic analysis of nerve plexus invasion in invasive ductal carcinoma of the pancreas and its prognostic impact.* Am J Surg Pathol, 2007. **31**(11): p. 1636-44.
103. Ceyhan, G.O., et al., *Neural invasion in pancreatic cancer: a mutual tropism between neurons and cancer cells.* Biochem Biophys Res Commun, 2008. **374**(3): p. 442-7.
104. Gil, Z., et al., *Paracrine regulation of pancreatic cancer cell invasion by peripheral nerves.* J Natl Cancer Inst. **102**(2): p. 107-18.
105. Cavel, O., et al., *Endoneurial macrophages induce perineural invasion of pancreatic cancer cells by secretion of GDNF and activation of RET tyrosine kinase receptor.* Cancer Res. **72**(22): p. 5733-43.
106. Ma, J., et al., *Expression of nerve growth factor and tyrosine kinase receptor A and correlation with perineural invasion in pancreatic cancer.* J Gastroenterol Hepatol, 2008. **23**(12): p. 1852-9.
107. Kolokythas, A., et al., *Nerve growth factor and tyrosine kinase A receptor in oral squamous cell carcinoma: is there an association*

with perineural invasion? J Oral Maxillofac Surg. **68**(6): p. 1290-5.
108. Chen-Tsai, C.P., M. Colome-Grimmer, and R.F. Wagner, Jr., *Correlations among neural cell adhesion molecule, nerve growth factor, and its receptors, TrkA, TrkB, TrkC, and p75, in perineural invasion by basal cell and cutaneous squamous cell carcinomas.* Dermatol Surg, 2004. **30**(7): p. 1009-16.
109. Demir, I.E., et al., *Neuronal plasticity in chronic pancreatitis is mediated via the neurturin/GFRalpha2 axis.* Am J Physiol Gastrointest Liver Physiol. **303**(9): p. G1017-28.
110. Muller, M.W., et al., *Association of axon guidance factor semaphorin 3A with poor outcome in pancreatic cancer.* Int J Cancer, 2007. **121**(11): p. 2421-33.
111. Macias, H., et al., *SLIT/ROBO1 signaling suppresses mammary branching morphogenesis by limiting basal cell number.* Dev Cell. **20**(6): p. 827-40.
112. Macias, H. and L. Hinck, *Mammary gland development.* Wiley Interdiscip Rev Dev Biol. **1**(4): p. 533-57.
113. Grieshammer, U., et al., *SLIT2-mediated ROBO2 signaling restricts kidney induction to a single site.* Dev Cell, 2004. **6**(5): p. 709-17.
114. Domyan, E.T., et al., *Roundabout receptors are critical for foregut separation from the body wall.* Dev Cell. **24**(1): p. 52-63.
115. Xian, J., et al., *Inadequate lung development and bronchial hyperplasia in mice with a targeted deletion in the Dutt1/Robo1 gene.* Proc Natl Acad Sci U S A, 2001. **98**(26): p. 15062-6.
116. Xian, J., et al., *Targeted disruption of the 3p12 gene, Dutt1/Robo1, predisposes mice to lung adenocarcinomas and lymphomas with methylation of the gene promoter.* Cancer Res, 2004. **64**(18): p. 6432-7.
117. Clark, K., E. Hammond, and P. Rabbitts, *Temporal and spatial expression of two isoforms of the Dutt1/Robo1 gene in mouse development.* FEBS Lett, 2002. **523**(1-3): p. 12-6.
118. Greenberg, J.M., et al., *Slit and robo expression in the developing mouse lung.* Dev Dyn, 2004. **230**(2): p. 350-60.
119. Liu, Y., et al., *Novel role for Netrins in regulating epithelial behavior during lung branching morphogenesis.* Curr Biol, 2004. **14**(10): p. 897-905.
120. MacMullin, A. and J.R. Jacobs, *Slit coordinates cardiac morphogenesis in Drosophila.* Dev Biol, 2006. **293**(1): p. 154-64.
121. Helenius, I.T. and G.J. Beitel, *The first "Slit" is the deepest: the secret to a hollow heart.* J Cell Biol, 2008. **182**(2): p. 221-3.
122. Santiago-Martinez, E., N.H. Soplop, and S.G. Kramer, *Lateral positioning at the dorsal midline: Slit and Roundabout receptors guide Drosophila heart cell migration.* Proc Natl Acad Sci U S A, 2006. **103**(33): p. 12441-6.
123. Liao, W.X., et al., *Perspectives of SLIT/ROBO signaling in placental angiogenesis.* Histol Histopathol. **25**(9): p. 1181-90.
124. Hebrok, M. and L.F. Reichardt, *Brain meets pancreas: netrin, an axon guidance molecule, controls epithelial cell migration.* Trends Cell Biol, 2004. **14**(4): p. 153-5.
125. Hinck, L., *The versatile roles of "axon guidance" cues in tissue morphogenesis.* Dev Cell, 2004. **7**(6): p. 783-93.

126. Goldberg, D., et al., *Slit/Robo-mediated chemorepulsion of vagal sensory axons in the fetal gut.* Dev Dyn. **242**(1): p. 9-15.
127. Ratcliffe, E.M., et al., *Netrin/DCC-mediated attraction of vagal sensory axons to the fetal mouse gut.* J Comp Neurol, 2006. **498**(5): p. 567-80.
128. Ratcliffe, E.M., F. D'Autreaux, and M.D. Gershon, *Laminin terminates the Netrin/DCC mediated attraction of vagal sensory axons.* Dev Neurobiol, 2008. **68**(7): p. 960-71.
129. Gitler, A.D., M.M. Lu, and J.A. Epstein, *PlexinD1 and semaphorin signaling are required in endothelial cells for cardiovascular development.* Dev Cell, 2004. **7**(1): p. 107-16.
130. Torres-Vazquez, J., et al., *Semaphorin-plexin signaling guides patterning of the developing vasculature.* Dev Cell, 2004. **7**(1): p. 117-23.
131. Villegas, G. and A. Tufro, *Ontogeny of semaphorins 3A and 3F and their receptors neuropilins 1 and 2 in the kidney.* Gene Expr Patterns, 2002. **2**(1-2): p. 151-5.
132. De Breuck, S., et al., *Netrin-1 expression in fetal and regenerating rat pancreas and its effect on the migration of human pancreatic duct and porcine islet precursor cells.* Diabetologia, 2003. **46**(7): p. 926-33.
133. Ito, T., et al., *Repulsive axon guidance molecule Sema3A inhibits branching morphogenesis of fetal mouse lung.* Mech Dev, 2000. **97**(1-2): p. 35-45.
134. Kagoshima, M. and T. Ito, *Diverse gene expression and function of semaphorins in developing lung: positive and negative regulatory roles of semaphorins in lung branching morphogenesis.* Genes Cells, 2001. **6**(6): p. 559-71.
135. Goel, H.L., et al., *Neuropilin-2 promotes branching morphogenesis in the mouse mammary gland.* Development. **138**(14): p. 2969-76.
136. Perala, N., et al., *Sema4C-Plexin B2 signalling modulates ureteric branching in developing kidney.* Differentiation. **81**(2): p. 81-91.
137. Yebra, M., et al., *Recognition of the neural chemoattractant Netrin-1 by integrins alpha6beta4 and alpha3beta1 regulates epithelial cell adhesion and migration.* Dev Cell, 2003. **5**(5): p. 695-707.
138. Yebra, M., et al., *Endothelium-derived Netrin-4 supports pancreatic epithelial cell adhesion and differentiation through integrins alpha2beta1 and alpha3beta1.* PLoS One. **6**(7): p. e22750.
139. Staton, C.A., *Class 3 semaphorins and their receptors in physiological and pathological angiogenesis.* Biochem Soc Trans. **39**(6): p. 1565-70.
140. Staton, C.A., et al., *Expression of class 3 semaphorins and their receptors in human breast neoplasia.* Histopathology. **59**(2): p. 274-82.
141. Ramesh, G., A. Berg, and C. Jayakumar, *Plasma netrin-1 is a diagnostic biomarker of human cancers.* Biomarkers. **16**(2): p. 172-80.
142. Castro-Rivera, E., et al., *Semaphorin 3B inhibits the phosphatidylinositol 3-kinase/Akt pathway through neuropilin-1 in*

lung and breast cancer cells. Cancer Res, 2008. **68**(20): p. 8295-303.
143. Yacoub, M., et al., *Differential expression of the semaphorin 3A pathway in prostatic cancer.* Histopathology, 2009. **55**(4): p. 392-8.
144. Kato, S., et al., *Semaphorin 4D, a lymphocyte semaphorin, enhances tumor cell motility through binding its receptor, plexinB1, in pancreatic cancer.* Cancer Sci. **102**(11): p. 2029-37.
145. Gabrovska, P.N., et al., *Semaphorin-plexin signalling genes associated with human breast tumourigenesis.* Gene. **489**(2): p. 63-9.
146. Pan, H., et al., *Autocrine semaphorin3A stimulates alpha2 beta1 integrin expression/function in breast tumor cells.* Breast Cancer Res Treat, 2009. **118**(1): p. 197-205.
147. Tseng, C.H., et al., *Sema3E/plexin-D1 mediated epithelial-to-mesenchymal transition in ovarian endometrioid cancer.* PLoS One. **6**(4): p. e19396.
148. Dumartin, L., et al., *Netrin-1 mediates early events in pancreatic adenocarcinoma progression, acting on tumor and endothelial cells.* Gastroenterology. **138**(4): p. 1595-606, 1606 e1-8.
149. Nüsslein-Volhard, C., E. Wieschaus, and H. Kluding, *Mutations affecting the pattern of the larval cuticle inDrosophila melanogaster.* Wilhelm Roux's archives of developmental biology, 1984. **193**(5): p. 267-282.
150. Rothberg, J.M., et al., *slit: an EGF-homologous locus of D. melanogaster involved in the development of the embryonic central nervous system.* Cell, 1988. **55**(6): p. 1047-59.
151. Brose, K., et al., *Slit proteins bind Robo receptors and have an evolutionarily conserved role in repulsive axon guidance.* Cell, 1999. **96**(6): p. 795-806.
152. Chedotal, A., *Slits and their receptors.* Adv Exp Med Biol, 2007. **621**: p. 65-80.
153. Mehlen, P., C. Delloye-Bourgeois, and A. Chedotal, *Novel roles for Slits and netrins: axon guidance cues as anticancer targets?* Nat Rev Cancer. **11**(3): p. 188-97.
154. Itoh, A., et al., *Cloning and expressions of three mammalian homologues of Drosophila slit suggest possible roles for Slit in the formation and maintenance of the nervous system.* Brain Res Mol Brain Res, 1998. **62**(2): p. 175-86.
155. Howitt, J.A., N.J. Clout, and E. Hohenester, *Binding site for Robo receptors revealed by dissection of the leucine-rich repeat region of Slit.* EMBO J, 2004. **23**(22): p. 4406-12.
156. Rothberg, J.M., et al., *slit: an extracellular protein necessary for development of midline glia and commissural axon pathways contains both EGF and LRR domains.* Genes Dev, 1990. **4**(12A): p. 2169-87.
157. Nguyen-Ba-Charvet, K.T. and A. Chedotal, *Role of Slit proteins in the vertebrate brain.* J Physiol Paris, 2002. **96**(1-2): p. 91-8.
158. Rothberg, J.M. and S. Artavanis-Tsakonas, *Modularity of the slit protein. Characterization of a conserved carboxy-terminal sequence in secreted proteins and a motif implicated in extracellular protein interactions.* J Mol Biol, 1992. **227**(2): p. 367-70.

159. Hohenester, E., et al., *The crystal structure of a laminin G-like module reveals the molecular basis of alpha-dystroglycan binding to laminins, perlecan, and agrin.* Mol Cell, 1999. **4**(5): p. 783-92.
160. Hohenester, E., *Structural insight into Slit-Robo signalling.* Biochem Soc Trans, 2008. **36**(Pt 2): p. 251-6.
161. Ballard, M.S. and L. Hinck, *A roundabout way to cancer.* Adv Cancer Res. **114**: p. 187-235.
162. Nguyen Ba-Charvet, K.T., et al., *Diversity and specificity of actions of Slit2 proteolytic fragments in axon guidance.* J Neurosci, 2001. **21**(12): p. 4281-9.
163. Zhang, F., et al., *Structural determinants of heparan sulfate interactions with Slit proteins.* Biochem Biophys Res Commun, 2004. **317**(2): p. 352-7.
164. Seeger, M., et al., *Mutations affecting growth cone guidance in Drosophila: genes necessary for guidance toward or away from the midline.* Neuron, 1993. **10**(3): p. 409-26.
165. Liu, Z., et al., *Extracellular Ig domains 1 and 2 of Robo are important for ligand (Slit) binding.* Mol Cell Neurosci, 2004. **26**(2): p. 232-40.
166. Sundaresan, V., et al., *The DUTT1 gene, a novel NCAM family member is expressed in developing murine neural tissues and has an unusually broad pattern of expression.* Mol Cell Neurosci, 1998. **11**(1-2): p. 29-35.
167. Kidd, T., K.S. Bland, and C.S. Goodman, *Slit is the midline repellent for the robo receptor in Drosophila.* Cell, 1999. **96**(6): p. 785-94.
168. Ypsilanti, A.R., Y. Zagar, and A. Chedotal, *Moving away from the midline: new developments for Slit and Robo.* Development. **137**(12): p. 1939-52.
169. Wong, K., et al., *Signal transduction in neuronal migration: roles of GTPase activating proteins and the small GTPase Cdc42 in the Slit-Robo pathway.* Cell, 2001. **107**(2): p. 209-21.
170. Lundstrom, A., et al., *Vilse, a conserved Rac/Cdc42 GAP mediating Robo repulsion in tracheal cells and axons.* Genes Dev, 2004. **18**(17): p. 2161-71.
171. Yang, L. and G.J. Bashaw, *Son of sevenless directly links the Robo receptor to rac activation to control axon repulsion at the midline.* Neuron, 2006. **52**(4): p. 595-607.
172. Guo, S. and S. Bao, *srGAP2 arginine methylation regulates cell migration and cell spreading through promoting dimerization.* J Biol Chem. **285**(45): p. 35133-41.
173. Sheldon, H., et al., *Active involvement of Robo1 and Robo4 in filopodia formation and endothelial cell motility mediated via WASP and other actin nucleation-promoting factors.* Faseb J, 2009. **23**(2): p. 513-22.
174. Ning, Y., et al., *Slit2-N inhibits PDGF-induced migration in rat airway smooth muscle cells: WASP and Arp2/3 involved.* Toxicology. **283**(1): p. 32-40.
175. Dunaway, C.M., et al., *Cooperative signaling between Slit2 and Ephrin-A1 regulates a balance between angiogenesis and angiostasis.* Mol Cell Biol. **31**(3): p. 404-16.
176. Ye, B.Q., et al., *Slit2 regulates attractive eosinophil and repulsive neutrophil chemotaxis through differential srGAP1*

expression during lung inflammation. J Immunol. **185**(10): p. 6294-305.
177. Bacon, C., et al., *Evidence for a role of srGAP3 in the positioning of commissural axons within the ventrolateral funiculus of the mouse spinal cord.* PLoS One. **6**(5): p. e19887.
178. Keleman, K., et al., *Comm sorts robo to control axon guidance at the Drosophila midline.* Cell, 2002. **110**(4): p. 415-27.
179. Kastenhuber, E., et al., *Netrin-DCC, Robo-Slit, and heparan sulfate proteoglycans coordinate lateral positioning of longitudinal dopaminergic diencephalospinal axons.* J Neurosci, 2009. **29**(28): p. 8914-26.
180. Rajagopalan, S., et al., *Crossing the midline: roles and regulation of Robo receptors.* Neuron, 2000. **28**(3): p. 767-77.
181. Simpson, J.H., et al., *Short-range and long-range guidance by Slit and its Robo receptors: a combinatorial code of Robo receptors controls lateral position.* Cell, 2000. **103**(7): p. 1019-32.
182. Simpson, J.H., et al., *Short-range and long-range guidance by slit and its Robo receptors. Robo and Robo2 play distinct roles in midline guidance.* Neuron, 2000. **28**(3): p. 753-66.
183. Spitzweck, B., M. Brankatschk, and B.J. Dickson, *Distinct protein domains and expression patterns confer divergent axon guidance functions for Drosophila Robo receptors.* Cell. **140**(3): p. 409-20.
184. Wang, K.H., et al., *Biochemical purification of a mammalian slit protein as a positive regulator of sensory axon elongation and branching.* Cell, 1999. **96**(6): p. 771-84.
185. Li, H.S., et al., *Vertebrate slit, a secreted ligand for the transmembrane protein roundabout, is a repellent for olfactory bulb axons.* Cell, 1999. **96**(6): p. 807-18.
186. Englund, C., et al., *Attractive and repulsive functions of Slit are mediated by different receptors in the Drosophila trachea.* Development, 2002. **129**(21): p. 4941-51.
187. Gallio, M., et al., *Rhomboid 3 orchestrates Slit-independent repulsion of tracheal branches at the CNS midline.* Development, 2004. **131**(15): p. 3605-14.
188. Zhang, H.Y., et al., *Slit1 promotes regenerative neurite outgrowth of adult dorsal root ganglion neurons in vitro via binding to the Robo receptor.* J Chem Neuroanat. **39**(4): p. 256-61.
189. Philipp, M., et al., *RabGDI controls axonal midline crossing by regulating Robo1 surface expression.* Neural Dev. **7**: p. 36.
190. Slovakova, J., et al., *The actin-binding protein Canoe/AF-6 forms a complex with Robo and is required for Slit-Robo signaling during axon pathfinding at the CNS midline.* J Neurosci. **32**(29): p. 10035-44.
191. Keleman, K., C. Ribeiro, and B.J. Dickson, *Comm function in commissural axon guidance: cell-autonomous sorting of Robo in vivo.* Nat Neurosci, 2005. **8**(2): p. 156-63.
192. Sabatier, C., et al., *The divergent Robo family protein rig-1/Robo3 is a negative regulator of slit responsiveness required for midline crossing by commissural axons.* Cell, 2004. **117**(2): p. 157-69.
193. Stein, E. and M. Tessier-Lavigne, *Hierarchical organization of guidance receptors: silencing of netrin attraction by slit through a*

Robo/DCC receptor complex. Science, 2001. **291**(5510): p. 1928-38.
194. Xu, C. and C.M. Fan, *Expression of Robo/Slit and Semaphorin/Plexin/Neuropilin family members in the developing hypothalamic paraventricular and supraoptic nuclei.* Gene Expr Patterns, 2008. **8**(7-8): p. 502-7.
195. Yamamoto, H. and K. Agata, *Optic chiasm formation in planarian I: Cooperative netrin- and robo-mediated signals are required for the early stage of optic chiasm formation.* Dev Growth Differ. **53**(3): p. 300-11.
196. Bernadskaya, Y.Y., et al., *UNC-40/DCC, SAX-3/Robo, and VAB-1/Eph polarize F-actin during embryonic morphogenesis by regulating the WAVE/SCAR actin nucleation complex.* PLoS Genet. **8**(8): p. e1002863.
197. Park, K.W., et al., *Robo4 is a vascular-specific receptor that inhibits endothelial migration.* Dev Biol, 2003. **261**(1): p. 251-67.
198. Huminiecki, L., et al., *Magic roundabout is a new member of the roundabout receptor family that is endothelial specific and expressed at sites of active angiogenesis.* Genomics, 2002. **79**(4): p. 547-52.
199. Suchting, S., et al., *Soluble Robo4 receptor inhibits in vivo angiogenesis and endothelial cell migration.* Faseb J, 2005. **19**(1): p. 121-3.
200. Huminiecki, L. and R. Bicknell, *In silico cloning of novel endothelial-specific genes.* Genome Res, 2000. **10**(11): p. 1796-806.
201. Jones, C.A., et al., *Robo4 stabilizes the vascular network by inhibiting pathologic angiogenesis and endothelial hyperpermeability.* Nat Med, 2008. **14**(4): p. 448-53.
202. Weitzman, M., E.B. Bayley, and U.P. Naik, *Robo4: a guidance receptor that regulates angiogenesis.* Cell Adh Migr, 2008. **2**(4): p. 220-2.
203. Bedell, V.M., et al., *roundabout4 is essential for angiogenesis in vivo.* Proc Natl Acad Sci U S A, 2005. **102**(18): p. 6373-8.
204. Gerhardt, H., *VEGF and endothelial guidance in angiogenic sprouting.* Organogenesis, 2008. **4**(4): p. 241-6.
205. Benjamin, L.E., et al., *Selective ablation of immature blood vessels in established human tumors follows vascular endothelial growth factor withdrawal.* J Clin Invest, 1999. **103**(2): p. 159-65.
206. Carmeliet, P. and R.K. Jain, *Angiogenesis in cancer and other diseases.* Nature, 2000. **407**(6801): p. 249-57.
207. Carmeliet, P., *VEGF gene therapy: stimulating angiogenesis or angioma-genesis?* Nat Med, 2000. **6**(10): p. 1102-3.
208. Jones, C.A., et al., *Slit2-Robo4 signalling promotes vascular stability by blocking Arf6 activity.* Nat Cell Biol, 2009. **11**(11): p. 1325-31.
209. Han, X. and M.C. Zhang, *Potential anti-angiogenic role of Slit2 in corneal neovascularization.* Exp Eye Res. **90**(6): p. 742-9.
210. Wang, B., et al., *Induction of tumor angiogenesis by Slit-Robo signaling and inhibition of cancer growth by blocking Robo activity.* Cancer Cell, 2003. **4**(1): p. 19-29.
211. Yang, X.M., et al., *Slit-Robo signaling mediates lymphangiogenesis and promotes tumor lymphatic metastasis.* Biochem Biophys Res Commun. **396**(2): p. 571-7.

212. Yuan, W., et al., *The mouse SLIT family: secreted ligands for ROBO expressed in patterns that suggest a role in morphogenesis and axon guidance.* Dev Biol, 1999. **212**(2): p. 290-306.
213. Holmes, G.P., et al., *Distinct but overlapping expression patterns of two vertebrate slit homologs implies functional roles in CNS development and organogenesis.* Mech Dev, 1998. **79**(1-2): p. 57-72.
214. Holmes, G. and L. Niswander, *Expression of slit-2 and slit-3 during chick development.* Dev Dyn, 2001. **222**(2): p. 301-7.
215. Fish, J.E., et al., *A Slit/miR-218/Robo regulatory loop is required during heart tube formation in zebrafish.* Development. **138**(7): p. 1409-19.
216. Loes, S., et al., *Slit1 is specifically expressed in the primary and secondary enamel knots during molar tooth cusp formation.* Mech Dev, 2001. **107**(1-2): p. 155-7.
217. Dickinson, R.E. and W.C. Duncan, *The SLIT-ROBO pathway: a regulator of cell function with implications for the reproductive system.* Reproduction. **139**(4): p. 697-704.
218. Strickland, P., et al., *Slit2 and netrin 1 act synergistically as adhesive cues to generate tubular bi-layers during ductal morphogenesis.* Development, 2006. **133**(5): p. 823-32.
219. Stuart, R.O., K.T. Bush, and S.K. Nigam, *Changes in gene expression patterns in the ureteric bud and metanephric mesenchyme in models of kidney development.* Kidney Int, 2003. **64**(6): p. 1997-2008.
220. Giovannone, D., et al., *Slits affect the timely migration of neural crest cells via Robo receptor.* Dev Dyn. **241**(8): p. 1274-88.
221. Tseng, R.C., et al., *SLIT2 attenuation during lung cancer progression deregulates beta-catenin and E-cadherin and associates with poor prognosis.* Cancer Res. **70**(2): p. 543-51.
222. Stella, M.C., L. Trusolino, and P.M. Comoglio, *The Slit/Robo system suppresses hepatocyte growth factor-dependent invasion and morphogenesis.* Mol Biol Cell, 2009. **20**(2): p. 642-57.
223. Marlow, R., et al., *SLITs suppress tumor growth in vivo by silencing Sdf1/Cxcr4 within breast epithelium.* Cancer Res, 2008. **68**(19): p. 7819-27.
224. Chang, P.H., et al., *Activation of Robo1 signaling of breast cancer cells by Slit2 from stromal fibroblast restrains tumorigenesis via blocking PI3K/Akt/beta-catenin pathway.* Cancer Res. **72**(18): p. 4652-61.
225. Peifer, M., et al., *Integrative genome analyses identify key somatic driver mutations of small-cell lung cancer.* Nat Genet, 2012. **44**(10): p. 1104-10.
226. Shivapurkar, N., et al., *Deletions of chromosome 4 at multiple sites are frequent in malignant mesothelioma and small cell lung carcinoma.* Clin Cancer Res, 1999. **5**(1): p. 17-23.
227. Dallol, A., et al., *SLIT2, a human homologue of the Drosophila Slit2 gene, has tumor suppressor activity and is frequently inactivated in lung and breast cancers.* Cancer Res, 2002. **62**(20): p. 5874-80.
228. Dallol, A., et al., *SLIT2 axon guidance molecule is frequently inactivated in colorectal cancer and suppresses growth of colorectal carcinoma cells.* Cancer Res, 2003. **63**(5): p. 1054-8.

229. Singh, R.K., et al., *Deletions in chromosome 4 differentially associated with the development of cervical cancer: evidence of slit2 as a candidate tumor suppressor gene.* Hum Genet, 2007. **122**(1): p. 71-81.
230. Shivapurkar, N., et al., *Deletions of chromosome 4 occur early during the pathogenesis of colorectal carcinoma.* Hum Pathol, 2001. **32**(2): p. 169-77.
231. Yu, J., et al., *The neuronal repellent SLIT2 is a target for repression by EZH2 in prostate cancer.* Oncogene. **29**(39): p. 5370-80.
232. Dallol, A., et al., *Frequent epigenetic inactivation of the SLIT2 gene in gliomas.* Oncogene, 2003. **22**(29): p. 4611-6.
233. Dunwell, T.L., et al., *Frequent epigenetic inactivation of the SLIT2 gene in chronic and acute lymphocytic leukemia.* Epigenetics, 2009. **4**(4): p. 265-9.
234. Jin, J., et al., *Epigenetic inactivation of SLIT2 in human hepatocellular carcinomas.* Biochem Biophys Res Commun, 2009. **379**(1): p. 86-91.
235. Sharma, G., et al., *Promoter hypermethylation of p16INK4A, p14ARF, CyclinD2 and Slit2 in serum and tumor DNA from breast cancer patients.* Life Sci, 2007. **80**(20): p. 1873-81.
236. Grone, J., et al., *Robo1/Robo4: differential expression of angiogenic markers in colorectal cancer.* Oncol Rep, 2006. **15**(6): p. 1437-43.
237. Latil, A., et al., *Quantification of expression of netrins, slits and their receptors in human prostate tumors.* Int J Cancer, 2003. **103**(3): p. 306-15.
238. Munoz-Bravo, J.L., et al., *GDNF is required for neural colonization of the pancreas.* Development. **140**(17): p. 3669-79.
239. De Bellard, M.E., Y. Rao, and M. Bronner-Fraser, *Dual function of Slit2 in repulsion and enhanced migration of trunk, but not vagal, neural crest cells.* J Cell Biol, 2003. **162**(2): p. 269-79.
240. Jaworski, A. and M. Tessier-Lavigne, *Autocrine/juxtaparacrine regulation of axon fasciculation by Slit-Robo signaling.* Nat Neurosci. **15**(3): p. 367-9.
241. Kaneko, N., et al., *New neurons clear the path of astrocytic processes for their rapid migration in the adult brain.* Neuron. **67**(2): p. 213-23.
242. Ito, Y., et al., *Expression of glial cell line-derived neurotrophic factor family members and their receptors in pancreatic cancers.* Surgery, 2005. **138**(4): p. 788-94.
243. Sambrook, J. and D.W. Russell, *Molecular Cloning: A Laboratory Manual*. Molecular Cloning: A Laboratory Manual. 2001: Cold Spring Harbor Laboratory Press.
244. Schulz, P., *Die biologische Signifikanz des Tumorsuppressors p16^{INK4a} und des proangiogenen Faktors Angiopoietin 2 im orthotopen humanen Pankreaskarzinommodell*. 2007, Fakultät III Prozesswissenschaften der Technischen Universität Berlin: Berlin. p. 116.
245. Furukawa, T., et al., *Long-term culture and immortalization of epithelial cells from normal adult human pancreatic ducts transfected by the E6E7 gene of human papilloma virus 16.* Am J Pathol, 1996. **148**(6): p. 1763-70.

246. Ouyang, H., et al., *Immortal human pancreatic duct epithelial cell lines with near normal genotype and phenotype.* Am J Pathol, 2000. **157**(5): p. 1623-31.
247. Livak, K.J. and T.D. Schmittgen, *Analysis of relative gene expression data using real-time quantitative PCR and the 2(-Delta Delta C(T)) Method.* Methods, 2001. **25**(4): p. 402-8.
248. Laemmli, U.K., *Cleavage of structural proteins during the assembly of the head of bacteriophage T4.* Nature, 1970. **227**(5259): p. 680-5.
249. Hillen, W. and C. Berens, *Mechanisms underlying expression of Tn10 encoded tetracycline resistance.* Annu Rev Microbiol, 1994. **48**: p. 345-69.
250. Gossen, M. and H. Bujard, *Tight control of gene expression in mammalian cells by tetracycline-responsive promoters.* Proc Natl Acad Sci U S A, 1992. **89**(12): p. 5547-51.
251. Wu, W., et al., *Directional guidance of neuronal migration in the olfactory system by the protein Slit.* Nature, 1999. **400**(6742): p. 331-6.
252. Geback, T., et al., *TScratch: a novel and simple software tool for automated analysis of monolayer wound healing assays.* Biotechniques, 2009. **46**(4): p. 265-74.
253. Hilfenhaus, G., et al., *Placental growth factor supports neuroendocrine tumor growth and predicts disease prognosis in patients.* Endocr Relat Cancer, 2013. **20**(3): p. 305-19.
254. Weidner, N., *Chapter 14. Measuring intratumoral microvessel density.* Methods Enzymol, 2008. **444**: p. 305-23.
255. Tan, A.C., et al., *Characterizing DNA methylation patterns in pancreatic cancer genome.* Mol Oncol, 2009. **3**(5-6): p. 425-38.
256. Vincent, A., et al., *Genome-wide analysis of promoter methylation associated with gene expression profile in pancreatic adenocarcinoma.* Clin Cancer Res. **17**(13): p. 4341-54.
257. Sipos, B., et al., *A comprehensive characterization of pancreatic ductal carcinoma cell lines: towards the establishment of an in vitro research platform.* Virchows Arch, 2003. **442**(5): p. 444-52.
258. Christman, J.K., *5-Azacytidine and 5-aza-2'-deoxycytidine as inhibitors of DNA methylation: mechanistic studies and their implications for cancer therapy.* Oncogene, 2002. **21**(35): p. 5483-95.
259. Kulis, M. and M. Esteller, *DNA methylation and cancer.* Adv Genet. **70**: p. 27-56.
260. Welman, A., J. Barraclough, and C. Dive, *Tetracycline regulated systems in functional oncogenomics.* Transl Oncogenomics, 2007. **2**: p. 17-33.
261. Friedl, P. and E.B. Brocker, *The biology of cell locomotion within three-dimensional extracellular matrix.* Cell Mol Life Sci, 2000. **57**(1): p. 41-64.
262. Tole, S., et al., *The axonal repellent, Slit2, inhibits directional migration of circulating neutrophils.* J Leukoc Biol, 2009. **86**(6): p. 1403-15.
263. Prasad, A., et al., *Slit-2/Robo-1 modulates the CXCL12/CXCR4-induced chemotaxis of T cells.* J Leukoc Biol, 2007. **82**(3): p. 465-76.

264. Guijarro-Munoz, I., et al., *The axonal repellent Slit2 inhibits pericyte migration: potential implications in angiogenesis.* Exp Cell Res. **318**(4): p. 371-8.
265. Wang, Y., H.L. Teng, and Z.H. Huang, *Repulsive migration of Schwann cells induced by Slit-2 through Ca2+-dependent RhoA-Myosin signaling.* Glia. **61**(5): p. 710-23.
266. Zhang, Y., et al., *Study human pancreatic cancer in mice: how close are they?* Biochim Biophys Acta. **1835**(1): p. 110-8.
267. Bockman, D.E., M. Buchler, and H.G. Beger, *Interaction of pancreatic ductal carcinoma with nerves leads to nerve damage.* Gastroenterology, 1994. **107**(1): p. 219-30.
268. Swanson, B.J., et al., *MUC1 is a counter-receptor for myelin-associated glycoprotein (Siglec-4a) and their interaction contributes to adhesion in pancreatic cancer perineural invasion.* Cancer Res, 2007. **67**(21): p. 10222-9.
269. Ayala, G.E., et al., *In vitro dorsal root ganglia and human prostate cell line interaction: redefining perineural invasion in prostate cancer.* Prostate, 2001. **49**(3): p. 213-23.
270. Malin, S.A., B.M. Davis, and D.C. Molliver, *Production of dissociated sensory neuron cultures and considerations for their use in studying neuronal function and plasticity.* Nat Protoc, 2007. **2**(1): p. 152-60.
271. Piper, M., et al., *Expression of the vertebrate Slit gene family and their putative receptors, the Robo genes, in the developing murine kidney.* Mech Dev, 2000. **94**(1-2): p. 213-7.
272. Anselmo, M.A., et al., *Slit and robo: expression patterns in lung development.* Gene Expr Patterns, 2003. **3**(1): p. 13-9.
273. Nasarre, P., et al., *Guidance molecules in lung cancer.* Cell Adh Migr. **4**(1): p. 130-45.
274. Medioni, C., et al., *Expression of Slit and Robo genes in the developing mouse heart.* Dev Dyn. **239**(12): p. 3303-11.
275. Harpaz, N., et al., *Multiplexin promotes heart but not aorta morphogenesis by polarized enhancement of slit/robo activity at the heart lumen.* PLoS Genet. **9**(6): p. e1003597.
276. Mommersteeg, M.T., et al., *Slit-roundabout signaling regulates the development of the cardiac systemic venous return and pericardium.* Circ Res. **112**(3): p. 465-75.
277. Ratcliffe, E.M., *Molecular development of the extrinsic sensory innervation of the gastrointestinal tract.* Auton Neurosci. **161**(1-2): p. 1-5.
278. Lu, P. and Z. Werb, *Patterning mechanisms of branched organs.* Science, 2008. **322**(5907): p. 1506-9.
279. Dickinson, R.E., M. Myers, and W.C. Duncan, *Novel regulated expression of the SLIT/ROBO pathway in the ovary: possible role during luteolysis in women.* Endocrinology, 2008. **149**(10): p. 5024-34.
280. Jarikji, Z., et al., *The tetraspanin Tm4sf3 is localized to the ventral pancreas and regulates fusion of the dorsal and ventral pancreatic buds.* Development, 2009. **136**(11): p. 1791-800.
281. Yang, Y.H., et al., *Intraislet SLIT-ROBO signaling is required for beta-cell survival and potentiates insulin secretion.* Proc Natl Acad Sci U S A.
282. Yang, Y.H., et al., *Paracrine signalling loops in adult human and mouse pancreatic islets: netrins modulate beta cell apoptosis*

signalling via dependence receptors. Diabetologia. **54**(4): p. 828-42.
283. Plump, A.S., et al., *Slit1 and Slit2 cooperate to prevent premature midline crossing of retinal axons in the mouse visual system.* Neuron, 2002. **33**(2): p. 219-32.
284. Bagri, A., et al., *Slit proteins prevent midline crossing and determine the dorsoventral position of major axonal pathways in the mammalian forebrain.* Neuron, 2002. **33**(2): p. 233-48.
285. Kim, H.N., et al., *Gene expression profiling in lymph node-positive and lymph node-negative pancreatic cancer.* Pancreas, 2007. **34**(3): p. 325-34.
286. Brantley-Sieders, D.M., et al., *Angiocrine factors modulate tumor proliferation and motility through EphA2 repression of Slit2 tumor suppressor function in endothelium.* Cancer Res. **71**(3): p. 976-87.
287. Zhou, W.J., et al., *Slit-Robo signaling induces malignant transformation through Hakai-mediated E-cadherin degradation during colorectal epithelial cell carcinogenesis.* Cell Res. **21**(4): p. 609-26.
288. Long, J., et al., *Development of a unique mouse model for pancreatic cancer lymphatic metastasis.* Int J Oncol, 2012. **41**(5): p. 1662-8.
289. He, H., et al., *The microRNA-218 and ROBO-1 signaling axis correlates with the lymphatic metastasis of pancreatic cancer.* Oncol Rep, 2013. **30**(2): p. 651-8.
290. Yang, L., et al., *Silencing of miRNA-218 promotes migration and invasion of breast cancer via Slit2-Robo1 pathway.* Biomed Pharmacother, 2012. **66**(7): p. 535-40.
291. Dickinson, R.E., et al., *Epigenetic inactivation of SLIT3 and SLIT1 genes in human cancers.* Br J Cancer, 2004. **91**(12): p. 2071-8.
292. Kim, H.K., et al., *Slit2 inhibits growth and metastasis of fibrosarcoma and squamous cell carcinoma.* Neoplasia, 2008. **10**(12): p. 1411-20.
293. Mouratidis, P.X., K.W. Colston, and A.G. Dalgleish, *Doxycycline induces caspase-dependent apoptosis in human pancreatic cancer cells.* Int J Cancer, 2007. **120**(4): p. 743-52.
294. Son, K., et al., *Doxycycline induces apoptosis in PANC-1 pancreatic cancer cells.* Anticancer Res, 2009. **29**(10): p. 3995-4003.
295. Yiin, J.J., et al., *Slit2 inhibits glioma cell invasion in the brain by suppression of Cdc42 activity.* Neuro Oncol, 2009. **11**(6): p. 779-89.
296. Prasad, A., et al., *Slit protein-mediated inhibition of CXCR4-induced chemotactic and chemoinvasive signaling pathways in breast cancer cells.* J Biol Chem, 2004. **279**(10): p. 9115-24.
297. Prasad, A., et al., *Slit-2 induces a tumor-suppressive effect by regulating beta-catenin in breast cancer cells.* J Biol Chem, 2008. **283**(39): p. 26624-33.
298. Yuasa-Kawada, J., et al., *Deubiquitinating enzyme USP33/VDU1 is required for Slit signaling in inhibiting breast cancer cell migration.* Proc Natl Acad Sci U S A, 2009. **106**(34): p. 14530-5.
299. Werbowetski-Ogilvie, T.E., et al., *Inhibition of medulloblastoma cell invasion by Slit.* Oncogene, 2006. **25**(37): p. 5103-12.

300. Mertsch, S., et al., *Slit2 involvement in glioma cell migration is mediated by Robo1 receptor.* J Neurooncol, 2008. **87**(1): p. 1-7.
301. Schmid, B.C., et al., *The neuronal guidance cue Slit2 induces targeted migration and may play a role in brain metastasis of breast cancer cells.* Breast Cancer Res Treat, 2007. **106**(3): p. 333-42.
302. Tie, J., et al., *MiR-218 inhibits invasion and metastasis of gastric cancer by targeting the Robo1 receptor.* PLoS Genet. **6**(3): p. e1000879.
303. Khusial, P.R., et al., *Src activates Abl to augment Robo1 expression in order to promote tumor cell migration.* Oncotarget. **1**(3): p. 198-209.
304. Ronca, F., et al., *Characterization of Slit protein interactions with glypican-1.* J Biol Chem, 2001. **276**(31): p. 29141-7.
305. Seiradake, E., et al., *Structure and functional relevance of the Slit2 homodimerization domain.* EMBO Rep, 2009. **10**(7): p. 736-41.
306. Chen, Z.B., et al., *Slit-Robo GTPase-activating proteins are differentially expressed in murine dorsal root ganglia: modulation by peripheral nerve injury.* Anat Rec (Hoboken). **295**(4): p. 652-60.
307. Camurri, L., et al., *Evidence for the existence of two Robo3 isoforms with divergent biochemical properties.* Mol Cell Neurosci, 2005. **30**(4): p. 485-93.
308. Acevedo, L.M., S.M. Weis, and D.A. Cheresh, *Robo4 counteracts VEGF signaling.* Nat Med, 2008. **14**(4): p. 372-3.
309. Liu, D., et al., *Neuronal chemorepellent Slit2 inhibits vascular smooth muscle cell migration by suppressing small GTPase Rac1 activation.* Circ Res, 2006. **98**(4): p. 480-9.
310. Gorbunova, E.E., I.N. Gavrilovskaya, and E.R. Mackow, *Slit2-Robo4 receptor responses inhibit ANDV directed permeability of human lung microvascular endothelial cells.* Antiviral Res. **99**(2): p. 108-12.
311. Seth, P., et al., *Magic roundabout, a tumor endothelial marker: expression and signaling.* Biochem Biophys Res Commun, 2005. **332**(2): p. 533-41.
312. Kaur, S., et al., *Robo4 signaling in endothelial cells implies attraction guidance mechanisms.* J Biol Chem, 2006. **281**(16): p. 11347-56.
313. Kaur, S., et al., *Silencing of directional migration in roundabout4 knockdown endothelial cells.* BMC Cell Biol, 2008. **9**: p. 61.
314. London, N.R. and D.Y. Li, *Robo4-dependent Slit signaling stabilizes the vasculature during pathologic angiogenesis and cytokine storm.* Curr Opin Hematol. **18**(3): p. 186-90.
315. Nguyen-Ba-Charvet, K.T., et al., *Sensory axon response to substrate-bound Slit2 is modulated by laminin and cyclic GMP.* Mol Cell Neurosci, 2001. **17**(6): p. 1048-58.
316. Zheng, W., et al., *Robo4 regulates the radial migration of newborn neurons in developing neocortex.* Cereb Cortex. **22**(11): p. 2587-601.
317. Fujisawa, K., J.L. Wrana, and J.G. Culotti, *The slit receptor EVA-1 coactivates a SAX-3/Robo mediated guidance signal in C. elegans.* Science, 2007. **317**(5846): p. 1934-8.

318. James, G., et al., *The Expression Pattern of EVA1C, a Novel Slit Receptor, Is Consistent with an Axon Guidance Role in the Mouse Nervous System.* PLoS One. **8**(9): p. e74115.
319. Wu, J.Y., et al., *The neuronal repellent Slit inhibits leukocyte chemotaxis induced by chemotactic factors.* Nature, 2001. **410**(6831): p. 948-52.
320. Geutskens, S.B., P.L. Hordijk, and P.B. van Hennik, *The chemorepellent Slit3 promotes monocyte migration.* J Immunol. **185**(12): p. 7691-8.
321. Shibata, F., et al., *Roundabout 4 is expressed on hematopoietic stem cells and potentially involved in the niche-mediated regulation of the side population phenotype.* Stem Cells, 2009. **27**(1): p. 183-90.
322. London, N.R., et al., *Targeting Robo4-dependent Slit signaling to survive the cytokine storm in sepsis and influenza.* Sci Transl Med. **2**(23): p. 23ra19.
323. Eibl, G. and H.A. Reber, *A xenograft nude mouse model for perineural invasion and recurrence in pancreatic cancer.* Pancreas, 2005. **31**(3): p. 258-62.
324. Koide, N., et al., *Establishment of perineural invasion models and analysis of gene expression revealed an invariant chain (CD74) as a possible molecule involved in perineural invasion in pancreatic cancer.* Clin Cancer Res, 2006. **12**(8): p. 2419-26.
325. Gil, Z., et al., *Nerve-sparing therapy with oncolytic herpes virus for cancers with neural invasion.* Clin Cancer Res, 2007. **13**(21): p. 6479-85.
326. Gil, Z., et al., *Utility of a herpes oncolytic virus for the detection of neural invasion by cancer.* Neoplasia, 2008. **10**(4): p. 347-53.
327. Dai, H., et al., *Enhanced survival in perineural invasion of pancreatic cancer: an in vitro approach.* Hum Pathol, 2007. **38**(2): p. 299-307.
328. Yang, G., et al., *Perineural invasion of prostate carcinoma cells is associated with reduced apoptotic index.* Cancer, 1996. **78**(6): p. 1267-71.
329. Ghashghaei, H.T., C. Lai, and E.S. Anton, *Neuronal migration in the adult brain: are we there yet?* Nat Rev Neurosci, 2007. **8**(2): p. 141-51.
330. Kasemeier-Kulesa, J.C., et al., *Eph/ephrins and N-cadherin coordinate to control the pattern of sympathetic ganglia.* Development, 2006. **133**(24): p. 4839-47.
331. Kasemeier-Kulesa, J.C., et al., *CXCR4 controls ventral migration of sympathetic precursor cells.* J Neurosci. **30**(39): p. 13078-88.
332. Kearns, S.M., et al., *Extracellular matrix effects on neurosphere cell motility.* Exp Neurol, 2003. **182**(1): p. 240-4.
333. Schmidt, S. and P. Friedl, *Interstitial cell migration: integrin-dependent and alternative adhesion mechanisms.* Cell Tissue Res. **339**(1): p. 83-92.
334. Mehes, E., et al., *Dystroglycan is involved in laminin-1-stimulated motility of Muller glial cells: combined velocity and directionality analysis.* Glia, 2005. **49**(4): p. 492-500.
335. Palecek, S.P., et al., *Integrin-ligand binding properties govern cell migration speed through cell-substratum adhesiveness.* Nature, 1997. **385**(6616): p. 537-40.

336. Fereol, S., et al., *Micropatterned ECM substrates reveal complementary contribution of low and high affinity ligands to neurite outgrowth.* Cytoskeleton (Hoboken). **68**(7): p. 373-88.
337. Gritsenko, P.G., O. Ilina, and P. Friedl, *Interstitial guidance of cancer invasion.* J Pathol. **226**(2): p. 185-99.
338. Zaman, M.H., et al., *Migration of tumor cells in 3D matrices is governed by matrix stiffness along with cell-matrix adhesion and proteolysis.* Proc Natl Acad Sci U S A, 2006. **103**(29): p. 10889-94.
339. Baker, E.L., R.T. Bonnecaze, and M.H. Zaman, *Extracellular matrix stiffness and architecture govern intracellular rheology in cancer.* Biophys J, 2009. **97**(4): p. 1013-21.
340. Friedl, P., E.B. Brocker, and K.S. Zanker, *Integrins, cell matrix interactions and cell migration strategies: fundamental differences in leukocytes and tumor cells.* Cell Adhes Commun, 1998. **6**(2-3): p. 225-36.
341. Friedl, P., K.S. Zanker, and E.B. Brocker, *Cell migration strategies in 3-D extracellular matrix: differences in morphology, cell matrix interactions, and integrin function.* Microsc Res Tech, 1998. **43**(5): p. 369-78.
342. Rhee, J., et al., *Cables links Robo-bound Abl kinase to N-cadherin-bound beta-catenin to mediate Slit-induced modulation of adhesion and transcription.* Nat Cell Biol, 2007. **9**(8): p. 883-92.
343. Shih, W. and S. Yamada, *N-cadherin as a key regulator of collective cell migration in a 3D environment.* Cell Adh Migr. **6**(6): p. 513-7.
344. Camand, E., et al., *N-cadherin expression level modulates integrin-mediated polarity and strongly impacts on the speed and directionality of glial cell migration.* J Cell Sci. **125**(Pt 4): p. 844-57.
345. Bauer, K., et al., *Slit-2 facilitates interaction of P-cadherin with Robo-3 and inhibits cell migration in an oral squamous cell carcinoma cell line.* Carcinogenesis. **32**(6): p. 935-43.
346. Santiago-Martinez, E., et al., *Repulsion by Slit and Roundabout prevents Shotgun/E-cadherin-mediated cell adhesion during Drosophila heart tube lumen formation.* J Cell Biol, 2008. **182**(2): p. 241-8.
347. Loveless, T. and J. Hardin, *Cadherin complexity: recent insights into cadherin superfamily function in C. elegans.* Curr Opin Cell Biol. **24**(5): p. 695-701.
348. Hohenester, E., S. Hussain, and J.A. Howitt, *Interaction of the guidance molecule Slit with cellular receptors.* Biochem Soc Trans, 2006. **34**(Pt 3): p. 418-21.
349. Blockus, H. and A. Chedotal, *Dystroglycan adds more sugars to the midline cocktail.* Neuron. **76**(5): p. 864-7.
350. Wright, K.M., et al., *Dystroglycan organizes axon guidance cue localization and axonal pathfinding.* Neuron. **76**(5): p. 931-44.
351. Kraut, R. and K. Zinn, *Roundabout 2 regulates migration of sensory neurons by signaling in trans.* Curr Biol, 2004. **14**(15): p. 1319-29.
352. Ward, M., et al., *Distinguishing between directional guidance and motility regulation in neuronal migration.* J Neurosci, 2003. **23**(12): p. 5170-7.

353. Chen, L., et al., *CONTROLLING THE MIGRATION OF GBM CELLS: LESSONS FROM NEUROGENIC NICHES.* Neuro-Oncology, 2011. **13**(suppl 3): p. iii145-iii153.
354. Xu, H.T., et al., *Calcium signaling in chemorepellant Slit2-dependent regulation of neuronal migration.* Proc Natl Acad Sci U S A, 2004. **101**(12): p. 4296-301.
355. Chernichenko, N., et al., *The role of Cdc42 in cancer cell perineural invasion.* Cancer Res, 2012. **72 (8 Suppl)**(8 Suppl): p. Abstract nr 460.
356. Demir, I.E., et al., *Perineural mast cells are specifically enriched in pancreatic neuritis and neuropathic pain in pancreatic cancer and chronic pancreatitis.* PLoS One. **8**(3): p. e60529.
357. Luo, X.L., et al., *The role of Schwann cell differentiation in perineural invasion of adenoid cystic and mucoepidermoid carcinoma of the salivary glands.* Int J Oral Maxillofac Surg, 2006. **35**(8): p. 733-9.
358. Thompson, D.M. and H.M. Buettner, *Oriented Schwann cell monolayers for directed neurite outgrowth.* Ann Biomed Eng, 2004. **32**(8): p. 1120-30.
359. Thompson, D.M. and H.M. Buettner, *Neurite outgrowth is directed by schwann cell alignment in the absence of other guidance cues.* Ann Biomed Eng, 2006. **34**(1): p. 161-8.
360. Koppes, A.N., A.M. Seggio, and D.M. Thompson, *Neurite outgrowth is significantly increased by the simultaneous presentation of Schwann cells and moderate exogenous electric fields.* J Neural Eng. **8**(4): p. 046023.
361. Seggio, A.M., et al., *Self-aligned Schwann cell monolayers demonstrate an inherent ability to direct neurite outgrowth.* J Neural Eng. **7**(4): p. 046001.
362. Suri, S. and C.E. Schmidt, *Cell-laden hydrogel constructs of hyaluronic acid, collagen, and laminin for neural tissue engineering.* Tissue Eng Part A. **16**(5): p. 1703-16.
363. Mano, Y., et al., *Decreased roundabout 1 expression promotes development of intrahepatic cholangiocarcinoma.* Hum Pathol.

7. Supplementary

7.1 Immunohistochemical staining for Slit2

For the detection of Slit2 on frozen cryosections, we tried several immunohistochemical approaches. Unfortunately, different antibodies revealed different patterns of immunoreactivity, which could not be validated in cell lines with known Slit2 expression that were processed in parallel. As most published immunohistochemical stainings for Slit2 were conducted on paraffin embedded tissues, we collaborated with Dr. Ruza Arsenic (Department of Pathology, Charité), who conducted immunohistochemistry for Slit2 on paraffin embedded tissues in order to determine Slit2 expression on paraffin material of PDAC tissues [please refer to Suppl. Figure 1-2]. Paraffin-embedded samples of cultured PDAC cell lines for validation of Slit2 immunoreactivity were provided by our laboratory and also included. Two commercially available Slit2-antibodies (Chemicon AB5701, Sigma-Aldrich HPA023088) were tested, which have been reported as suitable for Slit2 immunohistochemistry, using published protocols. Paraffin sections from PDAC specimens were used, which also included areas of non-transformed pancreas and small intestine. In parallel, we quantified Slit2 mRNA levels in cryosections of the same tissues used for immunohistochemistry via qRT-PCR to verify the plausibility of the immunohistochemical results. Several problems were noted: First, striking differences in the distribution pattern of Slit2 immunoreactivity between the two applied antibodies were noticed. Second, data obtained by qRT-PCR analysis were not conform to the immunoreactivity observed. Finally, Slit2 immunoreactivity was present on sections of paraffin-embedded pancreatic tumor cell lines (please refer to Suppl. Figure 3), which were consistently tested negative in both qualitative and quantitative Slit2 PCR.

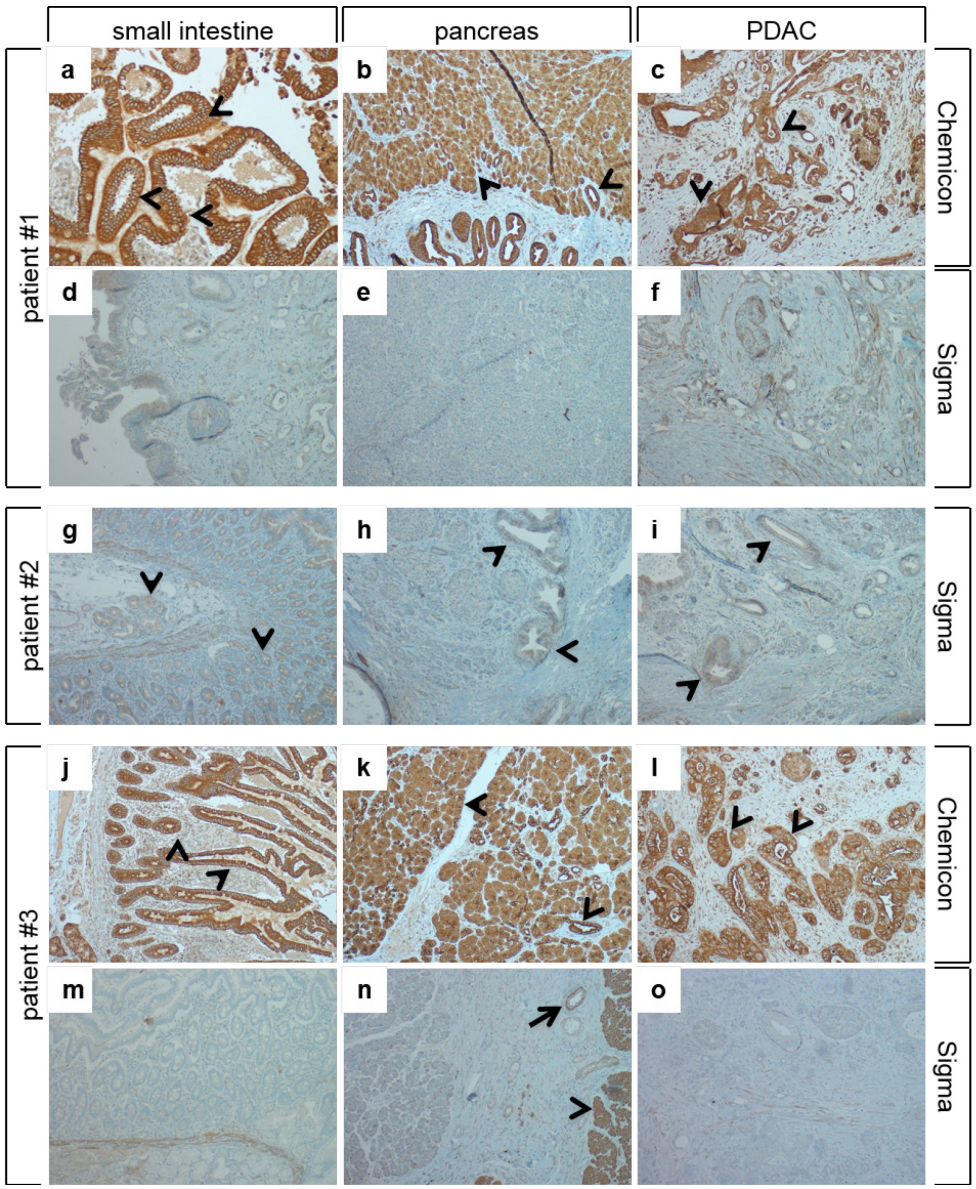

Suppl. Figure 1: Immunohistochemical staining for Slit2 on human small intestinal, pancreatic and PDAC tissues

Paraffin embedded clinical specimens from patients who underwent surgery due to PDAC were used for immunostaining utilizing two different Slit2 antibodies (Chemicon AB5701, dilution 1:200; Sigma HPA023088, dilution 1:25). Shown are representative areas of adjacent tissues of small intestine, pancreas and PDAC within the same clinical specimen. Of note, immunoreactivity for the Chemicon antibody localized to epithelial cells of non-transformed pancreas (arrowhead in b and k) and PDAC (arrowhead in c and l) but also equally intense to epithelial cells of the small intestine (arrowhead in a and j). Immunoreactivity for the Sigma antibody was best in vascular structures (arrow in n) and smooth musculature (arrowhead in n), and less in epithelia of small intestine, pancreas and PDAC (arrowheads in g-i).

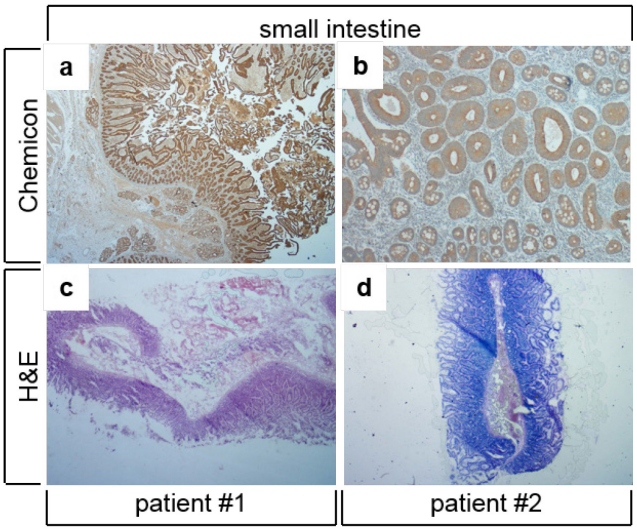

Suppl. Figure 2: Immunohistochemical staining for Slit2 on human small intestinal

Frozen tissues of small intestine (d and d) obtained from the same clinical specimens used for paraffin sections and Slit2 immunostaining (a, b) were harvested and used for subsequent Slit2 qRT-PCR analysis. H&E staining on several intermittent cryosections confirmed that these tissues were small intestinal origin only (c, d). Of note, whereas qRT-PCR data indicated a 100-200 fold lower Slit2 expression in small intestine than in the non-transformed pancreatic tissues, immunoreactivity against Slit2 antibodies was equally strong in small intestine (a, b) and non-transformed pancreatic tissue (please refer to Suppl. Figure 1).

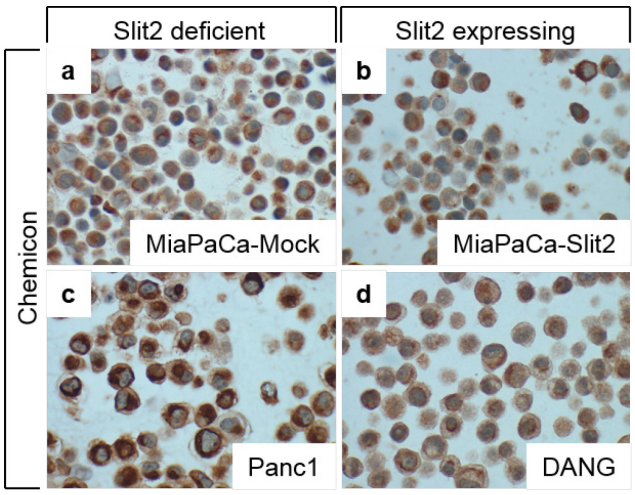

Suppl. Figure 3: Immunohistochemical staining formalin-fixed, paraffin-embedded tumor cell pellets

Formalin-fixed and paraffin-embedded (FFPE) cell pellets obtained from tumor cells with either ectopic or endogenous Slit2 expression (b and d) versus Mock-transfected and Slit2-deficient tumor cell lines (a and c) were used for immunostaining against Slit2. Of note, intense immunoreactivity was detected in Mock-transfected MiaPaCa and Panc1 cells which lack endogenous Slit2 expression (a, c).

Immunohistological staining approaches with antibodies against Slit2 were done in collaboration with Dr. Ruza Arsenic (Department of Pathology, Charité) and included in the supplementary section of this thesis with her permission.

7.2 MiaPaCa cell clones with inducible expression of full-length Slit2, Slit2N and Slit2C

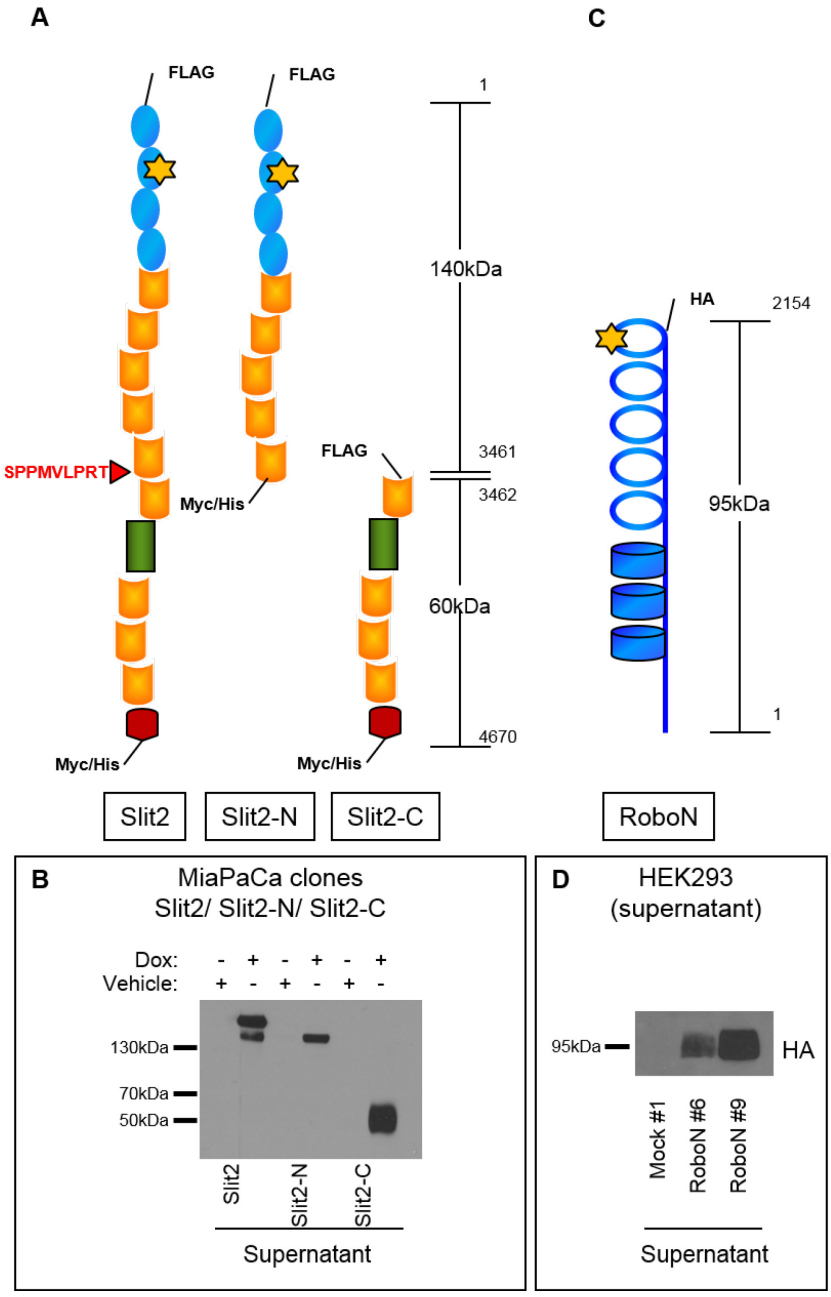

Suppl. Figure 4: Schematic representation of the recombinant Slit2 fragments and soluble RoboN used for the transfection

(A) Schematic representation of cDNA constructs encoding for full-length Slit2, Slit2N and Slit2C. The full-length Slit2 ligand consists of 1469aa (~200 kDa), comprising four leucine-rich domains (LRR), located at the N-terminus, followed by nine epidermal growth factor (EGF)-like repeats, which are separated by an ALPS domain (Agrin, Laminin, Perlecan, Slit) and a cysteine knot at the C-terminus. Full-length Slit2 is proteolytically cleaved at aa1110-1118 (SPPMVLPRT) creating an additional N-terminal (B; ~140 kDa) and a C-terminal (C; ~60 kDa) fragment. **(B)** Using the

doxycycline-inducible T-Rex™ vector system, MiaPaCa$^{TR\text{-}Slit2}$ cells with inducible expression of full-length human Slit2, Slit2N and Slit2C were generated by transfection with a Slit2-cDNA constructs that comprise either the nucleotides 1-4670 (full-length; ~200 kDa), 1-3461 (N-terminal fragment; ~140 kDa) or 3462-4670 (C-terminal fragment; ~60 kDa) . For convenient detection of Slit2, an N-terminal Flag-tag and a C-terminal myc-HIS-tag flank each Slit2-fragment. Inducible expression and secretion of the Flag-tagged Slit2/-N/-C protein was confirmed using immunoblotting of TCA-precipitates from MiaPaCa$^{TR\text{-}Slit2/\text{-}N/\text{-}C}$ cell culture supernatants following treatment with doxycycline (Dox: 1 µg/ml for 48 h) as compared to vehicle treated controls. Proteolytic cleavage of full-length Slit2 (~200 kDa) resulted in the generation of the N-terminal Slit2 fragment (Slit2N, ~140 kDa). **(C)** Schematic representation of the cDNA construct encoding for the soluble N-terminal fragment of Robo1 (RoboN). The extracellular domain consists of several Ig domains and fibronectin type III repeats (Fn3), with varying numbers between the receptor isoforms. **(D)** HEK293 cells were stably transfected with RoboN and respective Mock-control vectors. Soluble RoboN (~95 kDa) was detected with an antibody against the HA-tag in supernatants of transfected HEK293 cells but not in Mock control cells.[IV]

[IV] RoboN immunoblot in suppl. figure 4D was kindly provided by M. Welzel

8. Index

8.1 Index of figures

8.2 Index of tables

Erklärung

Hiermit versichere ich, dass ich die vorliegende Dissertation eigenständig und nur unter der Verwendung, der angegebenen Hilfsmittel angefertigt habe. Ich versichere außerdem, dass ich mich weder anderwärts um einen Doktorgrad beworben habe, noch einen entsprechenden Doktorgrad besitze. Ich erkläre hiermit, dass mir die geltende Promotionsordnung vom 06.07.2009 bekannt ist.

Berlin, den

Andreas Göhrig

Publications and Conferences

Publications

- **A. Göhrig**, K. M. Detjen, G. Hilfenhaus, J. Körner, M. Welzel, R. Arsenic, R. Schmuck, M. Bahra, J. Y. Wu, B. Wiedenmann, and C. Fischer. Axon Guidance Factor SLIT2 Inhibits Neural Invasion and Metastasis in Pancreatic Cancer. Cancer Research, 2014 March 1.

- **G. Hilfenhaus**, **A. Göhrig**, U. F. Pape, T. Neumann, H. Jann, D. Zdunek, G. Hess, J. M. Stassen, B. Wiedenmann, K. Detjen, M. Pavel, and C. Fischer. Placental growth factor supports neuroendocrine tumor growth and predicts disease prognosis in patients. Endocrine-Related Cancer, 2013 May 20, Volume 20, Page 305-319.

Conferences

- **A. Göhrig**, K. M. Detjen, G. Hilfenhaus, J. Körner, M. Welzel, R. Arsenic, R. Schmuck, M. Bahra, J. Y. Wu, B. Wiedenmann, and C. Fischer. Das *Axon Guidance* Molekül Slit2 inhibiert Neurale Invasion und Metastasierung des Pankreaskarzinoms (Talk). Jahreskongress 2013 der Deutschen Gesellschaft für Allgemein- und Viszeralchirurgie. Nuremberg, Germany. September 2013 11-14. Published in Zeitschrift für Gastroenterologie 2013; 51 - K53

- **A. Göhrig**, K. M. Detjen, J. Körner, G. Hilfenhaus, M. Welzel, R. Arsenic, R. Schmuck, M. Bahra, J. Y. Wu, B. Wiedenmann, and C. Fischer. Novel role of Slit2 as tumor suppressor in pancreatic neuroendocrine tumors (Poster). MDC Cancer Day 2012. Berlin, Germany. 2013 November 14.

- **A. Göhrig**, K. M. Detjen, G. Hilfenhaus, J. Körner, M. Welzel, and C. Fischer. The axon guidance molecule Slit2 regulates the motility of neuroendocrine tumor cells (Poster). Cell Symposia - Angiogenesis, Metabolic Regulation and Cancer Biology. Leuven, Belgium. 2013 June 07.

Berlin, _____
Ort, Datum

_____
Unterschrift

Acknowledgement/ Danksagung

Als erstes bedanke ich mich ganz herzlich bei Dr. med. Christian Fischer dafür, dass ich meine Doktorarbeit in seiner Arbeitsgruppe durchführen durfte und dafür, dass er mich über die gesamte Dauer der vorliegenden Arbeit unterstützt und gefördert hat. Christian hat mich von Anfang an in den Forschungsverbund seiner Arbeitsgruppe eingebunden, gerade auch dann, wenn die gegebenen Fragestellungen für mich neu waren. Dadurch konnte ich mich schnell einarbeiten und mir das experimentelle Handwerk und vor allem die translationalen Aspekte meiner Arbeit, welche nicht Teil meiner bisherigen Ausbildung waren, schnell aneignen und für meine Doktorarbeit einsetzen. Ohne diesen starken Rückhalt durch Christian hätte ich meine Doktorarbeit nicht erfolgreich abschließen können.

Im Anschluss daran bedanke ich mich bei Dr. med. Katharina Detjen, an die ich mich jederzeit und zu allen Themen des wissenschaftlichen Diskurses wenden konnte. Kate hat die Diskussionen stets so geführt, dass man sich die wesentlichen Fragen, mit denen man an sie herangetreten ist, am Ende oft selbst beantworten konnte. Von diesen Diskussionen habe ich ungemein profitiert und es hat mich vor allem in Bezug auf die Herangehensweise an verschiedene wissenschaftliche Fragestellungen ungemein weitergebracht.

Ganz besonders bedanke ich mich auch bei Frau Professor Ulrike Stein dafür, dass Sie nicht nur die Betreuung meiner Arbeit an der Humboldt-Universität zu Berlin übernommen hat, sondern mir auch die Möglichkeit gegeben hat an den Seminaren und Weiterbildungen des Max-Delbrück Zentrums teilzunehmen und dafür, dass ich meine Daten einem wissenschaftlichen Komitee am Max-Delbrück Centrum vorstellen konnte.

Ich danke ganz herzlich Martina Welzel für ihre technische Unterstützung im Labor, ihre fundierten Methoden-Kenntnisse und für ihre ansteckende Gelassenheit in schwierigen Zeiten.

Ich bedanke mich bei Maik Schröder für seine Hilfestellung bei histologischen Fragestellungen und tierexperimentellen Methoden. Jemand der neu in eine Stadt kommt braucht so einen Freund.

Ich bedanke mich bei Andrea Behm, die genau zur rechten Zeit unser Team verstärkt und mich gegen Ende der Doktorarbeit im Labor bei neuen Projekten sehr unterstützt hat.

Sehr dankbar bin ich Herrn Prof. Dr.-Ing. Dr. med. h.c. Frhr. von Villiez und der Sonnenfeldstiftung, für die Vergabe eines Stipendiums an meine Person. Ich habe mich sehr über die persönliche Betreuung durch Herr Prof. Villiez gefreut, der es sich hat nicht nehmen lassen, jeden seiner Stipendiaten persönlich zu besuchen.

Unabhängig von den Personen, die mich an den jeweiligen Stationen meiner Ausbildung und meiner Doktorarbeit unterstützt haben, danke ich meiner Familie und meinen Freunden.

Mein ganz herzlicher Dank gilt meiner Mutter Gabriele Göhrig, ihrem unermüdlichen Optimismus, ihrer Geduld und Fürsorge. Aus ähnlichen Gründen danke ich Iris, Johannes, Tobias und Daniel Wehr, sowie Bärbel, Irmgard und Walter Göhrig und Anette Quentin. Wann immer es möglich und immer, wenn es nötig war, wart Ihr für mich da. Ich kann nur andeuten, wie wichtig das für mich war und ist.

Außerdem bedanke ich mich bei Betteke van Noort für das Korrekturlesen meiner Arbeit.